

AD 608186

U. S. A R M Y

TRANSPORTATION RESEARCH COMMAND  
FORT EUSTIS, VIRGINIA

TRECOM TECHNICAL REPORT 64-47

EFFECTS OF PROPELLER SLIPSTREAM  
ON V/STOL AIRCRAFT  
PERFORMANCE AND STABILITY

Task 1D121401A14203  
Contract DA 44-177-AMC-48(T)

August 1964

prepared by:

DYNASCIENCES CORPORATION  
Fort Washington, Pennsylvania



### DISCLAIMER NOTICE

When Government drawings, specifications, or other data are used for any purpose other than in connection with a definitely related Government procurement operation, the United States Government thereby incurs no responsibility nor any obligation whatsoever; and the fact that the Government may have formulated, furnished, or in any way supplied the said drawings, specifications, or other data is not to be regarded by implication or otherwise as in any manner licensing the holder or any other person or corporation, or conveying any rights or permission, to manufacture, use, or sell any patented invention that may in any way be related thereto.

\* \* \* \*

### DDC AVAILABILITY NOTICE

Qualified requesters may obtain copies of this report from

Defense Documentation Center  
Cameron Station  
Alexandria, Virginia 22314

\* \* \* \*

This report has been released to the Office of Technical Services, U. S. Department of Commerce, Washington 25, D. C., for sale to the general public.

\* \* \* \*

Reproduction of this document in whole or in part is prohibited except with specific written permission of the Commanding Officer, U. S. Army Transportation Research Command.

\* \* \* \*


The findings and recommendations contained in this report are those of the contractor and do not necessarily reflect the views of the U. S. Army Mobility Command, the U. S. Army Materiel Command, or the Department of the Army.

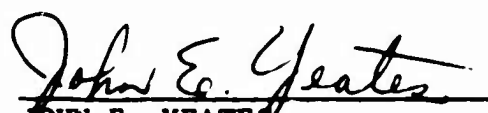
HEADQUARTERS  
U S ARMY TRANSPORTATION RESEARCH COMMAND  
FORT EUSTIS, VIRGINIA 23604

This report presents a theoretical development of propeller slipstream wing lift and drag contributions and the effects of these contributions on V/STOL aircraft performance and stability.

The principal contract under which this effort was initiated has been extended and will result in a follow-on report.

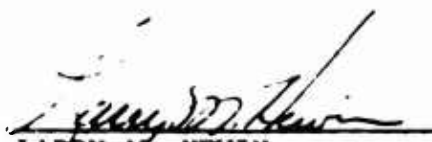
This command has reviewed the report and considers it to be technically sound.

  
FRANCIS E. LA CASSE, 2/Lt

  
JOHN E. YEATES  
Group Leader  
Aeromechanics Group

APPROVED.

FOR THE COMMANDER:

  
LARRY M. HEWIN  
Technical Director

Task 1D121401A14203

Contract DA 44-177-AMC-48(T)

TRECOM Technical Report 64-47

August 1964

EFFECTS OF PROPELLER SLIPSTREAM

ON V/STOL AIRCRAFT

PERFORMANCE AND STABILITY

Dynasciences Report No. DCR-137

Prepared by:

Dynasciences Corporation  
Fort Washington, Pennsylvania

for

U. S. Army Transportation Research Command  
Fort Eustis, Virginia

## PREFACE

This report presents the results of an investigation of propeller slipstream effects on V/STOL aircraft performance and stability. The work was performed for the U. S. Army Transportation Research Command, under Contract Number DA 44-177-AMC-48(T), during the period from 24 April 1963 to 24 March 1964.

Lt. F. E. La Casse and Dr. L. Goland were, respectively, the Army and Contractor's project engineers. Dr. Goland, Mr. N. Miller and Mr. L. Butler were the principal investigators.

## CONTENTS

	Page
PREFACE	iii
CONTENTS	v
ILLUSTRATIONS	vi
SYMBOLS	x
SUMMARY	1
I INTRODUCTION	2
II THEORETICAL ANALYSIS OF THE SLIPSTREAM CONTRIBUTION TO WING LIFT	3
III DEVELOPMENT OF LIFT AND LONGITUDINAL FORCE COEFFICIENTS FOR WING PROPELLER COMBINATIONS	15
IV ADDITIONAL SLIPSTREAM CONSIDERATIONS	30
V CORRELATION OF THEORY WITH TEST DATA	35
VI V/STOL AIRCRAFT STABILITY AND CONTROL	69
VII CONCLUSIONS AND RECOMMENDATIONS	84
VIII BIBLIOGRAPHY	85
APPENDIX. STOL TAKE-OFF AND LANDING PERFORMANCE ANALYSIS	90
DISTRIBUTION LIST	107

## ILLUSTRATIONS

Figure		Page
1	Wing Spanning a Circular Jet	5
2	Flow Pattern Around a Delta Wing (Top View)	8
3	Propeller Slipstream Notation	17
4	Model Configurations A, B, and C General Arrangement Drawing	36
5	Model Configuration D General Arrangement Drawing	37
6	Model Configuration E General Arrangement Drawing	38
7	Model Configuration F General Arrangement Drawing	39
8	Correlation of Predicted and Experimental Lift Coefficients, Configuration A, $C_{T,S} = 0.98$ and $\delta_f = 0$ Degrees	40
9	Correlation of Predicted and Experimental Lift Coefficients, Configuration B, $C_{T,S} = 0.98$ and $\delta_f = 0$ Degrees	41
10	Correlation of Predicted and Experimental Lift Coefficients Configuration C, $C_{T,S} = 0.98$ and $\delta_f = 0$ Degrees	42
11	Correlation of Predicted and Experimental Lift Coefficients, Configuration A, $C_{T,S} = 0.58$ and $\delta_f = 0$ Degrees	44
12	Correlation of Predicted and Experimental Lift Coefficients, Configuration B, $C_{T,S} = 0.58$ and $\delta_f = 0$ Degrees	45

13	Correlation of Predicted and Experimental Lift Coefficients, Configuration C, $C_{T,S} = 0.57$ and $\delta_f = 0$ Degrees	46
14	Correlation of Predicted and Experimental Lift Coefficients, Configuration B, $C_{T,S} = 0.88$ and $\delta_f = 0$ Degrees	47
15	Correlation of Predicted and Experimental Longitudinal Force Coefficients, Configuration B, $C_{T,S} = 0.88$ and $\delta_f = 0$ Degrees	48
16	Correlation of Predicted and Experimental Longitudinal Force Coefficients, Configuration B, $C_{T,S} = 0.58$ and $\delta_f = 0$ Degrees	49
17	Correlation of Predicted and Experimental Lift Coefficients, Configuration D, $C_{T,S} = 0.91$ and $\delta_f = 0$ Degrees	50
18	Correlation of Predicted and Experimental Lift Coefficients, Configuration D, $C_{T,S} = 0.71$ and $\delta_f = 0$ Degrees	51
19	Correlation of Predicted and Experimental Lift Coefficients, Configuration E, $C_{T,S} = 0.90$ and $\delta_f = 0$ Degrees	53
20	Correlation of Predicted and Experimental Lift Coefficients, Configuration E, $C_{T,S} = 0.90$ and $\delta_f = 50$ Degrees	54
21	Correlation of Predicted and Experimental Lift Coefficients, Configuration F, $C_{T,S} = 0.91$ and $\delta_f = 0$ Degrees	55
22	Correlation of Predicted and Experimental Lift Coefficients, Configuration F, $C_{T,S} = 0.71$ and $\delta_f = 0$ Degrees	56
23	Correlation of Predicted and Experimental Lift Coefficients, Configuration F, $C_{T,S} = 0.91$ and $\delta_f = 10$ Degrees	57



24	Correlation of Predicted and Experimental Lift Coefficients, Configuration F, $C_{T,S} = 0.71$ and $\delta_f = 10$ Degrees	58
25	Correlation of Predicted and Experimental Lift Coefficients, Configuration F, $C_{T,S} = 0.91$ and $\delta_f = 50$ Degrees	59
26	Correlation of Predicted and Experimental Lift Coefficients as a Function of Flap Deflection, Configuration F, $C_{T,S} = 0.91$ and $\alpha_w = 0$ Degrees	60
27	Correlation of Predicted and Experimental Longitudinal Force Coefficients, Configuration F, $C_{T,S} = 0.91$ and $\delta_f = 0$ Degrees	61
28	Correlation of Predicted and Experimental Longitudinal Force Coefficients, Configuration F, $C_{T,S} = 0.91$ and $\delta_f = 20$ Degrees	62
29	Correlation of Predicted and Experimental Longitudinal Force Coefficients, Configuration F, $C_{T,S} = 0.91$ and $\delta_f = 30$ Degrees	63
30	Correlation of Predicted and Experimental Longitudinal Force Coefficients, Configuration F, $C_{T,S} = 0.71$ and $\delta_f = 0$ Degrees	64
31	Correlation of Predicted and Experimental Longitudinal Force Coefficients, Configuration F, $C_{T,S} = 0.71$ and $\delta_f = 30$ Degrees	65
32	Effect of Slipstream on the Roots of the Characteristic Equation for Hovering Flight	79
33	Effect of Trailing Edge Flap Stabilizer on the Roots of the Characteristic Equation for Hovering Flight	83
34	Profile of Landing Path	91

35	Landing Approach Distance from Reference 14	93
36	Landing Transition Distance	94
37	Landing Ground Run Distance from Reference 14	96
38	Total Landing Distance Over a 50-Foot Obstacle	98

### SYMBOLS

$R$	wing aspect ratio
$a$	wing lift curve slope without slipstream, per radian
$a_1$	aircraft acceleration during take-off, ft/sec <sup>2</sup>
$a_c$	aircraft deceleration encountered during landing, ft/sec <sup>2</sup>
$a_o$	two dimensional airfoil lift curve slope, per radian
$b$	number of propeller blades; also wing span, ft.
$c$	chord of wing, ft.
$c_b$	propeller blade chord at 0.75R, ft.
$c_f$	flap chord, or distance from the wing leading edge as defined in Figure 2, ft.
$C_d$	section drag coefficient of propeller blade at 0.75R, or wing section drag coefficient
$C_{Di}$	induced drag coefficient, $C_L^2 / \pi R e$
$C_{D,N}$	nacelle drag coefficient based on nacelle length and diameter
$C_{D0}$	profile drag coefficient
$C_F$	coefficient of friction between tires and runway during landing
$C_l$	section lift coefficient
$C_L$	lift coefficient based on $q$ , $L/qS$
$C_{L,S}$	lift coefficient based on $q_s$ , $L/q_s S$

$C_{L,W}$	denotes the basic wing contribution to the total wing lift coefficient, $\frac{q}{q_s} C_L$ .
$C_{M,ac}$	pitching moment coefficient about the wing aerodynamic center
$C_{M,CF}$	pitching moment coefficient due to propeller blade offset
$C_T$	propeller thrust coefficient, $\frac{T}{\rho \pi R^2 (\Omega R)^2}$
$C_{T,S}$	propeller thrust coefficient, $\frac{T}{q_s \left( \frac{\pi D^2}{4} \right)}$
$C_X$	body axis longitudinal force coefficient, $\frac{F_x}{q S}$
$C_{X,R}$	propeller longitudinal force coefficient, $\frac{F_{x,R}}{q_s S}$
$C_{X,S}$	longitudinal force coefficient, $\frac{F_x}{q_s S}$
$D$	propeller diameter, ft. or drag, lb.
$D_i$	induced drag, lb.
$D_N$	nacelle drag, lb.
$D_o$	profile drag, lb.
$D_S$	slipstream drag measured parallel with the slipstream flow
$d$	diameter of the fully developed slipstream, $2r_o$ , ft.
$d_N$	nacelle diameter, ft.
$e$	efficiency factor used in estimating induced drag
$F_x$	summation of forces parallel with the free-stream flow, lb.

$F_z$	summation of forces perpendicular to the free-stream flow (vertical), lb.
$g$	acceleration due to gravity
$h$	vertical height achieved during transition, ft.
$i_w$	angle between propeller thrust axis and wing chord line, radians
$k_s$	flap linkage constant
$L$	lift, lb.
$L_s$	slipstream lift perpendicular to jet flow, $N(\Delta C_{L,S} q_s S)$ , lb.
$l$	nacelle length, ft.
$l_a$	landing approach distance, ft.
$l_c$	distance required to climb to 50-foot altitude, ft.
$l_g$	aircraft ground run, ft.
$\ln$	denotes natural logarithm
$l_t$	landing transition distance, ft.
$l_{TT}$	take-off transition distance, ft.
$N$	number of propellers
$q$ or $q_o$	free-stream dynamic pressure, $\frac{1}{2} \rho V^2$ , or $\frac{1}{2} \rho V_o^2$ , lb/ft <sup>2</sup>
$q_s$	slipstream dynamic pressure, $\frac{1}{2} \rho V_j^2$ , lb/ft <sup>2</sup>
$R$	propeller radius, ft.
$R_n$	Reynolds number based on $c$ and $V_j$

$r$	distance measured radially from center of slipstream jet, ft.
$r_o$	radius of fully developed slipstream, ft.
$S$	wing area, ft. <sup>2</sup> , or total landing distance, ft.
$S_f$	flap area, ft. <sup>2</sup>
$S_s$	total wing area immersed in slipstream, ft. <sup>2</sup>
$S_T$	total take-off distance over a 50 foot obstacle
$S_{To}$	take-off distance, ft.
$T$	propeller thrust, lb.
$U$	slipstream induced velocity, ft/sec
$V_c$	rate of climb, ft/sec
$V_j$	resultant flow velocity in slipstream, ft/sec
$V$ or $V_o$	free-stream velocity, ft/sec
$V_v$	rate of descent, ft/sec
$W$	aircraft weight, lb.
$X_a$	distance along X axis from wing quarter chord to center of gravity, ft.
$X_R$	distance along X axis from propeller center to center of gravity, ft.
$X_t$	distance along X axis from tail to center of gravity, ft.
$Z_a$	distance along Z axis from wing quarter chord to center of gravity, ft.

$z_R$	distance along Z axis from propeller center to center of gravity, ft.
$z_t$	distance along Z axis from tail to center of gravity, ft.
$\alpha$	airfoil section effective angle of attack, radians; only used in estimation of $C_L$
$\alpha_{LO}$	airfoil section angle of zero lift, rad.
$\alpha_T$	propeller thrust axis angle of attack, rad.
$\alpha_s$	effective angle of attack in slipstream, rad.
$\alpha_W$	wing geometric angle of attack with respect to freestream, rad.
$\beta_{.75R}$	propeller geometric pitch at .75R, rad.
$\Delta C_{DS}$	change in drag coefficient, due to slipstream
$\Delta C_L$	change in lift coefficient, due to the slipstream
$\Delta C_{L,S}$	change in lift coefficient, due to slipstream
$\Delta n$	increment of normal acceleration encountered during transition
$\delta_f$	flap deflection angle, rad.
$\theta$	aircraft pitch attitude, rad.
$\theta_p$	aircraft landing approach angle, rad.
$\theta_c$	aircraft climb angle, rad.
$\mu$	ratio of free-stream to jet velocity, $\frac{V \cos(\alpha_T - \phi)}{V_j}$
$\mu_L$	coefficient of friction during take-off

$\rho$	mass density of air, slugs/ft <sup>3</sup>
$\phi$	slipstream angular deflection, rad; also velocity potential, ft <sup>2</sup> /sec
$\phi_j$	velocity disturbance potential in the jet slipstream, ft <sup>2</sup> /sec
$\phi_o$	velocity disturbance potential outside of the jet (in free stream), ft <sup>2</sup> /sec
$\phi_s$	velocity disturbance potential on the surface of the airfoil, ft <sup>2</sup> /sec
$\Omega$	propeller rotational speed, rad/sec

#### SUBSCRIPTS

g	Gravity
i	Inertia
R	Propeller
S	Slipstream
t	Tail
W	Wing

NOTE: All angles are in radians unless otherwise specified.



**BLANK PAGE**

## SUMMARY

Presented herein is an analytical investigation of the aerodynamic forces acting on wing-propeller combinations including the effects of propeller slipstreams. The results of the developed theory are then applied to typical two- and four-propeller VTOL and STOL wing configurations. Correlation with existing test data is shown to be satisfactory.

Consideration is also given to such associated items as the effects of the slipstream on (1) wing stall (2) aircraft take-off and landing performance and (3) aircraft stability and control.

## I. INTRODUCTION

Recent interest in vertical and short take-off and landing aircraft (V/STOL) has put new emphasis on the problem of propeller slipstream-wing aerodynamic interaction. The low-speed performance and handling qualities of this type of aircraft are highly dependent on the nature of this interaction, since such aircraft have necessarily high-energy propeller slipstreams whose diameters are of the same order of magnitude as the wing semi-span and chord. These aircraft are subjected to the varying effects of this interaction especially during take-off, landing, and transition, when the free-stream velocity is small compared to that of the slipstream velocity. It is apparent that refinements of design and increased performance can be made only if this aerodynamic interaction can be adequately understood and utilized to the fullest extent.

Presented herein is a theory for the lift and drag of a wing immersed in a slipstream. The analysis is applicable to all ratios of free-stream to slipstream velocity and accounts for an angle of attack of the wing relative to the propeller thrust axis, as well as for an angle of attack of the thrust axis relative to the free-stream. The theory is correlated with experimental data of configurations such as two- and four-propeller tilt-wing-type aircraft. Attention is also focused on the effects of the slipstream interaction on the stalling and slow-speed characteristics of the aircraft. An analysis is then presented of the effect of the slipstream on the take-off and landing performance. Finally, an exploratory study is made of the propeller slipstream effect on the stability and control characteristics, and the feasibility of improving the slow-speed handling qualities by proper use of the slipstream.

## II. THEORETICAL ANALYSIS OF THE SLIPSTREAM CONTRIBUTION TO WING LIFT

### A. INTRODUCTION

The problem of a wing spanning a uniform jet for the case where the outside air (free-stream) velocity is zero (e.g., in a wind tunnel) has been extensively investigated both theoretically and experimentally.

The case in which the external air is in motion has not received as much attention, but the basic treatment was given by Koning (Reference 1). Koning was the first to determine the jet effect by including the important jet boundary conditions which must be satisfied. On account of the mathematical difficulties involved, however, he made the following simplifying assumptions:

1. The angle between the relative wind (free-stream) direction and the jet axis is equal to zero.
2. The jet is free from rotational components, and has constant velocity distribution over the circular cross section and along the jet axis.
3. The additional velocity in the jet is small compared with the free-stream velocity in order that the problem might be "linearized".
4. The change of the undisturbed flow, caused by the action of the wing, is identical with that related to a system of vortices; the system consists of a rectilinear line vortex, taking the place of the wing (the so-called "lifting vortex"), and a layer of "trailing vortices" extending from the lifting vortex to infinity.

Koning then decomposes the resulting flow field of the jet, wing and external flow into six different parts as follows:

1. undisturbed flow - the flow in the absence of wing and propeller, being a parallel flow with constant velocity.

2. propeller flow - the difference between (1) and the flow which would exist if the propeller were acting in the absence of the wing.
3. airfoil flow - the change in flow caused by the action of the wing when introduced into (1), the propeller being absent.
4. additional airfoil flow - the disturbance flow, related directly to the change in circulation around the wing, caused by the action of the propeller.
5. additional flow - the difference between the resulting flow (6) and the flow which would be obtained by simple superposition of (1), (2), (3), and (4).
6. resulting flow - the flow existing with both propeller and wing present.

The potentials of (1) through (4) can be superimposed in the usual way, but they do not represent the entire pattern of flow. The potential of (5), which is unknown, must be determined from the conditions at the jet slipstream boundary.

The conditions to be satisfied at the boundary of the slipstream are:

1. The pressure shall have the same value on each side of the jet boundary.
2. The jet boundary must be a streamline of the flow. In terms of the disturbance velocity potential,  $\phi$ , Reference 1 shows that the first boundary condition may be written as (see Figure 1),

$$v_j \frac{\partial \phi_j}{\partial x} = v_o \frac{\partial \phi_o}{\partial x} \quad \text{at } r = r_o \quad (2.1)$$

where the subscripts  $j$  and  $o$  refer to the regions inside and outside of the jet, respectively. Integrating in the streamwise direction from negative infinity to some station  $x$ , and recalling that  $\phi(-\infty)$  is an arbitrary constant, the first boundary condition is then obtained in the form,

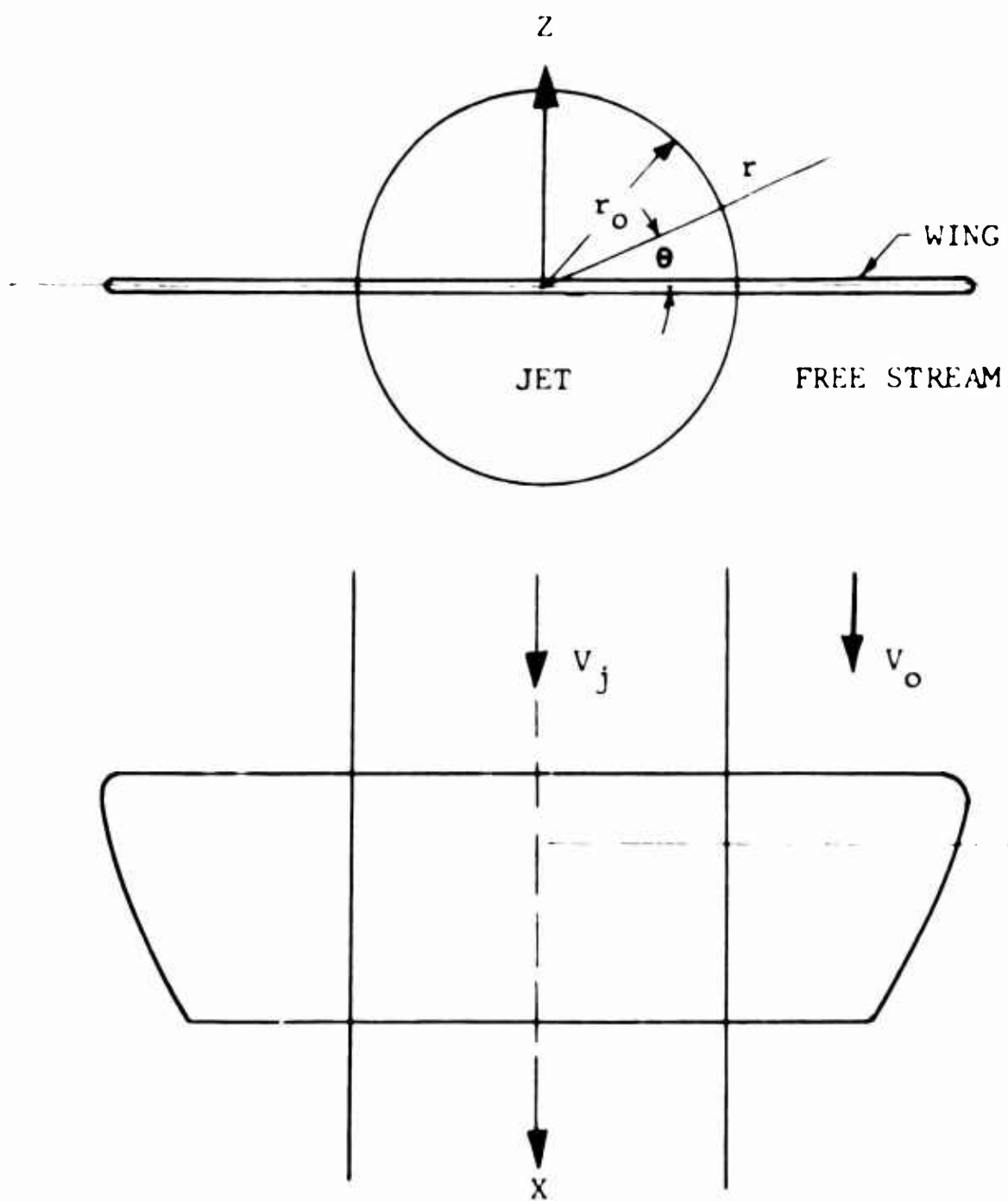


FIGURE 1: WING SPANNING A CIRCULAR JET

$$v_j \phi_j = v_o \phi_o \text{ at } r = r_o . \quad (2.2)$$

The second boundary condition expresses the fact that the inside and outside flow must be tangent at the boundary; that is, the boundary consists of streamlines. For a circular jet, the tangency condition is expressed as

$$v_j \frac{\partial \phi_o}{\partial r} = v_o \frac{\partial \phi_j}{\partial r} \text{ at } r = r_o . \quad (2.3)$$

As shown in Reference 1, the problem is more feasibly handled by studying the conditions in a plane far downstream from the wing (the Trefftz plane). At  $x = +\infty$ , the potentials of the airfoil flow, the additional airfoil flow, and the additional flow will be functions of  $y$  and  $z$  only, which moreover satisfy the Laplace equation,

$$\frac{\partial^2 \phi}{\partial y^2} + \frac{\partial^2 \phi}{\partial z^2} = 0 \quad (2.4)$$

and, hence, are two-dimensional potential functions. Thus, two-dimensional potential theory is used to satisfy boundary conditions 1 and 2 and the so-called "method of images" is utilized as well as the concept of horseshoe vortices.

The use of a line vortex system to represent the wing such as described above implies validity only for wings of high aspect ratio.

Thus the analysis of Reference 1 is applicable when :

- (1) the jet velocity is only slightly greater than the free-stream, and
- (2) the aspect ratio of the wing is large.

Most of the work accomplished since Reference 1 has started from Koning's basic system and includes various modifications involving the use of complex lifting surface approximations (Reference 2), semi-empirical methods (Reference 3), consideration of higher order terms to consider smaller values of the ratio

of free-stream to jet velocity ( $\mu$ ) as well as the treatment of infinite span wings (References 4 and 5), effects due to slipstream rotation (Reference 6), misalignment of slipstream and free-stream, and other effects.

The design of present-day aircraft (e.g., STOL and VTOL propeller types) calls for the diameter of the slipstream to be of the same order of magnitude as the wing chord and wing semi-span. The validity of a "lifting line" or infinite span wing theory discussed above is therefore to be questioned for application to the present problem of low-aspect-ratio wings. In Reference 7, R. T. Jones presents a low-aspect-ratio theory that is applicable to the present problem. As shown below its use enables the above restrictions to be removed so that a finite wing spanning the jet may be treated for all ratios of free-stream to jet velocity.

#### B. THEORY OF WINGS OF SMALL ASPECT RATIO

For wings of small aspect ratio, R. T. Jones proposed a theory which provides acceptable results for wings whose aspect ratio is less than approximately 1.5, which is the area of interest in the present problem. The theory is most suitable for the prediction of spanwise and chordwise lift, and induced drag, of wings with swept-back leading edges ending in straight trailing edges which are normal to the direction of flow. For wings of elliptic or rectangular planform, the spanwise lift and induced drag are also adequately predicted by the theory; however, for these configurations the analysis provides only qualitative information on the chordwise pressure distribution, viz, that the center of pressure moves toward the leading edge as the aspect ratio decreases. Since the prediction of spanwise lift is of prime interest in the present problem, this theory was expected to be applicable and is utilized herein.

The basic idea of the small aspect ratio theory, as described in Reference 7, may be obtained by considering a delta wing as shown in Figure 2, which moves with a uniform velocity,  $V$ , at an angle of attack,  $\alpha$ , in the negative direction of the X-axis. As the wing advances across the plane B-B, which is normal to the direction of motion of the wing, it transmits a downward component of velocity equal to  $V \tan \alpha$  or  $V\alpha$ , to the fluid. The field of flow in the plane B-B is therefore considered the same as that produced by a two-dimensional flat plate which moves downward with velocity,  $V\alpha$ . The field of



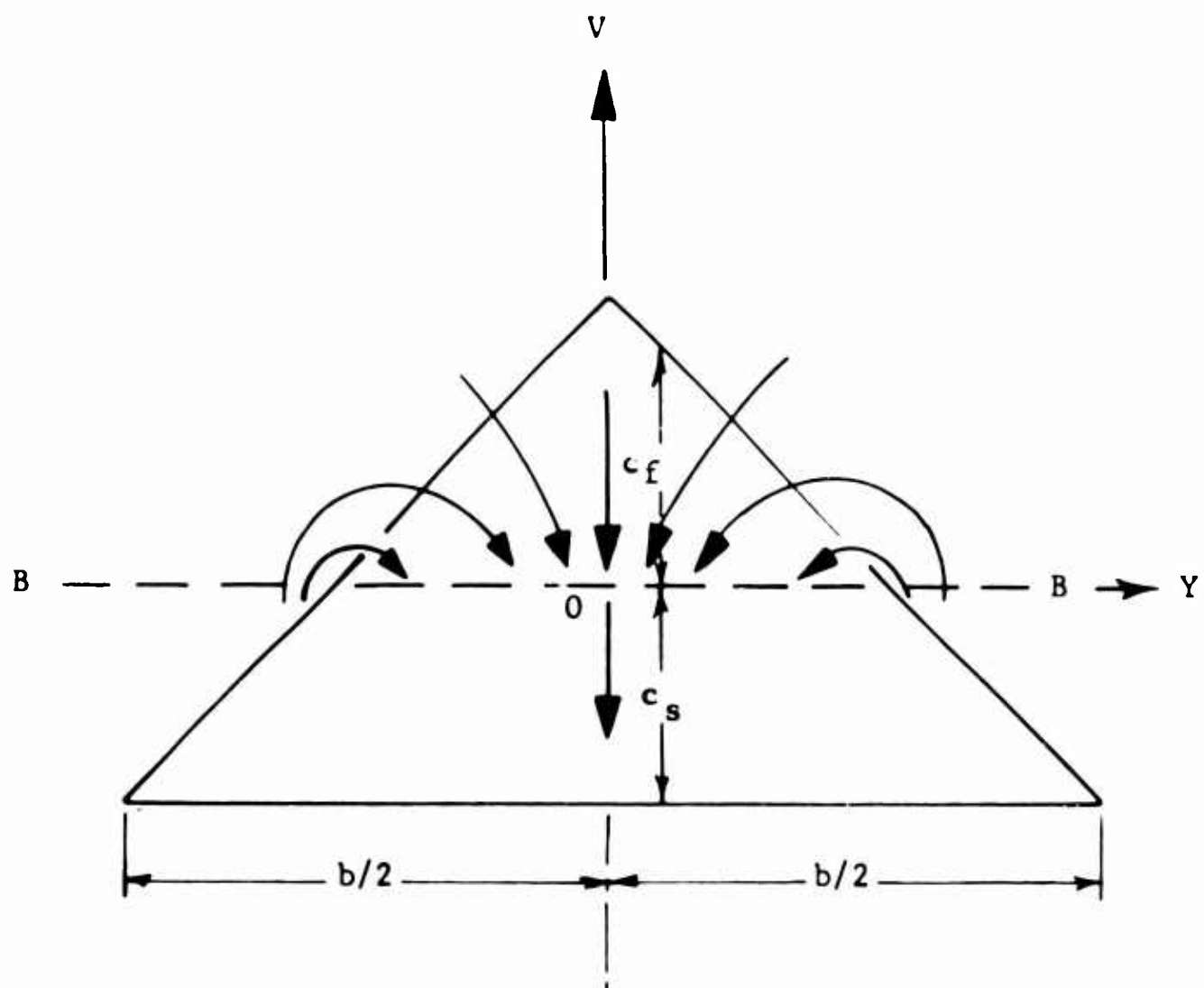


FIGURE 2: FLOW PATTERN AROUND A DELTA WING (Top View)

flow in B-B may therefore be represented by a velocity potential which satisfies the two dimensional Laplace equation

$$\frac{\partial^2 \phi}{\partial y^2} + \frac{\partial^2 \phi}{\partial z^2} = 0 \quad (2.4)$$

Equation 2.4 together with the above boundary conditions specify  $\phi$  in plane B-B.

The local pressure change is proportional to the local time rate of change of  $\phi$ . That is,

$$p = -\rho \frac{D\phi}{Dt} \quad (2.5)$$

Now, since  $\frac{D\phi}{Dt} = \frac{\partial \phi}{\partial x} \frac{dx}{dt}$

$$\text{and } V = \frac{dx}{dt} \quad (2.6)$$

Equation (2.5) may be written as,

$$p = -\rho V \frac{\partial \phi}{\partial x} \quad (2.7)$$

Integration of the pressures in a chordwise direction from forward of the leading edge downstream to the trailing edge and accounting for top and bottom airfoil surfaces, gives the span load distribution as,

$$\frac{\partial L}{\partial y} = 2 \int_{-c_f}^{c_s} p dx = 2\rho V \phi_s \quad (2.8)$$

where  $\phi_s$  is the velocity potential at the surface of the wing at the widest section, and  $c_f$  and  $c_s$  are defined in Figure 2. The wing lift is, therefore,

$$L = \int_{-b/2}^{b/2} 2 \rho V \phi_s dy \quad (2.9)$$

and the lift coefficient becomes

$$C_L = \frac{2 \rho V}{q_\infty} \int_{-b/2}^{b/2} \phi_s dy \quad (2.10)$$

The above theory will now be applied to the case of a finite wing spanning a uniform jet. The two-dimensional velocity potential,  $\phi$ , will therefore be obtained such as to satisfy the trailing edge as well as the jet boundary conditions.

### C. WING SPANNING UNIFORM JET

Considered here is the case of a wing of span,  $b = 2r_0$ , immersed in a uniform jet of velocity  $V_j$  which is aligned with a free-stream having a velocity  $V_\infty$ . From the foregoing discussions the problem reduces to the determination of the two-dimensional velocity potential subject to the following boundary conditions (Figure 1),

#### Boundary Condition

$$\text{wing:} \quad \frac{\partial \phi_j}{\partial z} = V_j \alpha \quad \text{at} \quad z = 0 \quad \text{and} \quad y \leq r_0 \quad (2.11)$$

$$\text{jet:} \quad V_j \frac{\partial \phi_0}{\partial r} = V_\infty \frac{\partial \phi_j}{\partial r} \quad \text{at} \quad r = r_0 \quad (2.12)$$

$$\text{jet:} \quad V_j \phi_j = V_\infty \phi_0 \quad \text{at} \quad r = r_0 \quad (2.13)$$

$$\text{free-stream:} \quad \phi_0 \longrightarrow 0 \quad \text{as} \quad r \longrightarrow \infty \quad (2.14)$$

$$\text{It is also to be noted that } \phi_j \text{ must be finite at } r = 0. \quad (2.15)$$

The flow is potential inside and outside the jet boundary; the potential function, however, need not be continuous at the

jet boundary.

In polar coordinates, Laplace's equation is,

$$\frac{\partial^2 \phi}{\partial r^2} + \frac{1}{r} \frac{\partial \phi}{\partial r} + \frac{1}{r^2} \frac{\partial^2 \phi}{\partial \theta^2} = 0. \quad (2.16)$$

The general solution to equation (2.16) is,

$$\phi = \sum_{m=0}^{\infty} (a_m r^m \cos m\theta + b_m r^m \sin m\theta + C_m r^{-m} \cos m\theta + D_m r^{-m} \sin m\theta). \quad (2.17)$$

Applying boundary conditions (2.14) and (2.15), there follows that,

$$\text{at } r < r_0 \quad \phi_j = a_0 + \sum_{m=1}^{\infty} b_m \left(\frac{r}{r_0}\right)^m \sin m\theta + \sum_{m=1}^{\infty} a_m \left(\frac{r}{r_0}\right)^m \cos m\theta \quad (2.18)$$

$$\text{at } r > r_0 \quad \phi_o = \sum_{m=1}^{\infty} D_m \left(\frac{r}{r_0}\right)^{-m} \sin m\theta + \sum_{m=1}^{\infty} C_m \left(\frac{r}{r_0}\right)^{-m} \cos m\theta \quad (2.19)$$

in which the distance,  $r$ , has been nondimensionalized by the jet radius,  $r_0$ . Now for  $r \leq r_0$  boundary condition, Equation (2.11) specifies that

$$\left(\frac{\partial \phi_j}{\partial z}\right)_{z=0} - \left(\frac{1}{r} \frac{\partial \phi_j}{\partial \theta}\right)_{\theta=0} = \sum_{m=1}^{\infty} m b_m \frac{r^{m-1}}{r_0^m} = -V_j \alpha. \quad (2.20)$$

Thus,  $b_1 = -V_j \alpha r_0$ ;  $b_m = 0$  for  $m = 2, 3, 4$ , etc.

Satisfying the boundary condition given by Equation (2.12),

$$-\sum_{m=1}^{\infty} m D_m \sin m\theta - \sum_{m=1}^{\infty} m C_m \cos m\theta = \mu \left[ -\frac{V_o \alpha r_0 \sin \theta}{\mu} + \sum_{m=1}^{\infty} m a_m \cos m\theta \right] \quad (2.21)$$

Consequently,

$$D_1 = V_0 \alpha r_0 ; D_m = 0 \text{ for } m = 2, 3, 4, \text{ etc.} \quad (2.22)$$

$$C_m = -\mu a_m .$$

Satisfying boundary condition Equation (2.13),

$$\begin{aligned} a_0 - \frac{V_0 \alpha r_0}{\mu} \sin \theta + \sum_{m=1}^{\infty} a_m \cos m\theta \\ - \mu \left[ V_0 \alpha r_0 \sin \theta - \mu \sum_{m=1}^{\infty} a_m \cos m\theta \right] \end{aligned} \quad (2.23)$$

which may be reduced to,

$$\frac{\mu a_0}{1 + \mu^2} - \mu \sum_{m=1}^{\infty} a_m \cos m\theta = V_0 \alpha r_0 \sin \theta \quad (2.24)$$

Now,

$$\sin \theta = \frac{2}{\pi} - \frac{4}{\pi} \sum_{m=2, 4, 6}^{\infty} \frac{\cos m\theta}{m^2 - 1} . \quad (2.25)$$

Substituting Equation (2.25) into Equation (2.24) and evaluating coefficients, there results that

$$\begin{aligned} a_0 &= \frac{1 + \mu^2}{\mu} \frac{2}{\pi} V_0 \alpha r_0 \\ a_m &= - \frac{4 V_0 \alpha r_0}{\pi \mu} \left( \frac{1}{m^2 - 1} \right) \text{ for } m=2, 4, 6 \text{ etc.} \end{aligned} \quad (2.26)$$

The velocity potential inside the jet may therefore be written as

$$\phi_j = V_0 \alpha r_0 \left[ \frac{1 + \mu^2}{\mu} \left( \frac{2}{\pi} \right) - \frac{r}{\mu r_0} \sin \theta - \frac{4}{\pi \mu} \sum_{m=2, 4, 6}^{\infty} \frac{\left( \frac{r}{r_0} \right)^m \cos m\theta}{m^2 - 1} \right] . \quad (2.27)$$

On the wing surface  $\theta = 0$ , and letting  $\bar{y} = \frac{r}{r_0}$ , the potential on the wing surface is,

$$\phi_s = v_o \alpha r_o \left[ \frac{1}{\mu} \left( \frac{2}{\pi} \right) - \frac{4}{\pi \mu} \sum_{m=2, 4, 6}^{\infty} \frac{\bar{y}^m}{m^2 - 1} \right] \quad (2.28)$$

By means of expression 601.2 of Reference 3, it may be shown that

$$\sum_{m=2, 4, 6}^{\infty} \frac{\bar{y}^m}{m^2 - 1} = \frac{1}{2} \left[ 1 - \frac{1}{2} \left( \bar{y} - \frac{1}{\bar{y}} \right) \ln \left( \frac{1 - \bar{y}}{1 - \bar{y}} \right) \right]; \quad (2.29)$$

thus,

$$\phi_s = \frac{2v_o \alpha r_o}{\pi \mu} \left[ \mu^2 - \frac{1}{2} \left( \bar{y} - \frac{1}{\bar{y}} \right) \ln \left( \frac{1 - \bar{y}}{1 - \bar{y}} \right) \right] \quad (2.30)$$

and the wing lift coefficient based on free-stream velocity and the wing area which is completely immersed in the slipstream becomes

$$C_L = \frac{4}{\mu v_o c} \int_0^1 \phi_s d\bar{y} \quad (2.31)$$

$$= \frac{8\alpha}{\pi c} \int_0^1 \left[ 1 - \frac{1}{2\mu^2} \left( \bar{y} - \frac{1}{\bar{y}} \right) \ln \left( \frac{1 - \bar{y}}{1 - \bar{y}} \right) \right] d\bar{y} \quad (2.32)$$

The following definite integrals are evaluated in Reference 8:

$$\int_0^1 \bar{y} \ln (1 - \bar{y}) d\bar{y} = -\frac{1}{4}$$

$$\int_0^1 \bar{y} \ln (1 - \bar{y}) d\bar{y} = -\frac{3}{4}$$

$$\int_0^1 \frac{\ln(1+\bar{y})}{\bar{y}} d\bar{y} = \frac{\pi^2}{12}$$

$$\int_0^1 \frac{\ln(1-\bar{y})}{\bar{y}} d\bar{y} = -\frac{\pi^2}{6} \quad . \quad (2.33)$$

Consequently,

$$C_L = \frac{8\alpha r_0}{\pi c} \left[ 1 + \frac{1}{2\mu^2} \left( \frac{\pi^2}{4} - 1 \right) \right] \quad . \quad (2.34)$$

In the absence of a slipstream jet,  $\mu = 1$  and

$$\left( C_L \right)_{\mu=1} = \frac{8\alpha r_0}{\pi c} \left[ 1 + \frac{1}{2} \left( \frac{\pi^2}{4} - 1 \right) \right] \quad . \quad (2.35)$$

Thus, the change in  $C_L$  due to the jet becomes,

$$\Delta C_L = \frac{8\alpha}{\pi} \left( \frac{r_0}{c} \right) \left[ \frac{1-\mu^2}{\mu^2} - \frac{1}{2} \left( \frac{\pi^2}{4} - 1 \right) \right] \quad (2.36)$$

$$= 1.87 \alpha \left( \frac{r_0}{c} \right) \cdot \left( \frac{1-\mu^2}{\mu^2} \right) \quad .$$

The change in spanwise lift distribution may similarly be obtained by use of Equations (2.8) and (2.30) and may be written as,

$$\Delta C_l = \frac{1}{q c} \frac{\partial (\Delta L)}{\partial \bar{y}} \quad (2.37)$$

$$= 1.27 \left( \frac{r_0}{c} \right) \cdot \left( \frac{1-\mu^2}{\mu^2} \right) \cdot \left( \frac{1}{\bar{y}} - \bar{y} \right) \cdot \ln \left( \frac{1+\bar{y}}{1-\bar{y}} \right) \quad .$$

### III. DEVELOPMENT OF LIFT AND LONGITUDINAL FORCE COEFFICIENTS FOR WING-PROPELLER COMBINATIONS

In this section expressions are developed for estimating the total lift and longitudinal force coefficients for various wing-propeller combinations throughout an angle of attack and " $\mu$ " range. The basic approach used is to account for the slipstream effects by adding to the basic wing lift coefficient ( $C_{L,W}$ ) the effect of the slipstream ( $\Delta C_{L,S}$ ) from Section II.

The major assumptions utilized in the development of the equations are:

1. Potential flow conditions exist, i.e., there is no separated flow over the wing or flap.
2. The slipstream is fully contracted at the wing leading edge.
3. The slipstream velocity is uniform and the effect of slipstream rotation is small.
4. The slipstream contraction is unaffected by the presence of the wing and nacelle.
5. For multi-propeller configurations no interaction exists between slipstreams.

#### A. GENERAL SLIPSTREAM WING AERODYNAMIC INFORMATION

Before proceeding with the development of the actual equations, some background information will be presented including standard expressions for estimating the aerodynamic characteristics of wings and slipstreams.

##### 1. Wing Lift Coefficient

The basic wing lift, i.e., the lift generated by the wing when the propeller thrust is zero, is considered first. For straight wings, with ordinary planforms, the classical expression for the wing lift coefficient is



$$C_L = \frac{a_0 AR \alpha}{AR + \frac{a_0}{\pi}} \approx \frac{a_0 AR \alpha}{AR + 2} \quad (3.1)$$

Equation (3.1) accounts for the effect of a finite span on aerodynamic loading in incompressible flow, which is of concern herein. It is accurate for those cases when the aspect ratio exceeds four (4) but gives too high numerical values below that. For the case of small aspect ratios, Jones (Reference 7 ) presents the equation

$$C_L = \frac{\pi}{2} \alpha AR \quad (3.2)$$

which has experimentally been shown to be quite accurate. Diederich (Reference 9 ) shows that the formula

$$C_L = \frac{a_0 AR \alpha}{(AR) \sqrt{1 + \left(\frac{a_0}{\pi AR}\right)^2} + \frac{a_0}{\pi}} \quad (3.3)$$

covers the whole range rather well, approaching Equation (3.1) in the limit of large  $AR$  and Equation (3.2) as  $AR$  goes to zero.

## 2. Propeller Slipstream Characteristics

### a. Induced Velocity, $U$

Referring to the notation in Figure 3, the induced velocity in a fully developed slipstream may be determined by use of Bernoulli's Equation and the continuity equation as

$$U = -V_0 \cos \alpha_T + \sqrt{(V_0 \cos \alpha_T)^2 + \frac{T}{\frac{\rho}{2} \left( \frac{\pi D^2}{4} \right)}} \quad (3.4)$$

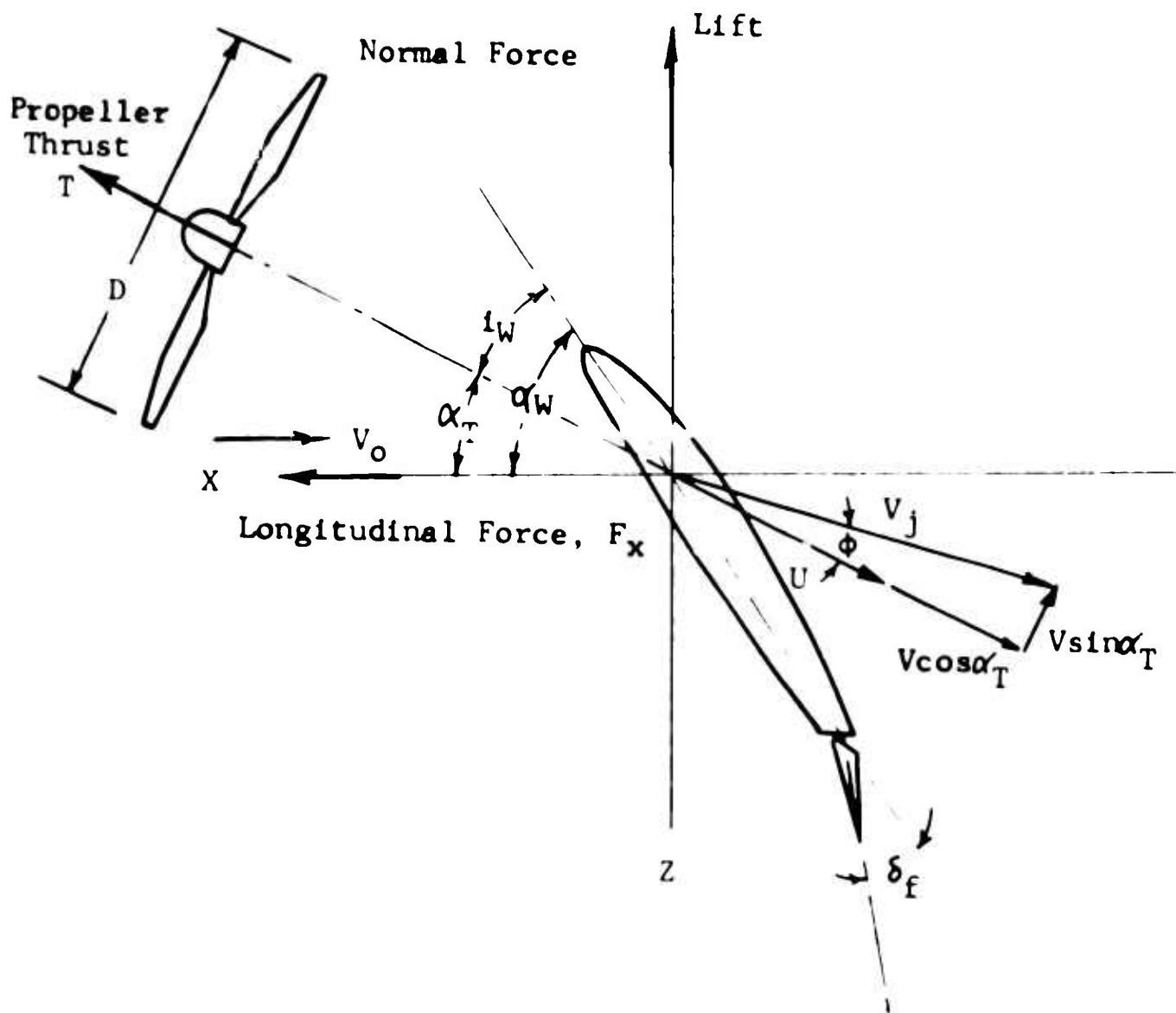


FIGURE 3: PROPELLER SLIPSTREAM NOTATION

b. Diameter of Slipstream, d

The diameter of a fully developed propeller slipstream can be determined from the continuity equation, and there results

$$d = D \sqrt{\frac{1}{2} \left( \frac{2V_o \cos \alpha_T + U}{V_o \cos \alpha_T + U} \right)} . \quad (3.5)$$

c. Resultant Velocity in Slipstream,  $V_j$

As shown in Figure 3, the resultant slipstream velocity is the vector sum of the free-stream and the induced velocities. Thus,

$$V_j^2 = (V \sin \alpha_T)^2 + (V_o \cos \alpha_T)^2 + U^2 + 2 V_o U \cos \alpha_T . \quad (3.6)$$

Substituting Equation (3.4) into Equation (3.6) and solving for  $V_j$ , there results

$$V_j = \sqrt{V_o^2 + \frac{T}{\frac{\rho}{2} \left( \frac{\pi D^2}{4} \right)}} . \quad (3.7)$$

d. Slipstream Dynamic Pressure,  $q_s$

The dynamic pressure of the flow in the slipstream is

$$\begin{aligned} q_s &= q_o + \left( \frac{T}{\frac{\pi D^2}{4}} \right) \\ &= \frac{1}{2} \rho V_j^2 . \end{aligned} \quad (3.8)$$

3. Wing Characteristics in Slipstream

The effective angle of attack,  $\alpha_s$ , of that portion of the wing located in the propeller slipstream is

$$\alpha_s = i_w + \phi - \alpha_{LO} + \delta_f \quad (3.9)$$

where it has been assumed that a flap deflection adds an increment  $\delta_f$  to the angle of attack of the wing within the slipstream, and where

$$\phi = \tan^{-1} \left( \frac{V_o \sin \alpha_T}{V_o \cos \alpha_T + U} \right) .$$

#### B. TOTAL LIFT COEFFICIENT, $C_{L,S}$

Summing all of the lift forces acting on the propeller-wing combination,  $C_{L,S}$  based on slipstream dynamic pressure,  $q_s$ , and total wing area,  $S$ , may be written as

$$C_{L,S} = \frac{L}{q_s S}$$

or

$$C_{L,S} = C_{L,T} + C_{L,NF} + C_{L,W} + \Delta C_{L,S} . \quad (3.10)$$

Where the coefficients representing the individual factors contributing to lift are:

##### 1. Propeller thrust contribution, $C_{L,T}$

$$C_{L,T} = N \left( \frac{T \sin \alpha_T}{q_s S} \right) \quad (3.11)$$

##### 2. Propeller Normal Force Contribution, $C_{L,NF}$

$$C_{L,NF} = \frac{N}{q_s S} \left( \frac{\rho}{4} \right) (C_d - c_b b) \Omega R^2 V_o \sin \alpha_T \cos \alpha_T \quad (3.12)$$

This equation is derived from Reference 11.

### 3. Basic Wing Contribution, $C_{L,W}$

The basic wing lift coefficient is given by Equation (3.3). There follows

$$C_{L,W} = \frac{q}{q_s} \left[ \frac{a_o AR \alpha}{AR \sqrt{1 + \left(\frac{a_o}{\pi AR}\right)^2} + \frac{a_o}{\pi}} \right] \quad (3.13)$$

where the effective wing angle of attack

$$\alpha = \alpha_W - \alpha_{LO} + \delta_f \left[ 1 - \frac{2\theta_h}{a} + \frac{2\sin\theta_h}{a} \right] \quad (3.14)$$

and where  $\theta_h$  is derived from Reference 10 as

$$\theta_h = 1 - 2 \cos \left\{ \tan^{-1} \left[ \frac{\sin \delta_f}{\frac{c}{c_f} - 1 \cdot \cos \delta_f} \right] \right\} \left[ 1 - \frac{c_f}{c} \right]. \quad (3.15)$$

### 4. Additional Contribution of Wing Area Exposed to Slipstream, $\Delta C_{L,S}$

Equation (2.36) gives the jet contribution to the wing lift coefficient based on  $q_o$  and  $S$ . Based on the slipstream dynamic pressure and on  $S$ , this contribution becomes

$$\Delta C_{L,S} = \frac{S_s}{S} \cos(\alpha_T - \phi) 1.87 \alpha_s \left( \frac{r_o}{c} \right) (1 - \mu^2). \quad (3.16)$$

Substituting the various lift coefficient contributions into Equation (3.10), there results

$$C_{L,S} = \frac{N T \sin \alpha_T}{q_s S} + \frac{N}{q_s S} \frac{\rho}{4} C_d c_b b \Omega R^2 V \sin \alpha_T \cos \alpha_T + \frac{q}{q_s} \left[ \frac{a_o AR \alpha}{AR \sqrt{1 + \left(\frac{a_o}{\pi AR}\right)^2} + \frac{a_o}{\pi}} \right] + \frac{S_s}{S} \cos(\alpha_T - \phi) 1.87 \alpha_s \frac{r_o}{c} (1 - \mu^2) \quad (3.17)$$

where for the general case of the propeller axis inclined to the free-stream velocity,

$$\mu = \frac{V_o \cos(\alpha_T - \phi)}{V_j} \quad (3.17a)$$

Based on the free-stream dynamic pressure,  $q$ , and the wing area,  $S$ , the lift equation becomes

$$C_L = \frac{L}{qS} = \frac{N T \sin \alpha_T}{qS} + \frac{N}{qS} \frac{\rho}{4} C_{dc} b \Omega R^2 V \sin \alpha_T \cos \alpha_T + \quad (3.18)$$

$$\frac{a_o}{AR} \frac{AR \alpha}{\sqrt{1 + \left(\frac{a_o}{\pi AR}\right)^2} + \frac{a_o}{\pi}} + \frac{S_s}{S} \frac{q_s}{q} \cos(\alpha_T - \phi) 1.87 \alpha_s \frac{r_o(1 - \mu^2)}{c}.$$

### C. TOTAL LONGITUDINAL FORCE COEFFICIENT, $C_{X,S}$

The longitudinal force coefficient,  $C_{X,S}$  is obtained by dividing the longitudinal component of the resultant forces,  $F_x$ , by  $q_s$  and  $S$ .

$$C_{X,S} = \frac{F_x}{q_s S} \quad (3.19)$$

$$= C_{X,T} - C_{X,NF} - C_{X,N} - C_{X,W} - \Delta C_{X,S}$$

The various contributions to  $C_{X,S}$  are as follows:

#### 1. Propeller Thrust Contribution, $C_{X,T}$

$$C_{X,T} = \frac{N T \cos \alpha_T}{q_s S} \quad (3.20)$$

#### 2. Propeller Normal Force Contribution, $C_{X,NF}$

$$C_{X,NF} = \frac{N}{q_s S} \frac{\rho}{4} C_{dc} b \Omega R^2 V_o \sin^2 \alpha_T \quad (3.21)$$

3. Nacelle Profile Drag Contribution,  $C_{X,N}$

$$C_{X,N} = \frac{D_N N}{q_s S} \cdot \cos(\alpha_T - \phi) \quad (3.22)$$

where  $D_N = C_{DN} q_s l d_N$

4. Contribution of Wing Outside of Slipstream,  $C_{X,W}$

$$C_{X,W} = \left[ \frac{(S-S_s)}{S} \cdot C_{D0} + \frac{(a\alpha)^2}{\pi AR} \right] \cdot \frac{q}{q_s} \quad (3.23)$$

where  $a = \frac{a_o AR \alpha}{AR \sqrt{1 + \left(\frac{a_o}{\pi AR}\right)^2} + \frac{a_o}{\pi}}$

5. Contribution of Wing Inside of Slipstream,  $\Delta C_{X,S}$

$$\Delta C_{X,S} = N \frac{S_s}{S} C_{D0} + \left\{ \left[ 1.87 \alpha_s \frac{r_o}{c} (1 - \mu^2) \right]^2 \frac{N}{\pi AR} \right\} \cos(\alpha_T - \phi) + \left[ 1.87 \alpha_s \frac{r_o}{c} (1 - \mu^2) \right] \frac{S_s}{S} \sin(\alpha_T - \phi) \quad (3.24)$$

The longitudinal force coefficient based on  $q_s$  is thus

$$C_{X,S} = N \frac{T \cos \alpha_T}{q_s S} - \frac{N}{q_s S} \frac{\rho}{4} C_{dcb} b \Omega R^2 V_o \sin^2 \alpha_T -$$

$$\frac{N D_N}{q_s S} \cos(\alpha_T - \phi) - \left[ \frac{(S-S_s)}{S} C_{D0} + \frac{(a\alpha)^2}{\pi AR} \right] \frac{q}{q_s} -$$

$$\frac{N S_s}{S} C_{DO} - \left[ 1.87 \alpha_s \left( \frac{r_o}{c} \right) (1 - \mu^2) \right]^2 \cdot \frac{N}{\pi AR} \cos(\alpha_T - \phi) - 1.87 \alpha_s \left( \frac{r_o}{c} \right) (1 - \mu^2) \frac{S}{S_s} \sin(\alpha_T - \phi) . \quad (3.25)$$

#### D. SAMPLE CALCULATION

The following is a sample calculation for wing-propeller configuration B shown in Figure 4, Section V. Test data for this configuration from Reference 12 are shown on Figures 14 and 15 of this report. The following data are assumed to be known:

##### Performance Data

$$\begin{aligned} C_{T,S} &= .88 \\ V_o &= 28.25 \text{ fps} \\ q &= .95 \text{ psf} \\ \alpha_w &= 20^\circ \\ \delta_f &= 0^\circ \end{aligned}$$

##### Wing Characteristics

$$\begin{aligned} S &= 5.0 \text{ ft}^2 & \alpha_{L0} &= 0^\circ \\ i_w &= 0^\circ & a_o &= 0.097/\text{deg.} \quad 5.55/\text{rad.} \\ AR &= 5.0 & c &= 1.0 \text{ ft.} \end{aligned}$$

Airfoil section NACA 0015

##### Nacelle Characteristics

$$\begin{aligned} l &= 0.93 \text{ ft.} \\ d_N &= 0.33 \text{ ft.} \end{aligned}$$



### Propeller Characteristics

$$N = 2$$

$$b = 3$$

$$D = 2.0 \text{ ft.}$$

$$c_b = 0.14 \text{ ft.}$$

$$\Omega = 555 \text{ rad/sec}$$

$$C_d = 0.02 \text{ for } \beta_{.75R} = 8^\circ$$

#### 1. Calculation of Slipstream Parameters

a. Propeller thrust is

$$\begin{aligned} T &= C_{T,S} q_s \frac{\pi D^2}{4} \\ &= (.88) (8.0) \frac{\pi}{4} (2)^2 \\ &= 22.12 \text{ lb.} \end{aligned}$$

b. Using Equation (3.7), the slipstream resultant velocity,  $V_j$ , is found as

$$\begin{aligned} V_j &= \sqrt{V_o^2 + \frac{T}{\frac{\rho}{2} \left( \frac{\pi D^2}{4} \right)}} \\ &= \sqrt{(28.25)^2 + \frac{22.12}{\frac{\rho}{2} \left( \frac{\pi 4}{4} \right)}} \\ &= 82 \text{ ft/sec} \end{aligned}$$

c. Next using Equation (3.8), the slipstream dynamic pressure,  $q_s$ , is calculated as

$$\begin{aligned} q_s &= \frac{1}{2} \rho V_j^2 \\ &= \frac{1}{2} \rho (82)^2 \\ &= 8.0 \text{ psf} \end{aligned}$$

d. The slipstream induced velocity,  $U$ , is

$$\begin{aligned}
 U &= -V_o \cos \alpha_T + \sqrt{(V_o \cos \alpha_T)^2 + \frac{T}{\frac{\rho}{2} \left( \frac{\pi D^2}{4} \right)}} \\
 &= -28.25 (\cos 20^\circ) + \sqrt{(28.25 \cos 20^\circ)^2 + \frac{22.1}{\frac{\rho}{2} \left( \frac{\pi 4}{4} \right)}} \\
 &= 54.7 \text{ ft/sec} .
 \end{aligned}$$

e. The radius of fully developed slipstream,  $r_o$ , is

$$\begin{aligned}
 r_o &= \frac{D}{2} \sqrt{\frac{1}{2} \left( \frac{2V_o \cos \alpha_T + U}{V_o \cos \alpha_T + U} \right)} \\
 &= \frac{2}{2} \sqrt{\frac{1}{2} \left( \frac{2(28.25)(.936) + 54.7}{28.25 (.936) + 54.7} \right)} \\
 &= 0.815 \text{ ft} .
 \end{aligned}$$

f. The effective angle of attack of the wing out of the slipstream,  $\alpha$ , is

$$\alpha = \alpha_W - \alpha_{LO} + \delta_f \left[ 1 - \frac{2\theta_h}{a} + \frac{2 \sin \theta_h}{a} \right]$$

since  $\alpha_{LO} = 0^\circ$  and  $\delta_f = 0^\circ$

$$\alpha = \alpha_W = 20^\circ = 0.349 \text{ radians} .$$

g. The lift curve slope is

$$a = \frac{a_o AR}{AR \sqrt{1 + \left( \frac{a_o}{\pi AR} \right)^2} + \frac{a_o}{\pi}} = \frac{(5) (5.55)}{5 \sqrt{1 + \left( \frac{5.55}{\pi 5} \right)^2} + \frac{5.55}{\pi}} = 3.93/\text{rad}$$

h. The angle of attack in slipstream,  $\alpha_s$ , is

$$\begin{aligned}\alpha_s &= i_w + \phi - \alpha_{LO} + \delta_f \\ &= 0 + \tan^{-1}\left(\frac{28.25 (.341)}{28.25(.936)+54.7}\right) - 0 + 0 \\ &= 6.75^\circ = .118 \text{ rad.}\end{aligned}$$

i. The velocity parameter,  $\mu$ , is

$$\begin{aligned}\mu &= \frac{V_o \cos(\alpha_T - \phi)}{V_j} \\ &= \frac{28.25 \cos(20^\circ - 6.75^\circ)}{82} \\ &= 0.334\end{aligned}$$

## 2. Calculation of lift Coefficient, $C_{L,S}$

a. Propeller thrust contribution,  $C_{L,T}$

$$\begin{aligned}C_{L,T} &= \frac{N T \sin \alpha_T}{q_s S} = \frac{2(22.12) (.341)}{8 (5)} \\ &= 0.377\end{aligned}$$

b. Propeller normal force,  $C_{L,NF}$

$$\begin{aligned}C_{L,NF} &= \frac{N}{q_s S} \frac{\rho}{4} C_{dcbb} \Omega R^2 V_o \sin \alpha_T \cos \alpha_T \\ &= \frac{2}{(8)5.0} \frac{\rho}{4} (.02) (.14) 3(555)(1.0)^2 (28.25)(.341)(.936) \\ &= 0.0012\end{aligned}$$

c. Basic wing contribution,  $C_{L,W}$

$$C_{L,W} = \frac{q}{q_s} a \alpha$$

$$= \frac{.95}{8} (3.93) (.349)$$

$$= 0.161$$

$$\text{or } C_{L,W} = \frac{q}{q_s} (C_L)_{T=0}$$

where the lift coefficient of the basic wing based on  $q$  at zero thrust,  $(C_L)_{T=0}$ , is obtained from test data.

d. Additional contribution of wing area exposed to slipstream,  $\Delta C_{L,S}$

$$\Delta C_{L,S} = 1.87 \alpha \frac{r_o}{s_c} (1 - \mu^2) \frac{S_s}{S} \cos(\alpha_T - \phi)$$

$$\text{where } S_s = N (2r_o c) = 2(2(.815)1.0) = 3.26 \text{ ft}^2$$

$$\begin{aligned} \Delta C_{L,S} &= 1.87(.118) \frac{.815}{1.0} (1 - .334^2) \frac{3.26}{5} \cos(20^\circ - 6.75^\circ) \\ &= 0.1012 \end{aligned}$$

e. Summation of Lift Contributions

$$\begin{aligned} C_{L,S} &= C_{L,T} + C_{L,NF} + C_{L,W} + \Delta C_{L,S} \\ &= 0.377 + 0.0012 + 0.161 + 0.1012 \\ &= 0.6404 \end{aligned}$$

This calculated value agrees well with the experimental data (Figure 8, Section V) which indicates that  $C_{L,S} = 0.67$ .

### 3. Calculation of Longitudinal Force Coefficient, $C_{X,S}$

a. Propeller thrust contribution,  $C_{X,T}$

$$C_{X,T} = \frac{N T \cos \alpha_T}{q_s S} = \frac{2(22.12)(.936)}{5(8.0)} = 1.039$$

- b. Propeller normal force contribution,  $C_{X,NF}$

$$C_{X,NF} = \frac{N}{q_s S} \frac{\rho}{4} C_d c_b b \Omega R^2 V_o \sin^2 \alpha_T$$

$$= \frac{2}{8.0(5)} \frac{\rho}{4} (.02)(.14) 3 (555)(1.0)^2 (28.25)(.341)^2$$

$$= .00044$$

- c. Nacelle profile drag contribution,  $C_{X,N}$

$$C_{X,N} = N \frac{D_N}{q_s S} \cos(\alpha_T - \phi)$$

$$= 2 \frac{.172}{8(5)} \cos(20^\circ - 6.75^\circ)$$

$$= .00836$$

where the nacelle drag ( $D_N = C_{DN} q_s l_{DN}$ ) is estimated to be 0.172 pounds using a drag coefficient of 0.07 from Reference 13.

- d. Contribution of the wing outside the slipstream,  $C_{X,W}$

$$C_{X,W} = \left[ \frac{(S - S_s)}{S} C_{D0} + \frac{(a\alpha)^2}{\pi AR} \right] \frac{q}{q_s}$$

$$= \left[ \frac{(5 - 3.26)}{5} (.15) + \frac{[(3.93)(.349)]^2}{\pi 5} \right] = 0.0202$$

where the profile drag coefficient,  $C_{D0}$ , of the wing out of the slipstream is 0.15 from test data, Reference 12.

- e. Contribution of wing inside of slipstream,  $\Delta C_{X,S}$

$$\Delta C_{X,S} = \frac{S_s}{S} C_{D0} + \left[ 1.87 \alpha_s \frac{r_o}{c} (1 - \mu^2) \right]^2 \frac{N}{\pi AR} \cos(\alpha_T - \phi) +$$

$$\left[ 1.87 \alpha_s \frac{r_o}{c} (1 - \mu^2) \right] \frac{S_s}{S} \sin(\alpha_T - \phi)$$

$$= \frac{3.26}{5} (.02) + \left[ 1.87 (.118) \frac{.815}{1.0} (1 - .334^2) \right]^2 \frac{2}{\pi 5} \cos(20^\circ - 6.75^\circ) +$$

$$\left[ 1.87 (.118) \frac{.815}{1.0} (1 - .334^2) \right] \frac{3.26}{5} \sin(20^\circ - 6.75^\circ)$$

$$= 0.0398$$

where the profile drag coefficient,  $C_{D0}$ , in the slipstream is .02 from test data, Reference 12.

f. Summation of longitudinal force contributions

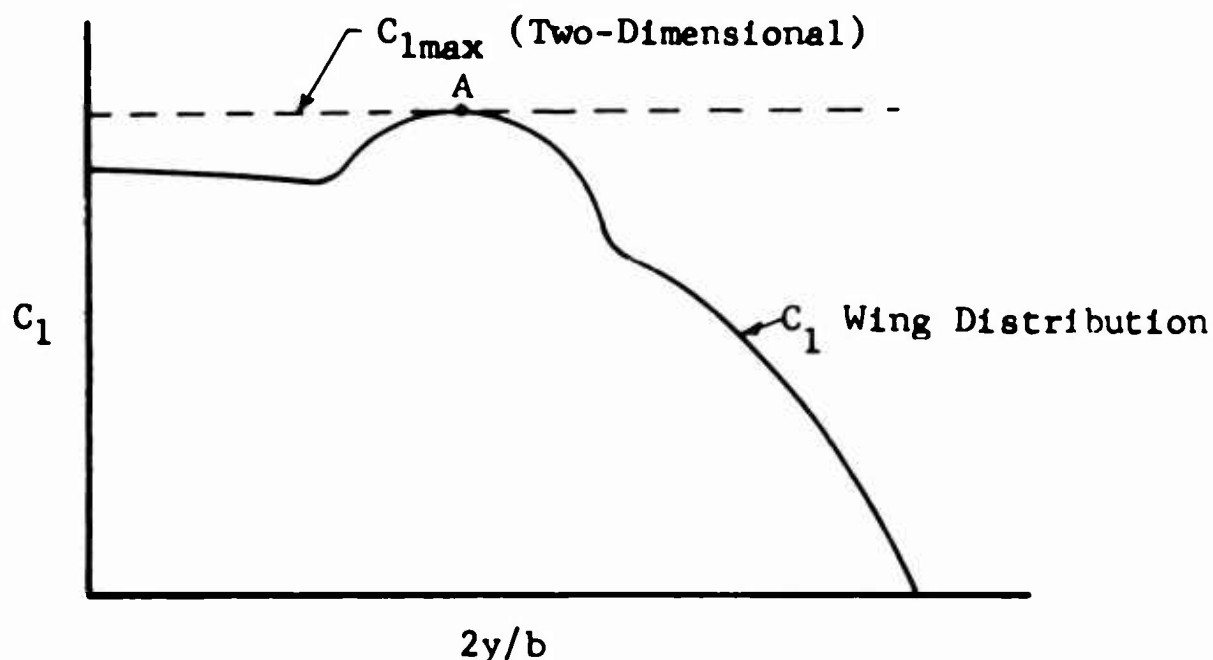
$$\begin{aligned}C_{X,S} &= C_{X,T} - C_{X,NF} - C_{X,N} - C_{X,W} - C_{X,S} \\&= 1.039 - .00044 - .00836 - .0202 - .0398 \\&= 0.9702\end{aligned}$$

Test data of Reference 12, shown in Figure 12 of this report, indicates the  $C_{X,S} = 0.96$

#### IV. ADDITIONAL SLIPSTREAM CONSIDERATIONS

##### A. STALL CHARACTERISTICS

It is generally recognized that a wing will stall first at or near the spanwise location where the section lift coefficient reaches its local (two-dimensional) maximum lift coefficient. Thus in the sketch below, stalling will start at a point "A" where the curves of  $C_l$  and  $C_{lmax}$  vs. span location are tangent.



The methods presented in the previous sections may be used to compute the stall conditions as affected by various parameters such as wing aspect ratio, twist, flap deflection, taper ratio, propeller thrust, propeller diameter, and angle of attack as well as other wing and propeller characteristics.

Considering a wing partially immersed in the propeller slipstream, there appear to be three critical spanwise stall locations. For a wing which has a constant geometric angle of attack, chord, and airfoil section, these critical stations for stall during transition are as follows:

1. In most cases, the wing root section which is outside of the slipstream would stall first. The maximum lift coefficient achieved by the root section at stall is equivalent to Section  $C_{l \max}$ , which may be expressed as

$$C_{l \max} = 4 AR \left( \frac{a_0}{\pi} \right) \left[ \frac{\alpha_{\text{stall}}}{AR \sqrt{1 + \left( \frac{a_0}{\pi AR} \right)^2} + \frac{a_0}{\pi}} \right]. \quad (4.1)$$

Thus, having the  $C_{l \max}$  of the airfoil section, the angle of attack at which stall would start,  $\alpha_{\text{stall}}$ , may be determined as a function of wing geometry and the two-dimensional lift curve slope,  $a_0$ .

2. The next critical station would be in the center of the slipstream. The lift coefficient at the center of the slipstream is

$$C_{l \max} = \frac{8 \alpha_{\text{stall}}}{\pi} \left( \frac{r_0}{c} \right) (1 + \mu^2). \quad (4.2)$$

Having the  $C_{l \max}$  of the airfoil section, the angle of attack at which stall would start,  $\alpha_{\text{stall}}$ , may be ascertained.

3. Another possible critical stall station could be close to the slipstream boundary where the effect of slipstream rotation is a maximum. The attainment of such a stall is, of course, highly dependent on the propeller torque and rotational speed.

The theory presented herein furnishes considerable insight into the requirements that must be met in order to avoid wing stall in the transition flight regime of tilt-wing aircraft. For the case of a wing fully immersed in the propeller slipstream, the maximum effective angle of attack is to a large extent dependent on the thrust coefficient and slipstream rotation. An increase in propeller thrust coefficient and a decrease in torque coefficient increases the allowable remote free-stream angle of attack before stall is incurred. It can be stated



that it is possible to perform the transition without encountering wing stall only if the proper balance of allowable effective angle of attack, remote free-stream angle of attack, and propeller disc loading is provided. During the landing, transition, and descent at low speeds, this is difficult to attain. The reduction of power for deceleration and let-down increases the effective angle of attack.

Obvious methods that tend to delay stall are the use of

- (1) leading edge devices to increase the allowable  $C_{l \max}$ .
- (2) increased power requirement through increased drag; aerodynamic drag devices must be utilized in the slipstream, as outside the slipstream they are ineffective at the low critical speeds.
- (3) increased wing area and high lift flaps; effectively, flaps turn the thrust vector toward the vertical through deflection of the slipstream while producing a very high drag increment which aids the stall problem as discussed in (2) above and thus decelerates the aircraft more rapidly during the landing transition. Thus the optimum use of flaps would reduce the speed for transition, and result in lower take-off and landing speeds.

## B. SLOW SPEED CHARACTERISTICS

The minimum flying speed is given by the classical expression

$$V_{\min} = \sqrt{\frac{W}{\frac{\rho}{2} C_{L\max} S}} \quad (4.3)$$

where  $C_{L \max}$  is based on the free-stream dynamic pressure,  $q$ , and the wing area,  $S$ .

The lift coefficient,  $C_{L \max}$ , is obtained by maximizing Equation (3.18). In the maximization process consideration must be given to the stalling of the wing as discussed in Section IV. A. The speed  $V_{\min}$  is the minimum flying speed before the onset of appreciable stall. Depending on the design,

it is possible to have a portion of the wing outside the slipstream in a stalled condition without detrimental effects. This is due to the fact that at very slow speeds for designs such as discussed in Section V, the majority of the lift is carried by the propellers and wing sections immersed in the slipstream. Thus maximum  $C_L$  may not be achieved until partial wing stall occurs. Of course, when the wing sections in the slipstream stall, serious effects on the performance and handling qualities can occur. For most practical tilt-wing designs, it would appear that stall on the wing outside the slipstream can be tolerated, but stall of the wing within the high-energy slipstream would be the limiting condition.

#### C. STOL TAKE-OFF AND LANDING

The analysis of STOL take-off and landing performance is presented in the Appendix. The analysis utilizes the methods discussed in References 14 and 15 along with the lift and longitudinal forces developed in Section III. The influence of the ground proximity on STOL performance is also discussed in the Appendix.

The take-off and landing performance was calculated for a typical STOL aircraft (Grumman OV-1 Mohawk) using the analysis presented in the Appendix. The results of the calculations are discussed in Section V.

#### D. OPTIMUM DESIGN CONSIDERATIONS

Based on the results presented herein, certain design considerations may be deduced. For cruise flight, the ratio of free-stream to slipstream velocity approaches one and therefore conventional aerodynamic analysis applies, which suggests the use of large-aspect-ratio wings for minimum power. However, in the transition speed range, the theory presented in this report indicates that for optimum design the following factors must be considered:

- (1) The propeller slipstream is extremely effective in delaying the onset of wing stall.

Consequently, high-disc-loading propellers are desirable from this point of view. Naturally, the hovering flight power requirement must be considered in establishing the propeller disc loading, and therefore the designer may be limited in his choice of

disc loading.

- (2) A wing whose span is completely immersed in the slipstream is very desirable.
- (3) Increases in wing chord would serve to reduce the severity of the stall, and therefore large  $c/D$  ratios should be used.
- (4) It should be possible to modify or eliminate the spanwise peaks in  $C_l$  for any given flight condition to reduce stall by varying the planform or spanwise distribution of wing twist. To this extent, proper use of differential flap deflection and slats can prove to be extremely beneficial.

## V. CORRELATION OF THEORY WITH TEST DATA

In this section calculated values of lift and longitudinal force coefficient, stall angle of attack, and take-off and landing performance are correlated with test data. The range of wing and propeller parameters over which satisfactory correlation has been obtained is also presented.

### A. $C_{L,S}$ AND $C_{X,S}$ CORRELATION

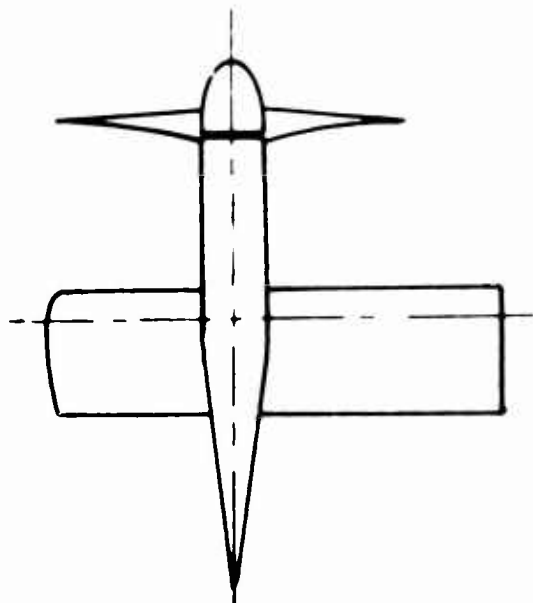
The test data of References 12, 16, and 17 are used to evaluate the degree of accuracy and range of  $C_{L,S}$  and  $C_{X,S}$  correlation possible using equations (3.17) and (3.25). All of these data are from model tests conducted by the National Aeronautics and Space Administration. Model data were selected due to the lack of adequate full scale data and because of the wide range of wing-propeller combinations tested. Correlation is shown in Figures 8 through 31 of this report.

Six configurations which are used for correlation are illustrated in Figures 4 through 7. In the following discussion they are referred to as configuration A, B, C, etc. For all tests a constant slipstream dynamic pressure of 8.0 pounds per square foot was maintained. Thrust coefficient,  $C_{T,S}$ , and tunnel free-stream dynamic pressure,  $q_0$ , were varied to obtain different values of  $\mu$ .

Values of parameters pertinent to the understanding of each plot of  $C_{L,S}$  or  $C_{X,S}$ , such as  $C_{T,S}$ ,  $V_0$ ,  $R_n$ , etc., are given on or in the title of each figure. Reynolds number,  $R_n$ , is based upon the slipstream velocity,  $V_j$ , and the average wing chord.

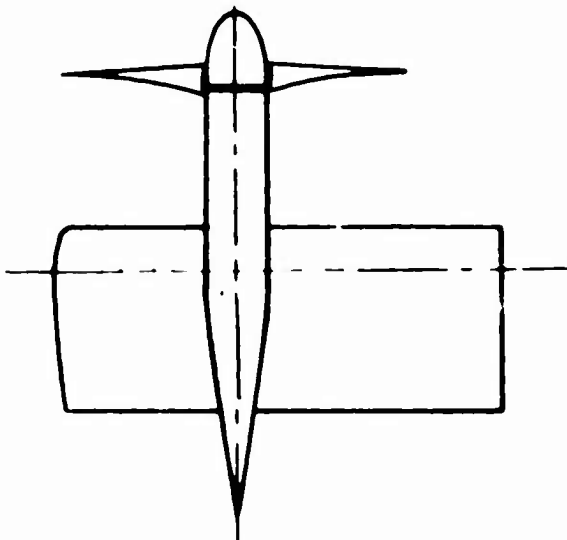
#### 1. Configurations A, B, and C (Reference 12)

By use of the data of Reference 12, the effects of variations in wing chord to propeller diameter ratio,  $c/D$ , on the accuracy of the analysis can be determined. Configurations A, B, and C have  $c/D$  values of 0.33, 0.50, and 0.75 respectively as shown in Figure 4. Data is presented for thrust coefficients,  $C_{T,S}$ , of 0.57, 0.58, 0.88, and 0.98. At high thrust ( $C_{T,S} = .98$ ), correlation is shown for the three  $c/D$  values in Figures 8, 9, and 10. At this thrust coefficient good agreement is obtained over the full range of angle of attack from 0 to 90 degrees. At a



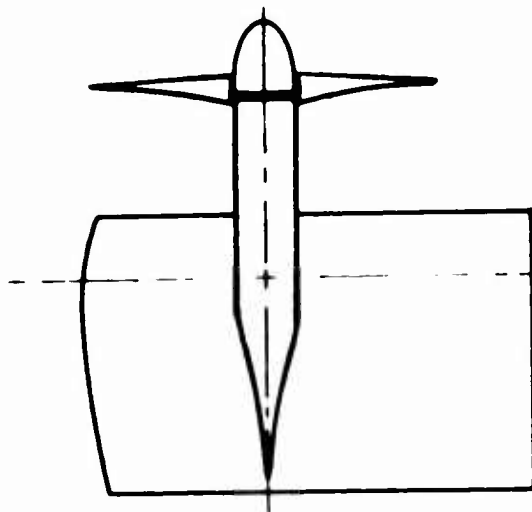
#### CONFIGURATION A

Aspect Ratio = 7.50  
 Area (Half Span) = 1.667 ft.<sup>2</sup>  
 Half Span = 2.50 ft.  
 Chord = 0.667 ft.  
 Propeller Dia = 2.0 ft.  
 Airfoil Section, 0015



#### CONFIGURATION B

Aspect Ratio = 5.00  
 Area (Half Span) = 2.500 ft.<sup>2</sup>  
 Half Span = 2.50 ft.  
 Chord = 1.00 ft.  
 Propeller Dia = 2.0 ft.  
 Airfoil Section, 0015



#### CONFIGURATION C

Aspect Ratio = 3.333  
 Area (Half Span) = 3.750 ft.<sup>2</sup>  
 Half Span = 2.50 ft.  
 Chord = 1.500 ft.  
 Propeller Dia = 2.0 ft.  
 Airfoil Section, 0015

FIGURE 4: MODEL CONFIGURATIONS A, B, AND C  
 GENERAL ARRANGEMENT DRAWING

CONFIGURATION D

Aspect Ratio	4.55	Average Chord	1.514 ft.
Area (Half Span)	5.12 ft. <sup>2</sup>	Propeller Dia	2 ft.
Half span	3.419 ft.		
Airfoil Section, 0015			

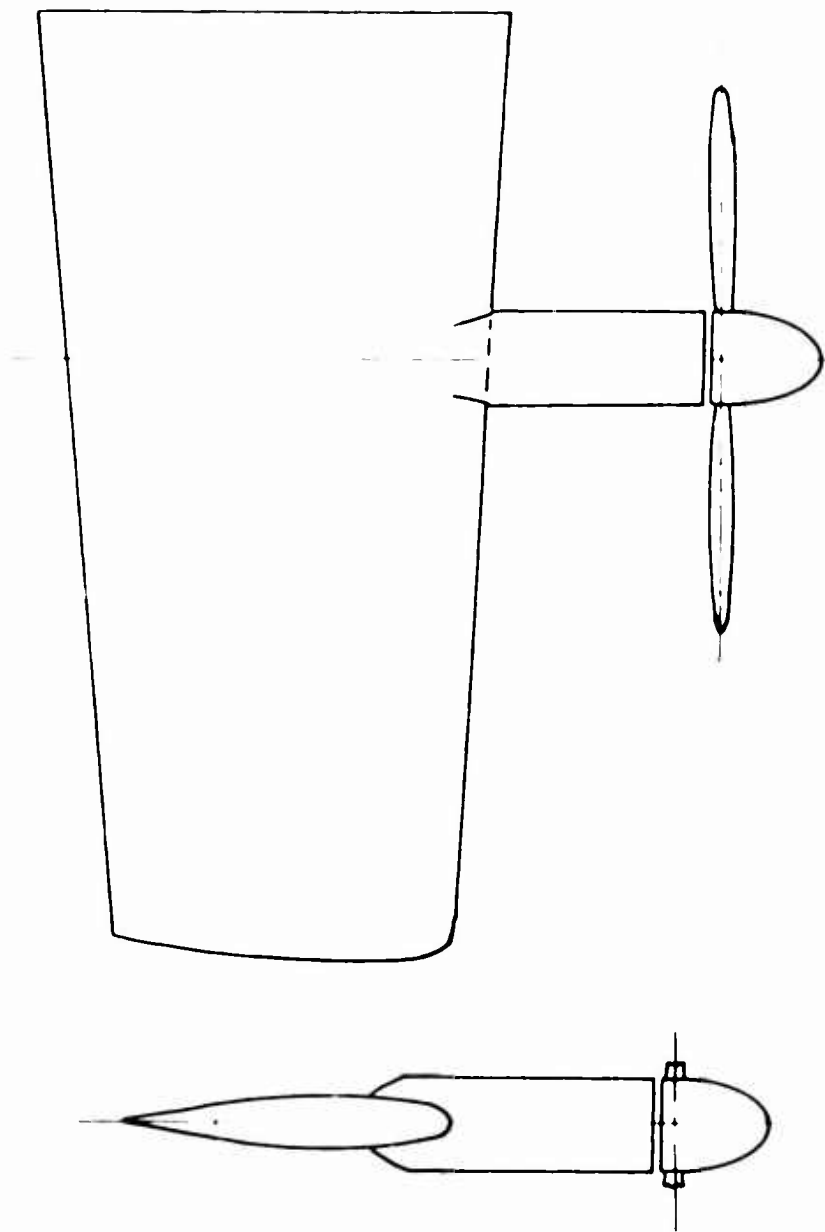
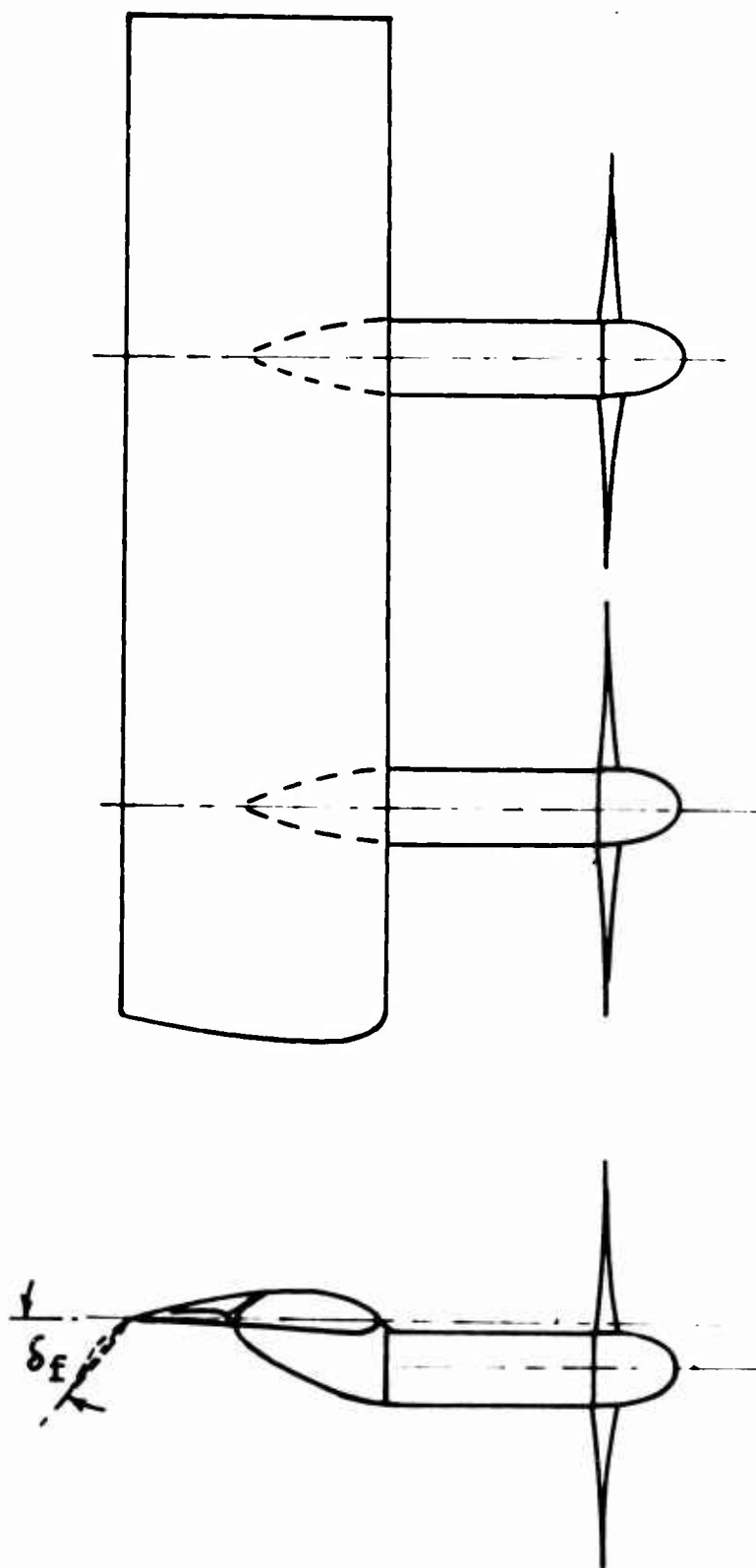


FIGURE 5: MODEL CONFIGURATION D  
GENERAL ARRANGEMENT DRAWING



# CONFIGURATION E

Aspect Ratio = 7.66  
 Area (Half Span) = 5.48 ft.<sup>2</sup>  
 Half Span = 4.58 ft.  
 Chord = 1.20 ft.  
 Propeller Dia = 2.00 ft.  
 Airfoil Section, 4415

FIGURE 6: MODEL CONFIGURATION E  
 GENERAL ARRANGEMENT DRAWING

### CONFIGURATION F

Aspect Ratio	= 4.55	Average Chord	= 1.514 ft.
Area (Half Span)	= 5.12 ft <sup>2</sup>	Propeller Dia	= 2.0 ft.
Half Span	= 3.416 ft.	Airfoil Section	, 0015

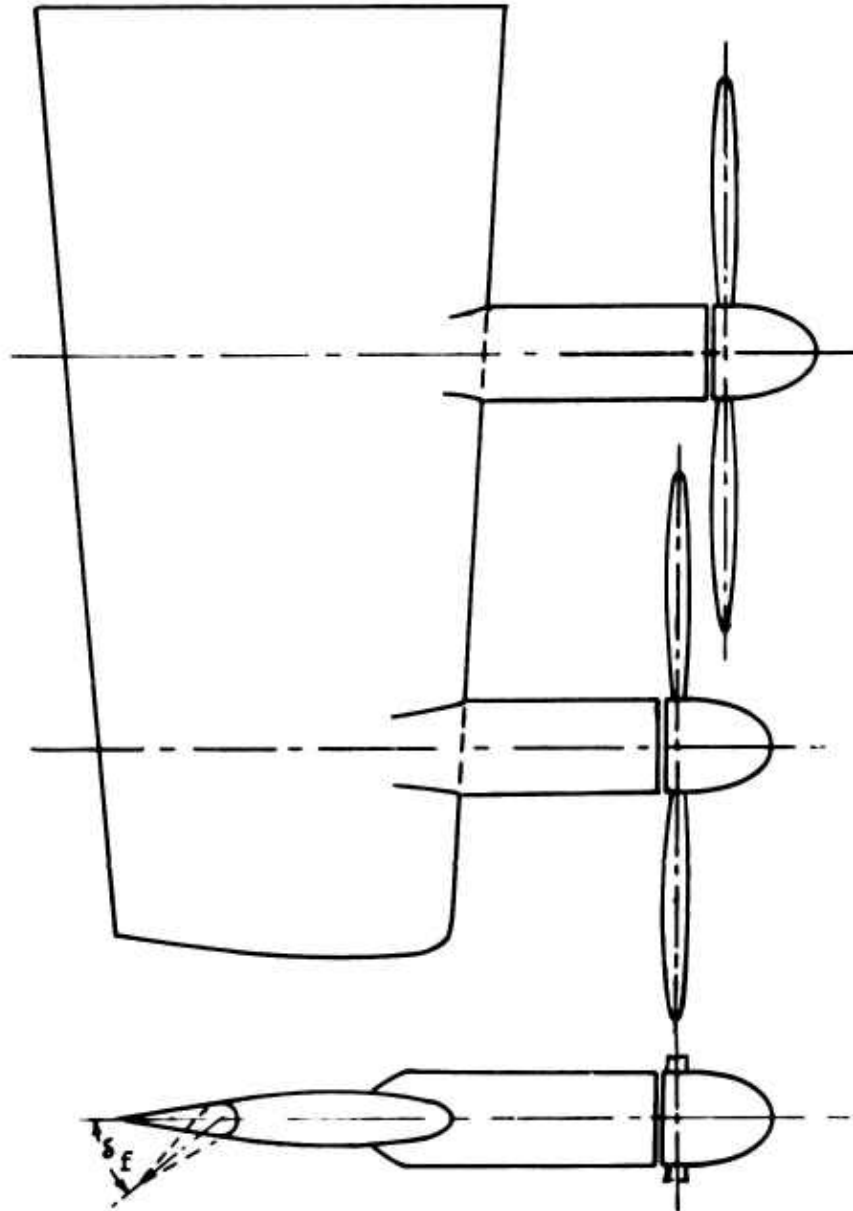


FIGURE 7: MODEL CONFIGURATION F  
GENERAL ARRANGEMENT DRAWING



$$c/D = 0.33 \quad V_o = 11.2 \text{ ft/sec}$$

$$i_w = 0^\circ \quad \frac{V_o}{V_j} = 0.137$$

$$N = 2 \quad R_n = 0.35 \times 10^6$$

⊙ TEST DATA REFERENCE 12

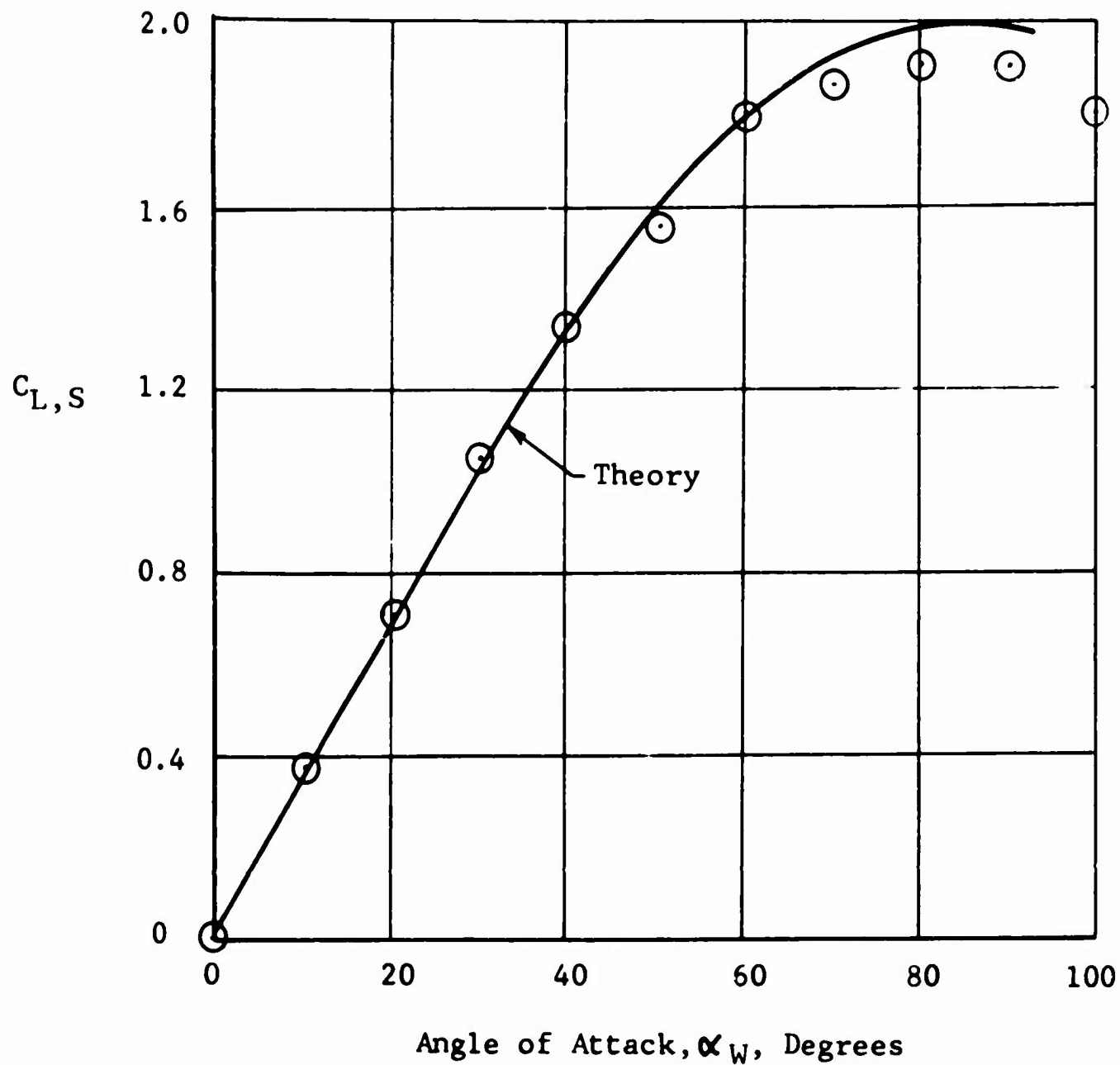


FIGURE 8: CORRELATION OF PREDICTED AND EXPERIMENTAL LIFT COEFFICIENTS, CONFIGURATION A,  $C_{T,S} = 0.98$  AND  $\delta_f = 0$  DEGREES

$c/D = 0.50$   $V_o = 11.2 \text{ ft/sec}$

$i_w = 0^\circ$   $\frac{V_o}{V_j} = 0.137$

$N = 2$   $R_n = 0.53 \times 10^6$

⊙ TEST DATA REFERENCE 12

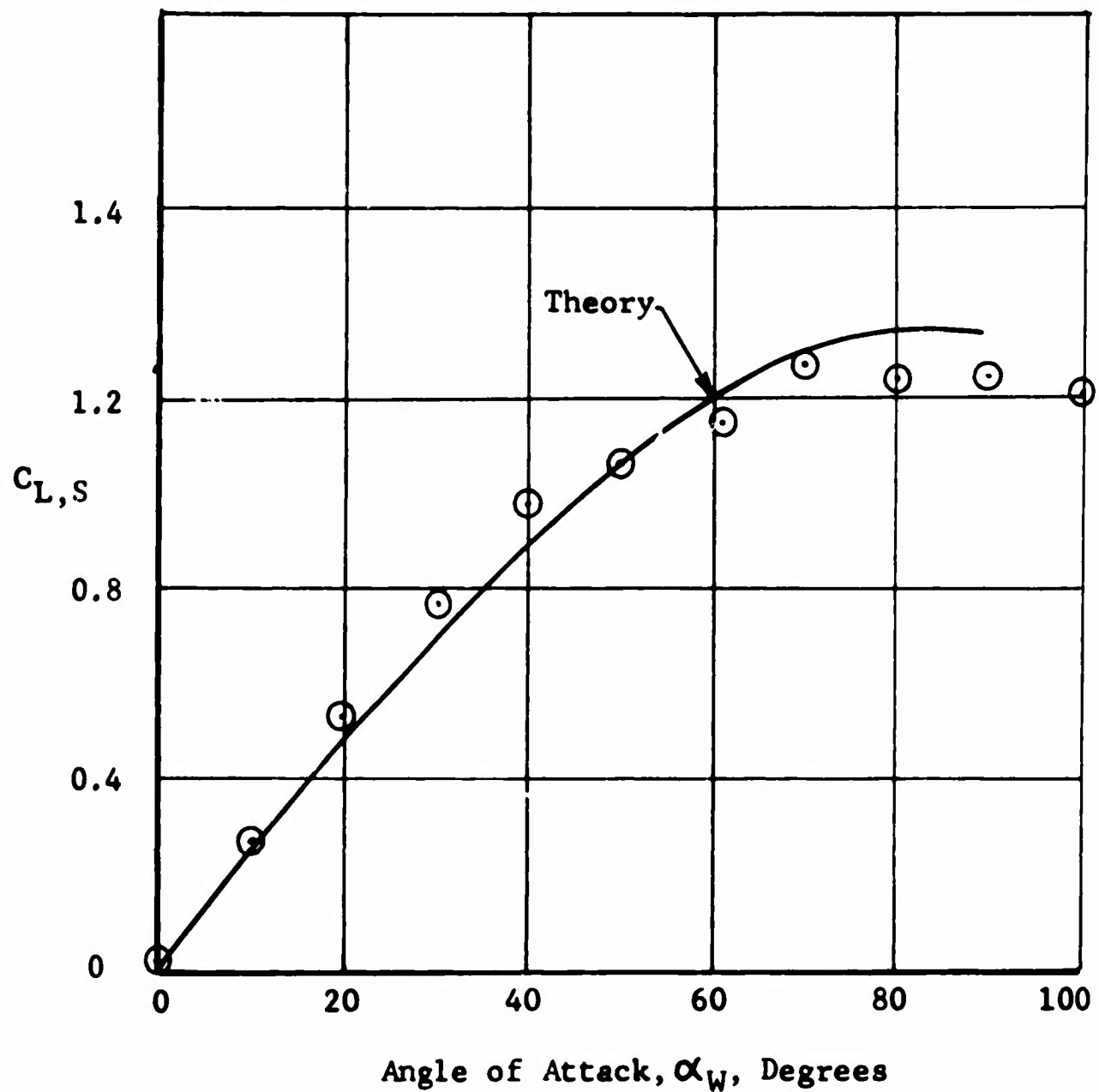


FIGURE 9: CORRELATION OF PREDICTED AND EXPERIMENTAL LIFT COEFFICIENTS, CONFIGURATION B,  $C_{T,S} = 0.98$  AND  $\delta_f = 0$  DEGREES

$$c/D = 0.75 \quad V_o = 11.2 \text{ ft/sec}$$

$$i_w = 0^\circ \quad \frac{V_o}{V_j} = 0.137$$

$$N = 2 \quad R_n = 0.79 \times 10^6$$

⊙ TEST DATA REFERENCE 12

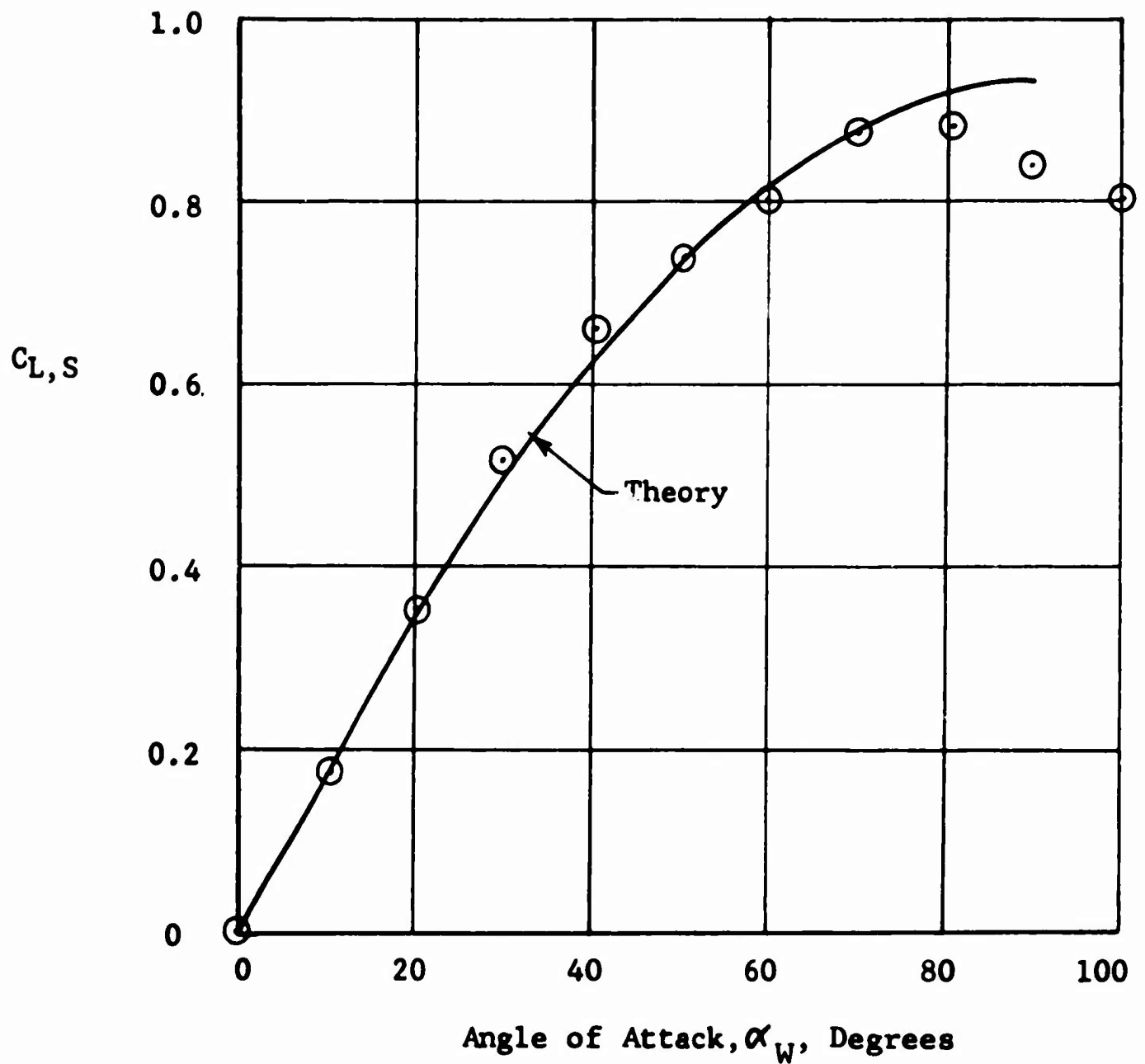


FIGURE 10: CORRELATION OF PREDICTED AND EXPERIMENTAL LIFT COEFFICIENTS CONFIGURATION C,  $C_{T,S} = 0.98$  AND  $\delta_f = 0$  DEGREES

lower value of thrust' ( $C_{T,S} = .58$  or  $.57$ ), as shown in Figures 11, 12, and 13, correlation is considered acceptable up to an angle of attack of approximately 20 degrees. The limited range of good correlation at the lower thrust coefficient can be attributed to the complete stalling of the wing outside of the slipstream combined with the onset of stall in the slipstream. The onset of stall being a consequence of the high effective angle of attack,  $\alpha_s$ , in the slipstream at low  $C_{T,S}$ . For example, using Equation (3.9) at  $\alpha_w = 30$  degrees and  $C_{T,S} = .58$ , the effective angle of attack in the slipstream,  $\alpha_s$ , is calculated to be 19 degrees. This compares with  $\alpha_s = 4$  degrees at  $\alpha_w = 30$  degrees and  $C_{T,S} = .98$ . The prediction of the onset of stall in the slipstream is discussed in detail in Section V B. Correlation for an intermediate value of thrust coefficient,  $C_{T,S} = .88$  is shown in Figure 14.

The above correlation indicates that the present theory gives good agreement with test data provided no stalling of the wing exists.

Longitudinal force correlation with Configuration B (for  $c/D = .5$ ) is shown in Figures 15 and 16. It is noted that agreement is obtained over a larger angle of attack range than was obtained for  $C_{L,S}$  at equivalent  $c/D$  ratios and thrust coefficients. This is due to the fact that the profile drag rise following stall is compensated for in the expression for longitudinal force (Equation(3.25)).

## 2. Configuration D (Reference 16)

The accuracy of the analysis may be further substantiated by correlating with data for the tapered wing configuration shown in Figure 5. This model has one propeller per semispan, a taper ratio of 0.71 and a  $c/D$  ratio of 0.76. Correlation is shown in Figures 17 and 18, and is comparable to that obtained with the straight wing configurations. The estimated values of  $C_{L,S}$  for the tapered wing are slightly lower than the test data in the lower  $\alpha_w$  range. Due to the limited data available it is not known if this is caused by wing taper or other effects.

## 3. Configuration E (Reference 17)

To determine the effects of propeller interaction, flap deflection, and airfoil camber on the accuracy of the analysis,

$$c/D = 0.33 \quad V_o = 53.7 \text{ ft/sec}$$

$$i_w = 0^\circ \quad \frac{V_o}{V_j} = 0.648$$

$$N = 2 \quad R_n = 0.35 \times 10^6$$

⊙ TEST DATA REFERENCE 12

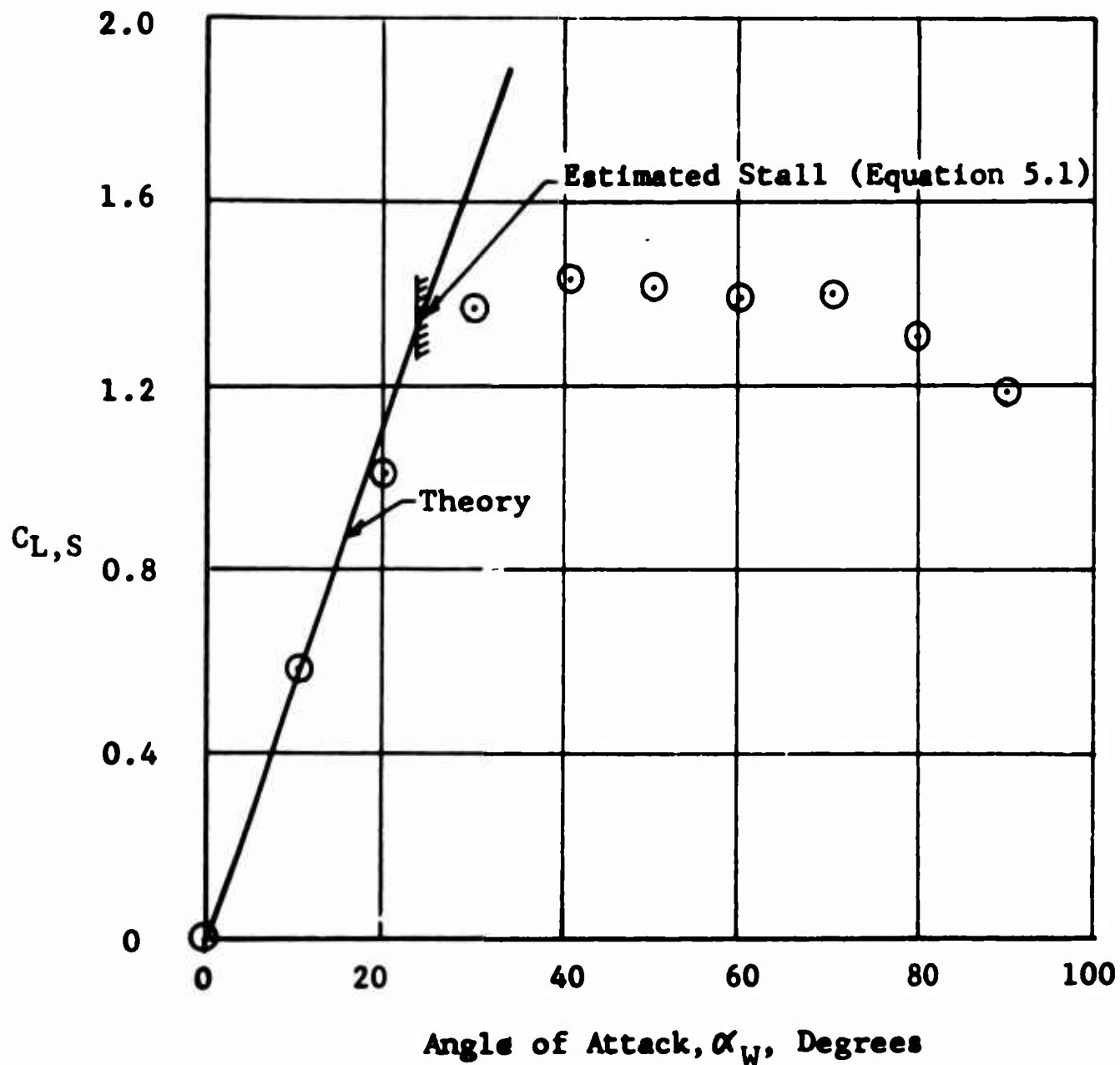


FIGURE 11: CORRELATION OF PREDICTED AND EXPERIMENTAL LIFT COEFFICIENTS, CONFIGURATION A,  $C_{T,S} = 0.58$  AND  $\delta_f = 0$  DEGREES

$$c/D = 0.50 \quad V_o = 53.1 \text{ ft/sec}$$

$$i_W = 0^\circ \quad \frac{V_o}{V_j} = 0.648$$

$$N = 2 \quad R_n = 0.53 \times 10^6$$

○ TEST DATA REFERENCE 12

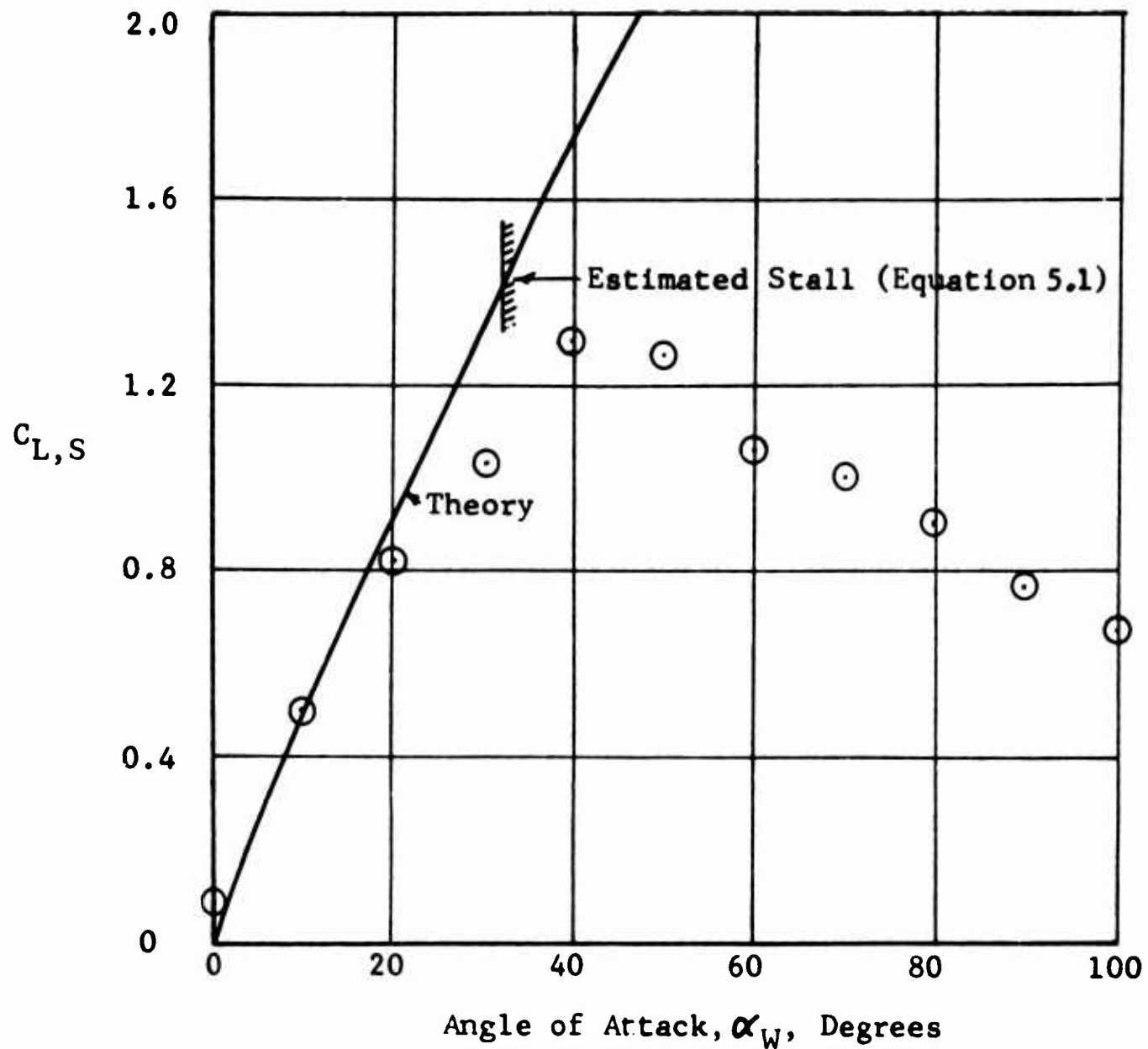


FIGURE 12: CORRELATION OF PREDICTED AND EXPERIMENTAL LIFT COEFFICIENTS, CONFIGURATION B,  $C_{T,S} = 0.58$  AND  $\delta_f = 0$  DEGREES

$$\begin{aligned}
 c/D &= 0.75 & V_o &= 53.7 \text{ ft/sec} \\
 i_W &= 0^\circ & \frac{V_o}{V_j} &= 0.655 \\
 N &= 2 & R_n &= 0.79 \times 10^6
 \end{aligned}$$

○ TEST DATA REFERENCE 12

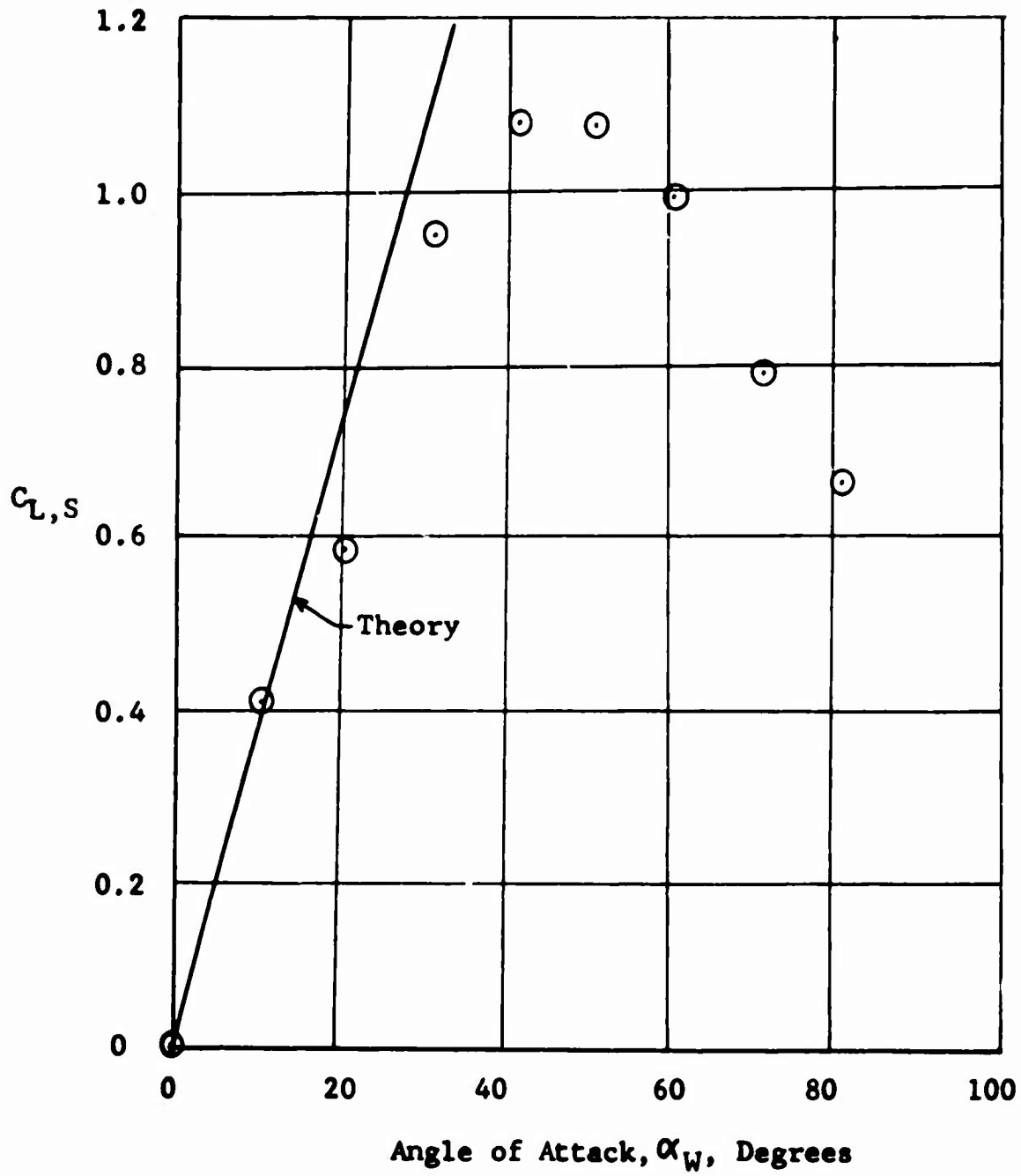


FIGURE 13: CORRELATION OF PREDICTED AND EXPERIMENTAL LIFT COEFFICIENTS, CONFIGURATION C,  $C_{T,S} = 0.57$  AND  $\delta_f = 0$  DEGREES

$$c/D = 0.50 \quad V_o = 28.25 \text{ ft/sec}$$

$$i_W = 0^\circ \quad \frac{V_o}{V_j} = 0.344$$

$$N = 2 \quad R_n = 0.53 \times 10^6$$

⊙ TEST DATA REFERENCE 12

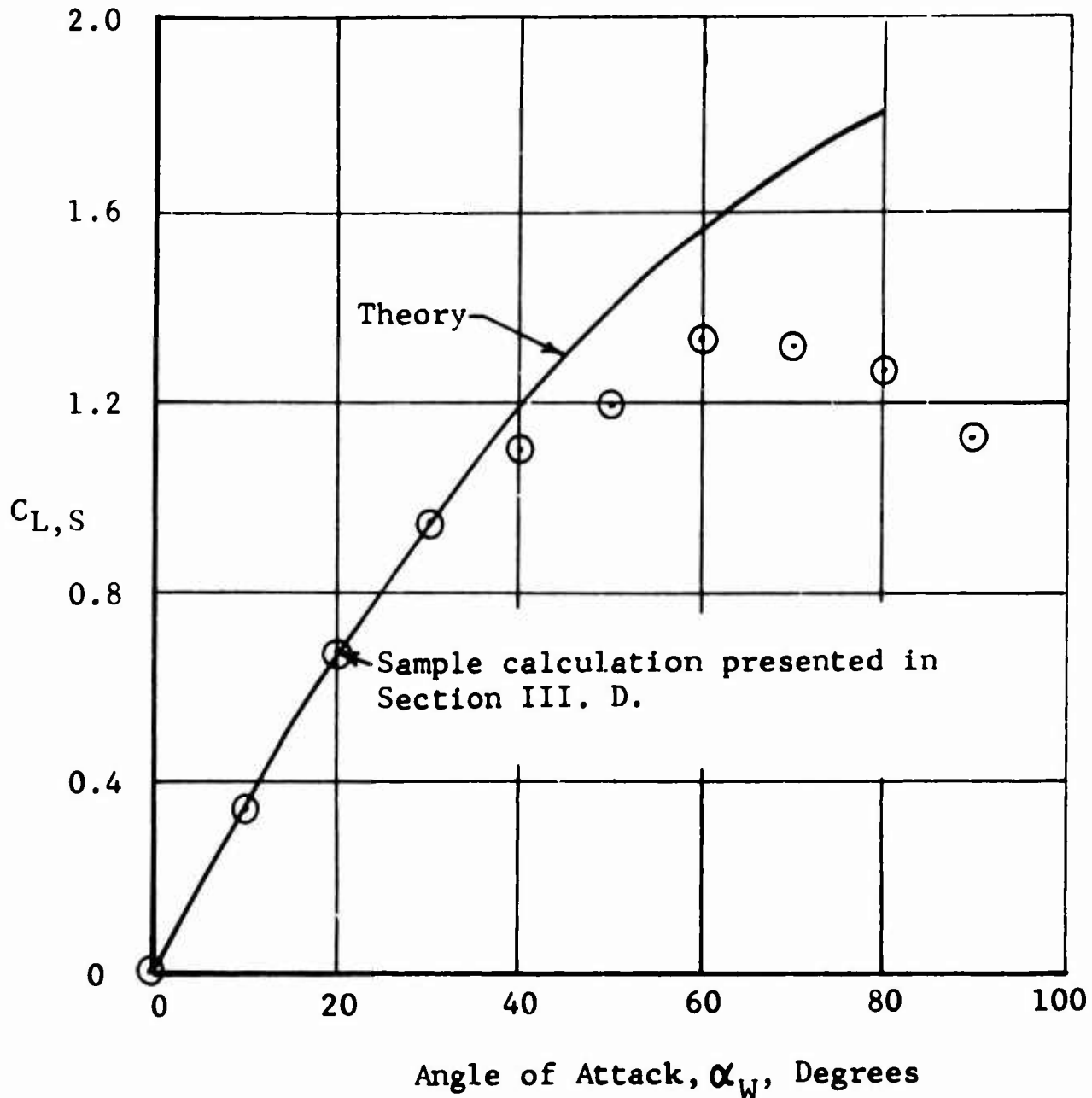


FIGURE 14: CORRELATION OF PREDICTED AND EXPERIMENTAL LIFT COEFFICIENTS, CONFIGURATION B,  $C_{T,S} = 0.88$ , AND  $\delta_f = 0$  DEGREES



$$c/D = 0.50 \quad V_o = 28.25 \text{ ft/sec}$$

$$i_w = 0^\circ \quad \frac{V_o}{V_j} = 0.344$$

$$N = 2 \quad R_n = 0.53 \times 10^6$$

△ TEST DATA REFERENCE 12

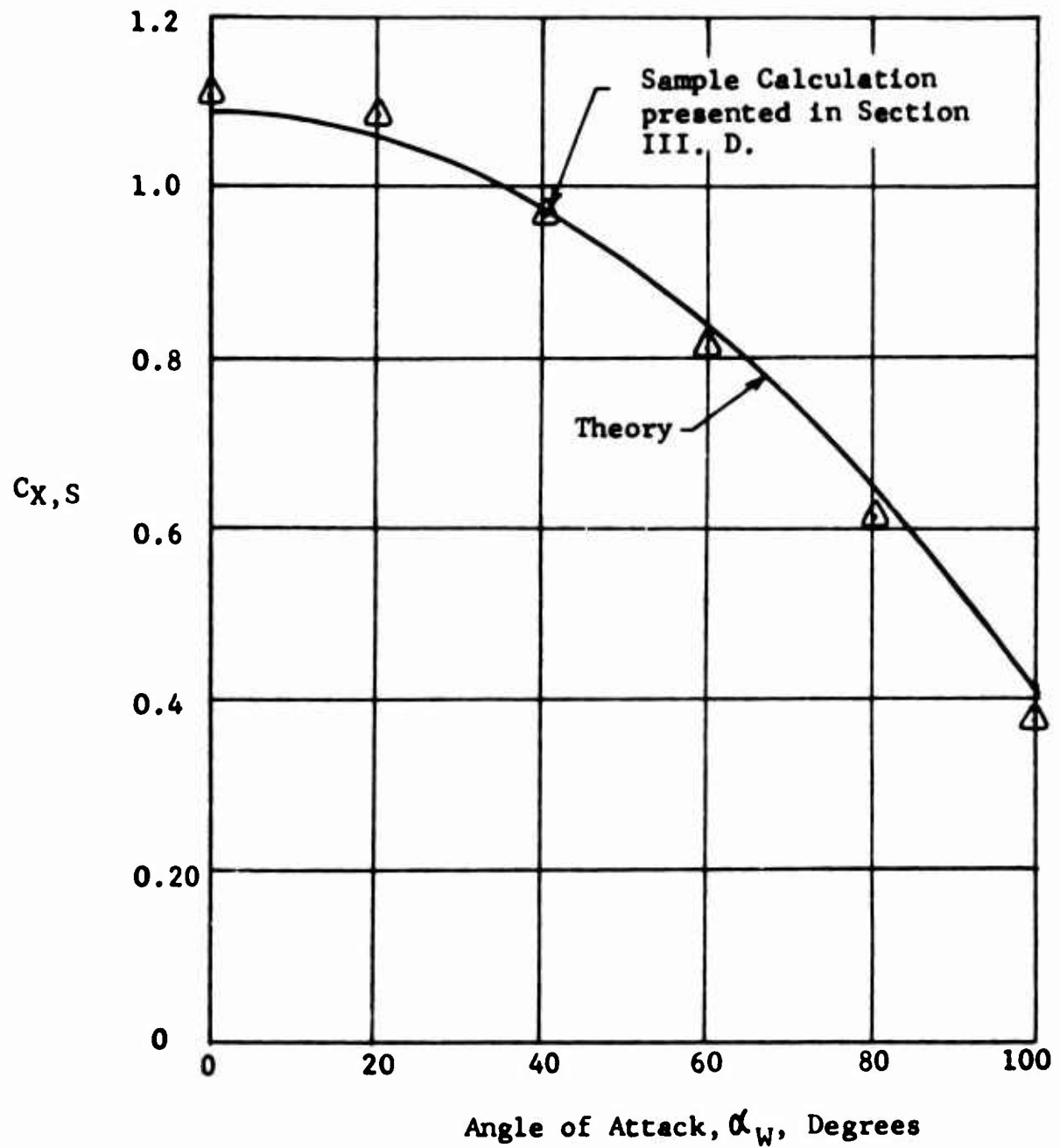


FIGURE 15: CORRELATION OF PREDICTED AND EXPERIMENTAL LONGITUDINAL FORCE COEFFICIENTS, CONFIGURATION B,  $C_{T,S} = 0.88$  AND  $\delta_f = 0$  DEGREES

$$c/D = 0.50 \quad V_o = 53.1 \text{ ft/sec}$$

$$i_W = 0^\circ \quad \frac{V_o}{V_j} = 0.648$$

$$N = 2 \quad R_n = 0.53 \times 10^6$$

△ TEST DATA REFERENCE 12

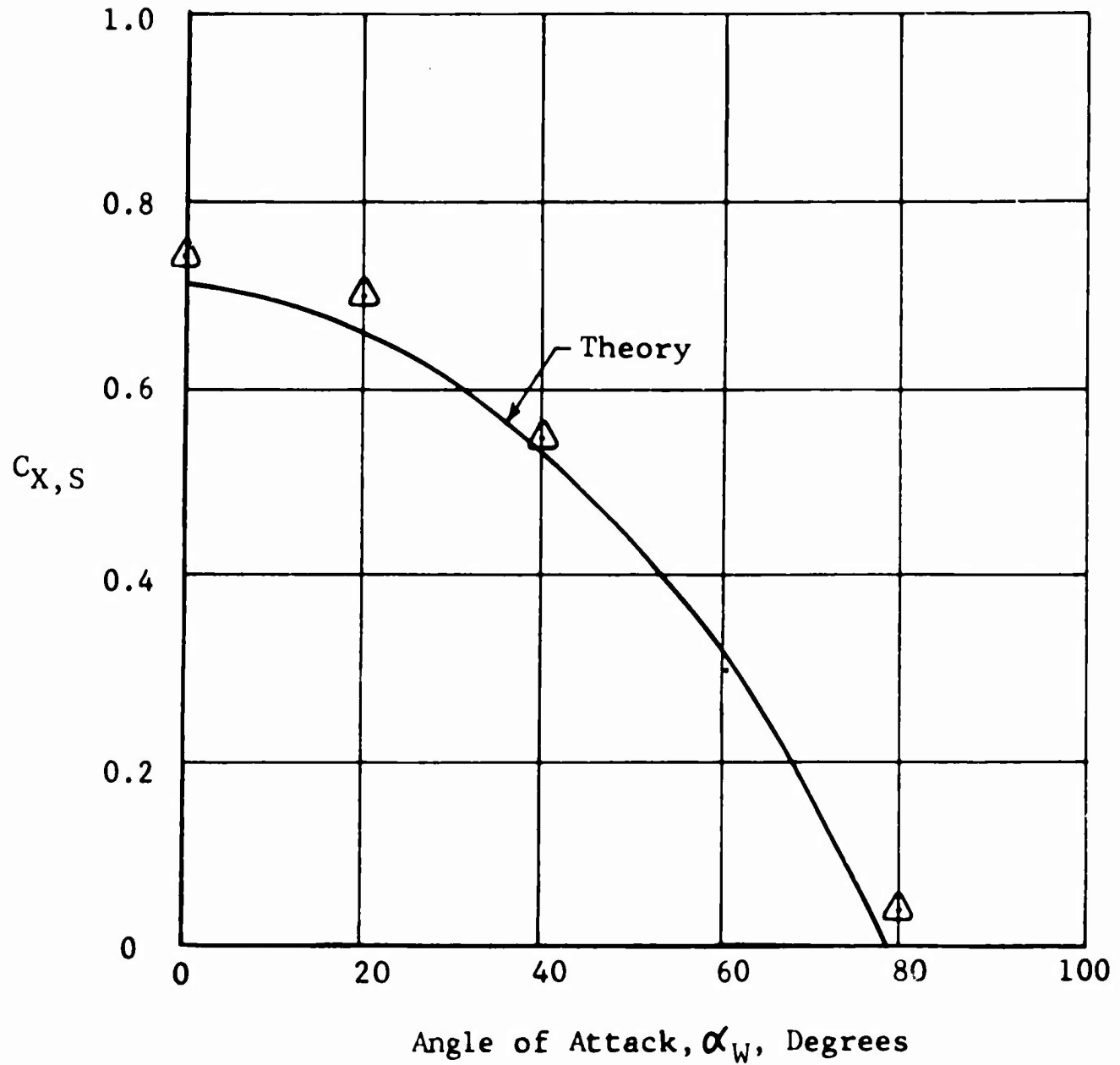


FIGURE 16: CORRELATION OF PREDICTED AND EXPERIMENTAL LONGITUDINAL FORCE COEFFICIENTS, CONFIGURATION B,  $C_{T,S} = 0.58$  AND  $\delta_f = 0$  DEGREES

$$c/D = 0.76 \quad V_o = 24.6 \text{ ft/sec}$$

$$i_w = 0^\circ \quad \frac{V_o}{V_j} = 0.300$$

$$N = 2 \quad R_n = 0.8 \times 10^6$$

⊙ TEST DATA REFERENCE 16

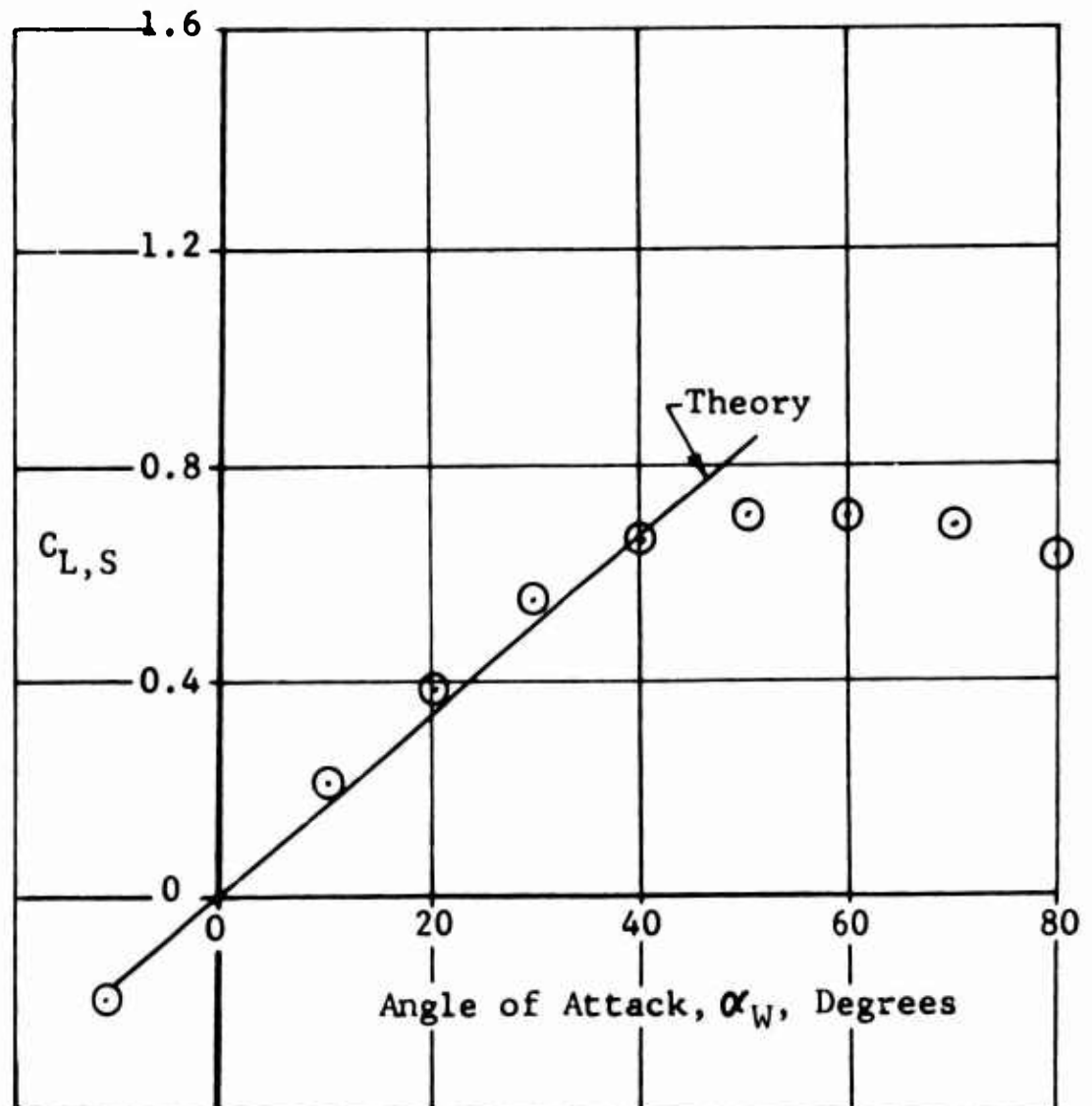


FIGURE 17: CORRELATION OF PREDICTED AND EXPERIMENTAL LIFT COEFFICIENTS, CONFIGURATION D,  $C_{T,S} = 0.91$  AND  $\delta_f = 0$  DEGREES

$$c/D = 0.76 \quad V_o = 44.1 \text{ ft/sec}$$

$$i_w = 0^\circ \quad \frac{V_o}{V_j} = 0.538$$

$$N = 2 \quad R_n = 0.8 \times 10^6$$

⊙ TEST DATA REFERENCE 16

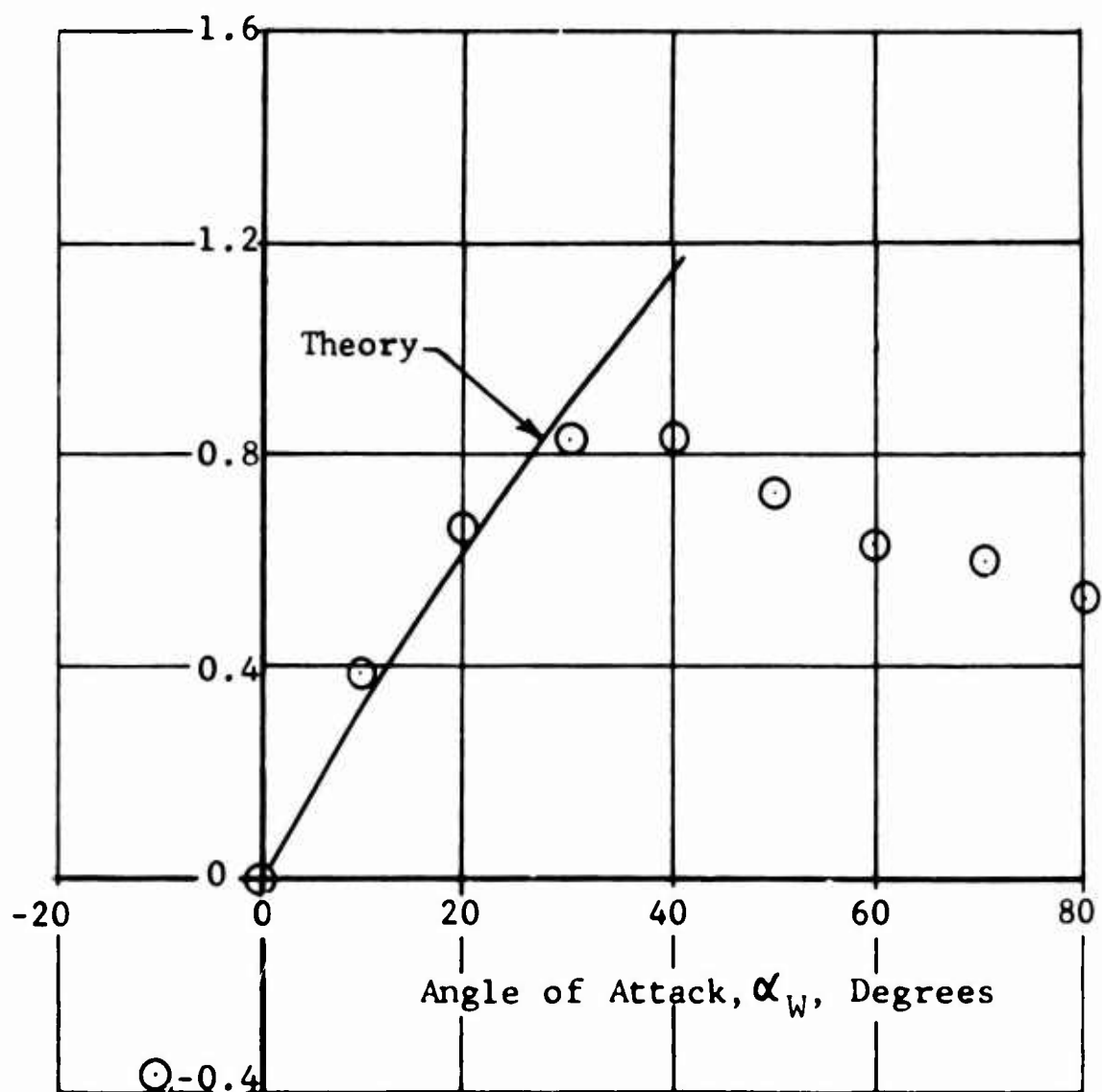


FIGURE 18: CORRELATION OF PREDICTED AND EXPERIMENTAL LIFT COEFFICIENTS, CONFIGURATION D,  $C_{T,S} = 0.71$  AND  $\delta_f = 0$  DEGREES

correlation with data from Reference 17 was utilized. As shown in Figure 6 Configuration E has two propellers per semispan, and is equipped with a fowler type trailing-edge flap. The extension of this flap results in a 40% increase in wing area. Correlation with the flap retracted is shown in Figure 19; and with the flap extended (at  $\delta_f = 50$  degrees) is shown in Figure 20. Agreement is good with and without flap up to stall. For this configuration calculated  $C_{L,S}$  is slightly lower than experiment in the angle of attack range up to stall. The effects of interaction between the slipstreams appear to be small for this configuration.

#### 4. Configuration F (Reference 16)

The effects of propeller overlap and the deflection of a plain trailing-edge flap on predicted performance was determined by correlation with the data of Configuration F from Reference 16. The pronounced propeller overlap of this configuration is evident in Figure 7. Lift coefficient correlation for flap deflections of 0 degrees, 10 degrees, and 50 degrees is shown in Figures 21 through 25. In general, agreement is good for various propeller thrust coefficients and flap deflections. However, referring to Figure 25, it is seen that the predicted values greatly exceed the test data for  $\delta_f = 50$  degrees. For this case the lower experimental values of  $C_{L,S}$  are due to stalled flow over the flap. This conclusion is substantiated in Figure 26 which is a plot of  $\delta_f$ -VS- $C_{L,S}$  for configuration F showing flap stall at  $\delta_f = 35$  degrees. Also referring to Figures 21 and 22, it is seen that the test points do not pass through zero as would be expected for a model of symmetrical airfoil section. The authors of Reference 16 indicate that this is caused by an induced upflow between the nacelles due to slipstream swirl. This fact is not considered in the present analysis hence it contributes to the underestimation of  $C_{L,S}$  in Figures 21 through 24.

Longitudinal force coefficient correlation for this configuration is shown in Figures 27 through 29 for  $C_{T,S} = 0.91$  and in Figures 30 and 31 for  $C_{T,S} = 0.71$ . In general, the theory is in agreement with test data; however, referring to Figures 27 and 28, it is seen that the predicted values of  $C_{X,S}$  exceed the experimental data. This implies that the drag contribution to the longitudinal force coefficient was underestimated. Modifications to the present analysis to achieve better correlation were investigated, however; it was found that

$$c/D = 0.60 \quad V_o = 25.9 \text{ ft/sec}$$

$$i_w = 0^\circ \quad \frac{V_o}{V_j} = 0.316$$

$$N = 4 \quad R_n^j = 0.63 \times 10^6$$

⊙ TEST DATA REFERENCE 17

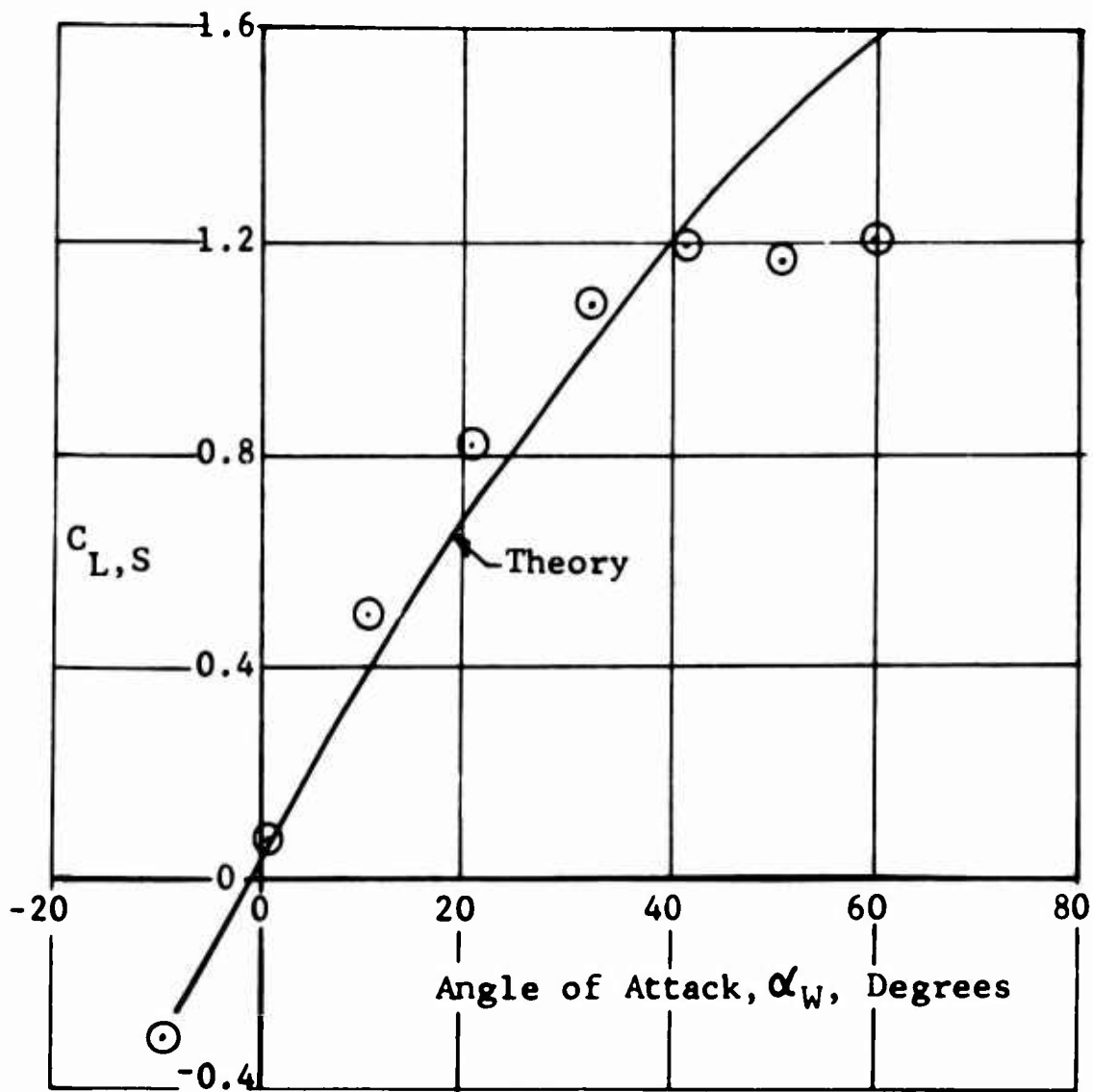


FIGURE 19: CORRELATION OF PREDICTED AND EXPERIMENTAL LIFT COEFFICIENTS, CONFIGURATION E,  $C_{T,S} = 0.90$  AND  $\delta_f = 0$  DEGREES

$$c/D = 0.60 \quad V_o = 25.9 \text{ ft/sec}$$

$$i_w = 0^\circ \quad \frac{V_o}{V_j} = 0.316$$

$$N = 4 \quad R_n = 0.63 \times 10^6$$

⊙ TEST DATA REFERENCE 18

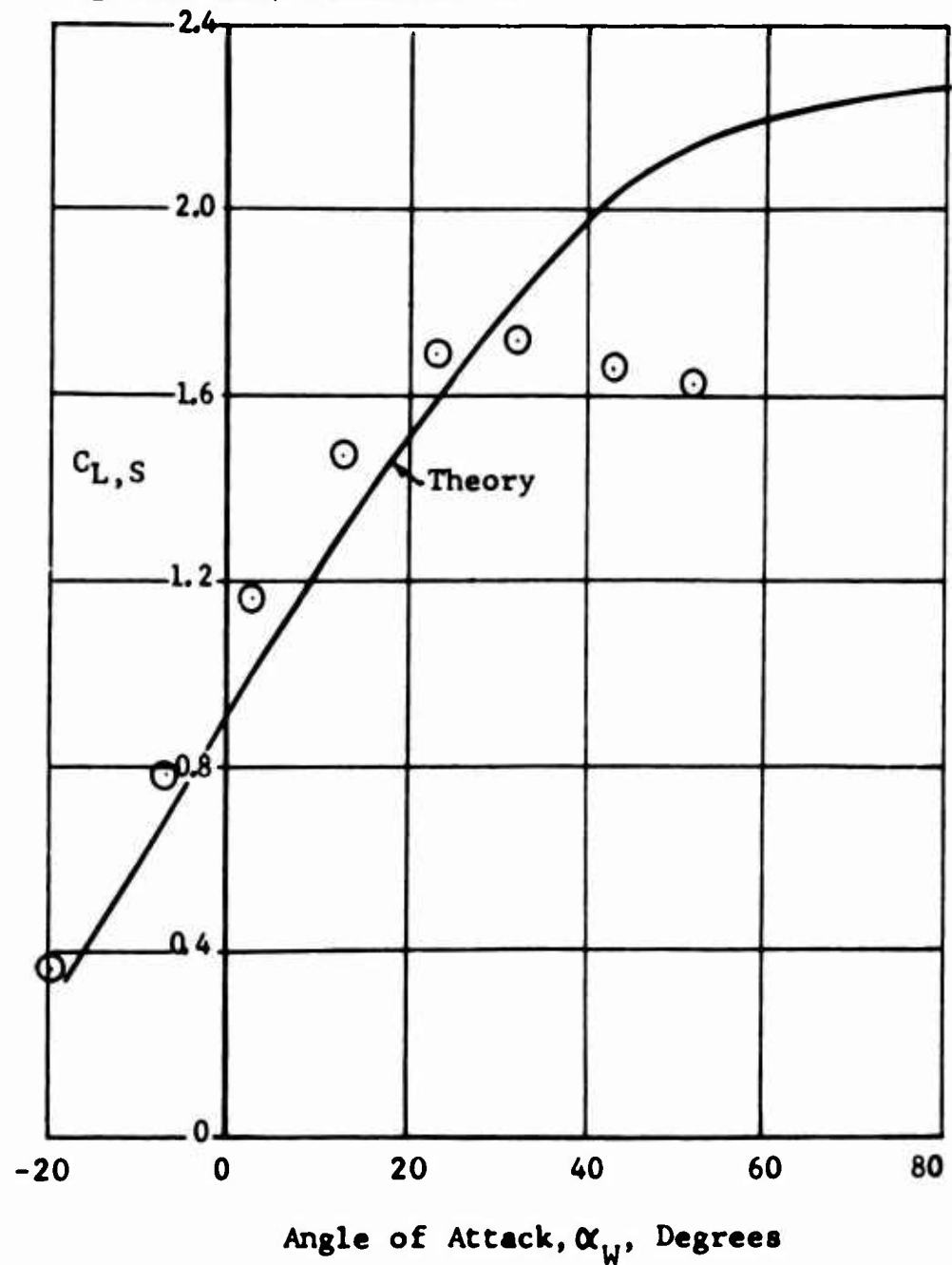


FIGURE 20: CORRELATION OF PREDICTED AND EXPERIMENTAL LIFT COEFFICIENTS, CONFIGURATION E,  $C_{T,S} = 0.90$  AND  $\delta_f = 50$  DEGREES

$$c/D = 0.76 \quad V_O = 24.6 \text{ ft/sec}$$

$$i_W = 0^\circ \quad \frac{V_O}{V_j} = 0.300$$

$$N = 4 \quad R_n = 0.80 \times 10^6$$

○ TEST DATA REFERENCE 16

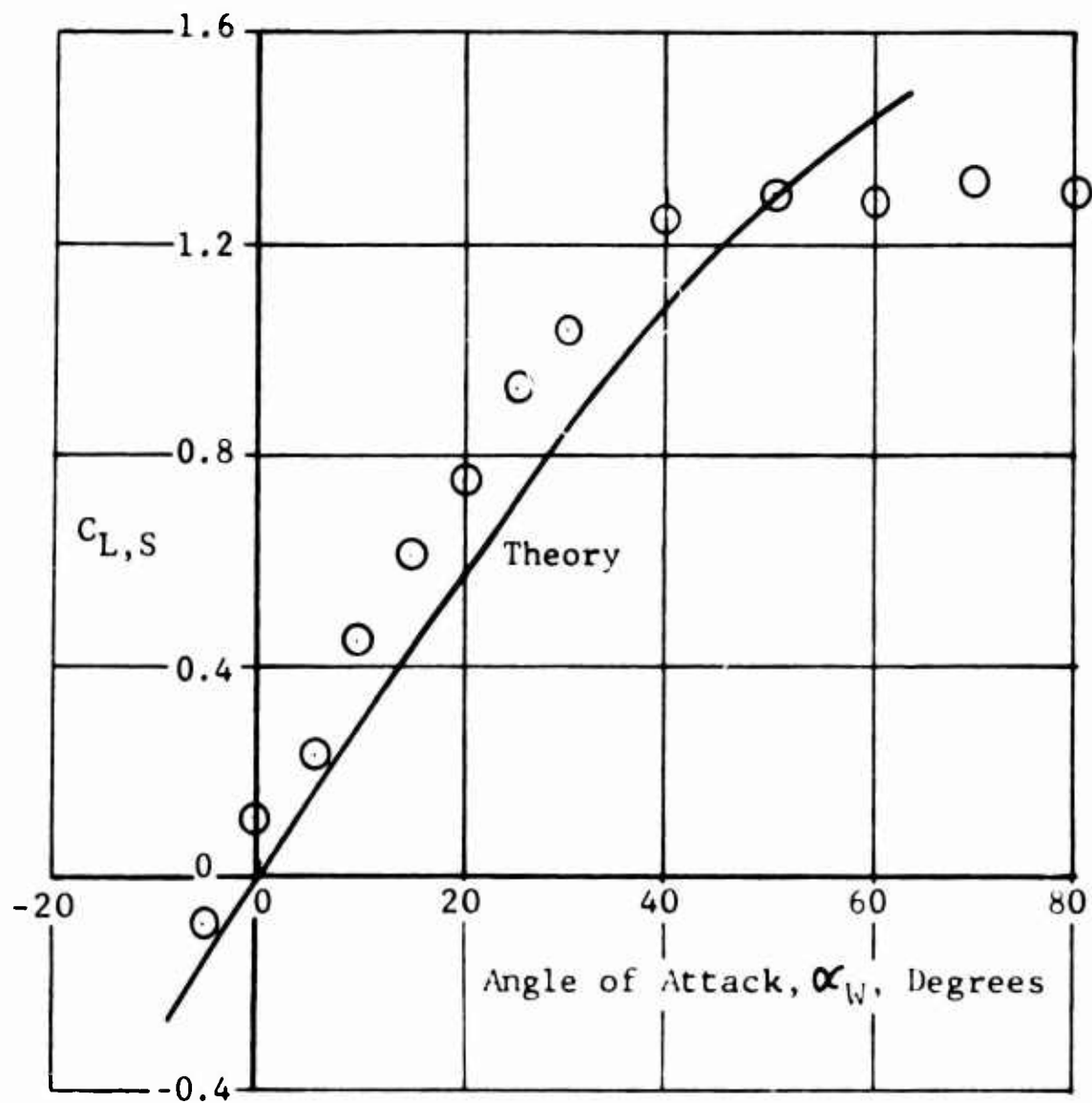


FIGURE 21: CORRELATION OF PREDICTED AND EXPERIMENTAL LIFT COEFFICIENTS, CONFIGURATION F,  $C_{T,S} = 0.91$  AND  $\delta_f = 0$  DEGREES



$$c/D = 0.76 \quad V_o = 44.1 \text{ ft/sec}$$

$$i_w = 0^\circ \quad \frac{V_o}{V_j} = 0.538$$

$$N = 4 \quad R_n = 0.8 \times 10^6$$

⊙ TEST DATA REFERENCE 16

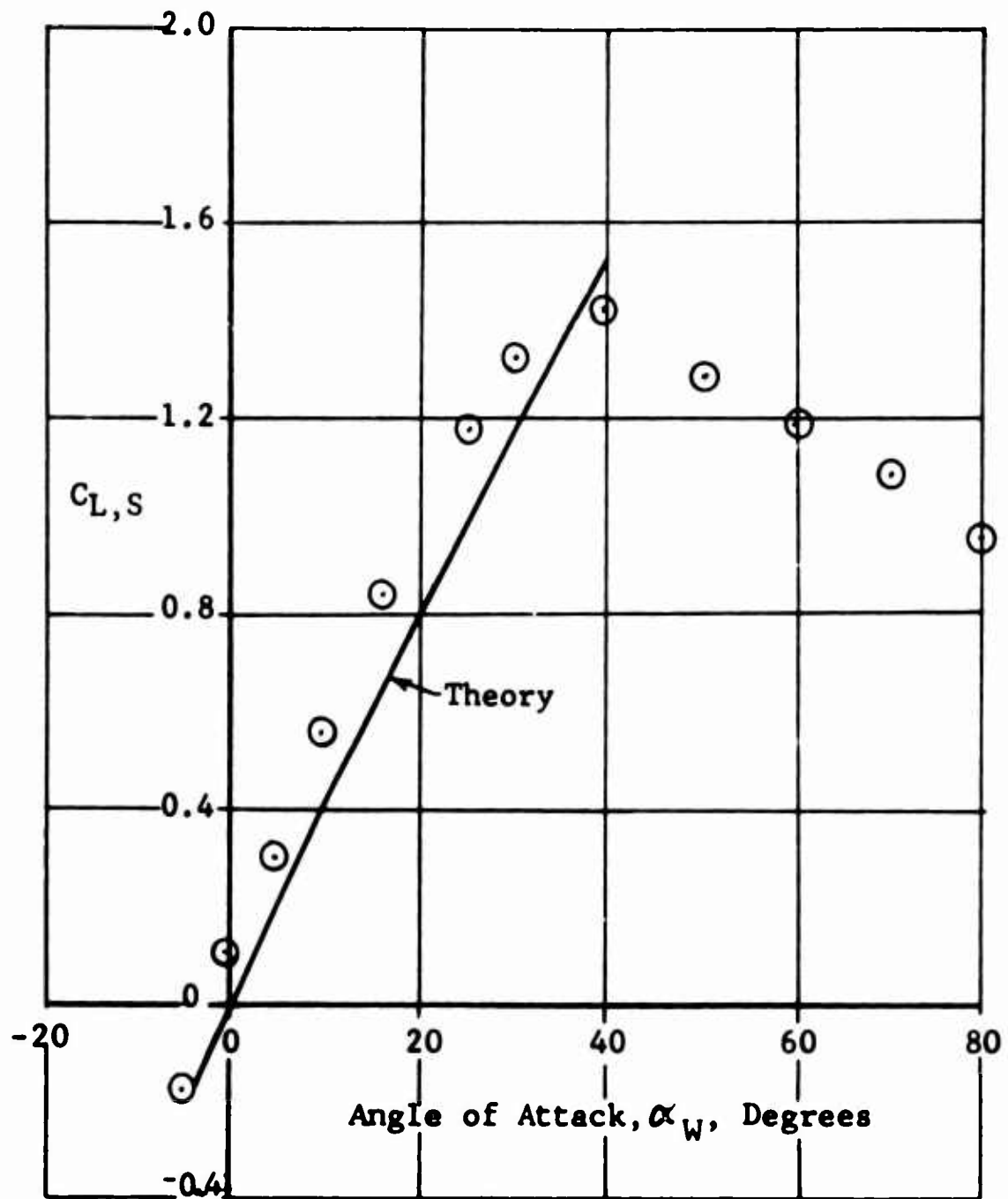


FIGURE 22: CORRELATION OF PREDICTED AND EXPERIMENTAL LIFT COEFFICIENTS, CONFIGURATION F,  $C_{T,S} = 0.71$  AND  $\delta_f = 0$  DEGREES

$$\begin{aligned}
 c/D &= 0.76 & V_o &= 24.6 \text{ ft/sec} \\
 i_w &= 0^\circ & \frac{V_o}{V_j} &= 0.300 \\
 N &= 4 & R_n &= 0.8 \times 10^6
 \end{aligned}$$

⊙ TEST DATA REFERENCE 16

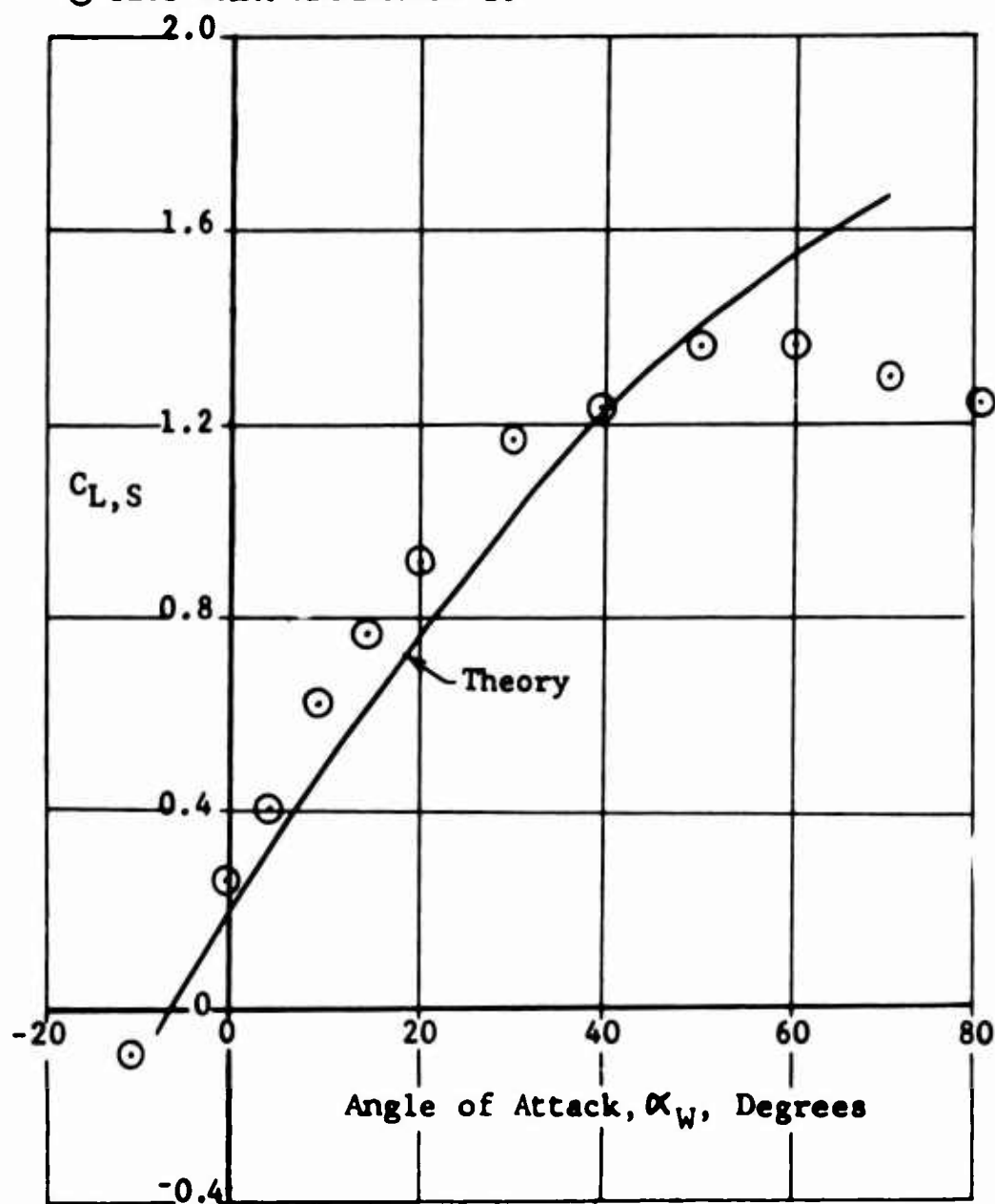


FIGURE 23: CORRELATION OF PREDICTED AND EXPERIMENTAL LIFT COEFFICIENTS, CONFIGURATION F,  $C_{T,S} = 0.91$  AND  $\delta_f = 10$  DEGREES

$$c/D = 0.76 \quad V_o = 44.1 \text{ ft/sec}$$

$$i_W = 0^\circ \quad \frac{V_o}{V_j} = 0.538$$

$$N = 4 \quad R_n = 0.8 \times 10^6$$

⊙ TEST DATA REFERENCE 16

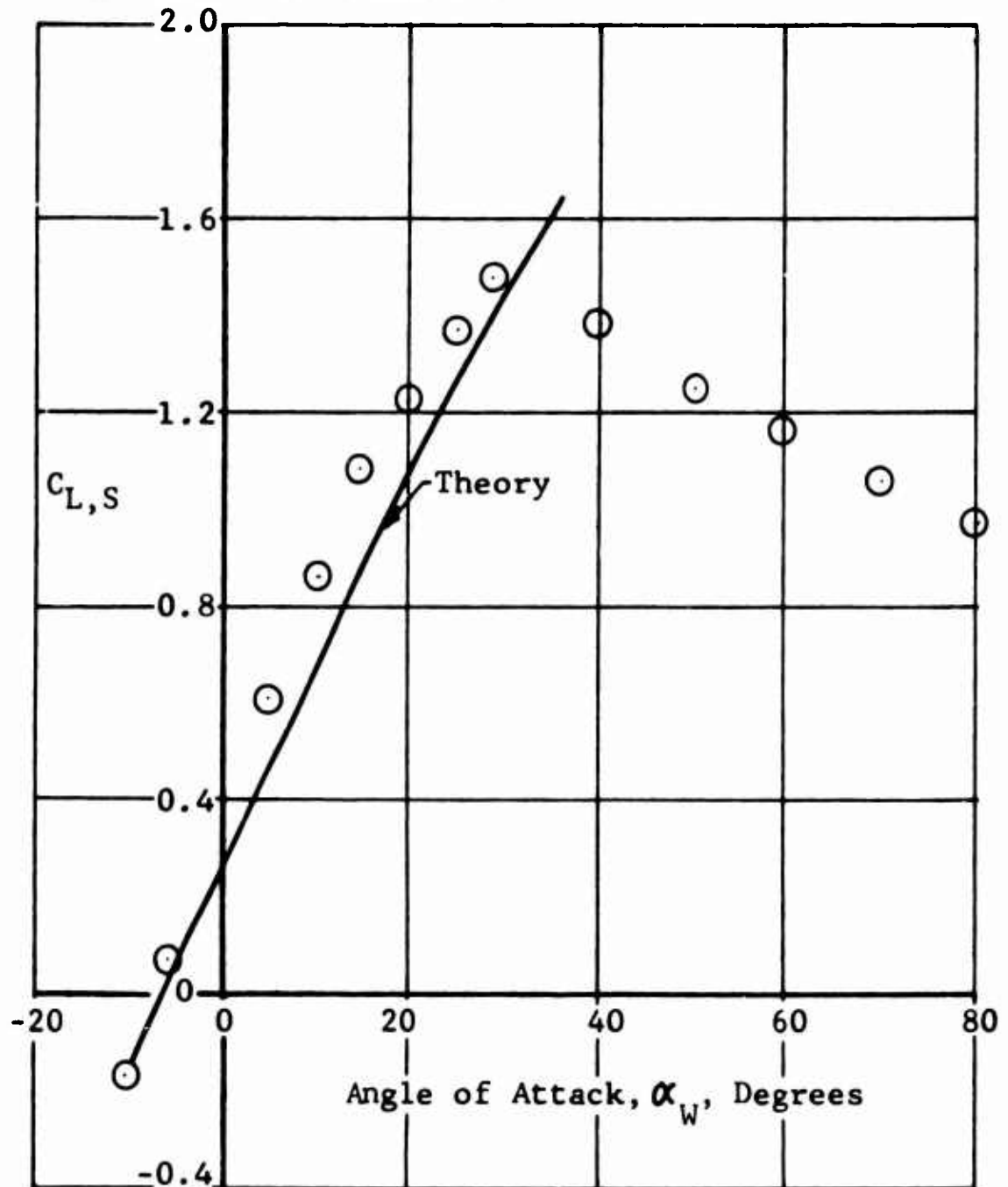


FIGURE 24: CORRELATION OF PREDICTED AND EXPERIMENTAL LIFT COEFFICIENTS, CONFIGURATION F,  $C_{T,S} = 0.71$  AND  $\delta_f = 10$  DEGREES

$$c/D = 0.76 \quad V_o = 24.6 \text{ ft/sec}$$

$$i_W = 0^\circ \quad \frac{V_o}{V_j} = 0.300$$

$$N = 4 \quad R_n^j = 0.8 \times 10^6$$

⊙ TEST DATA REFERENCE 16

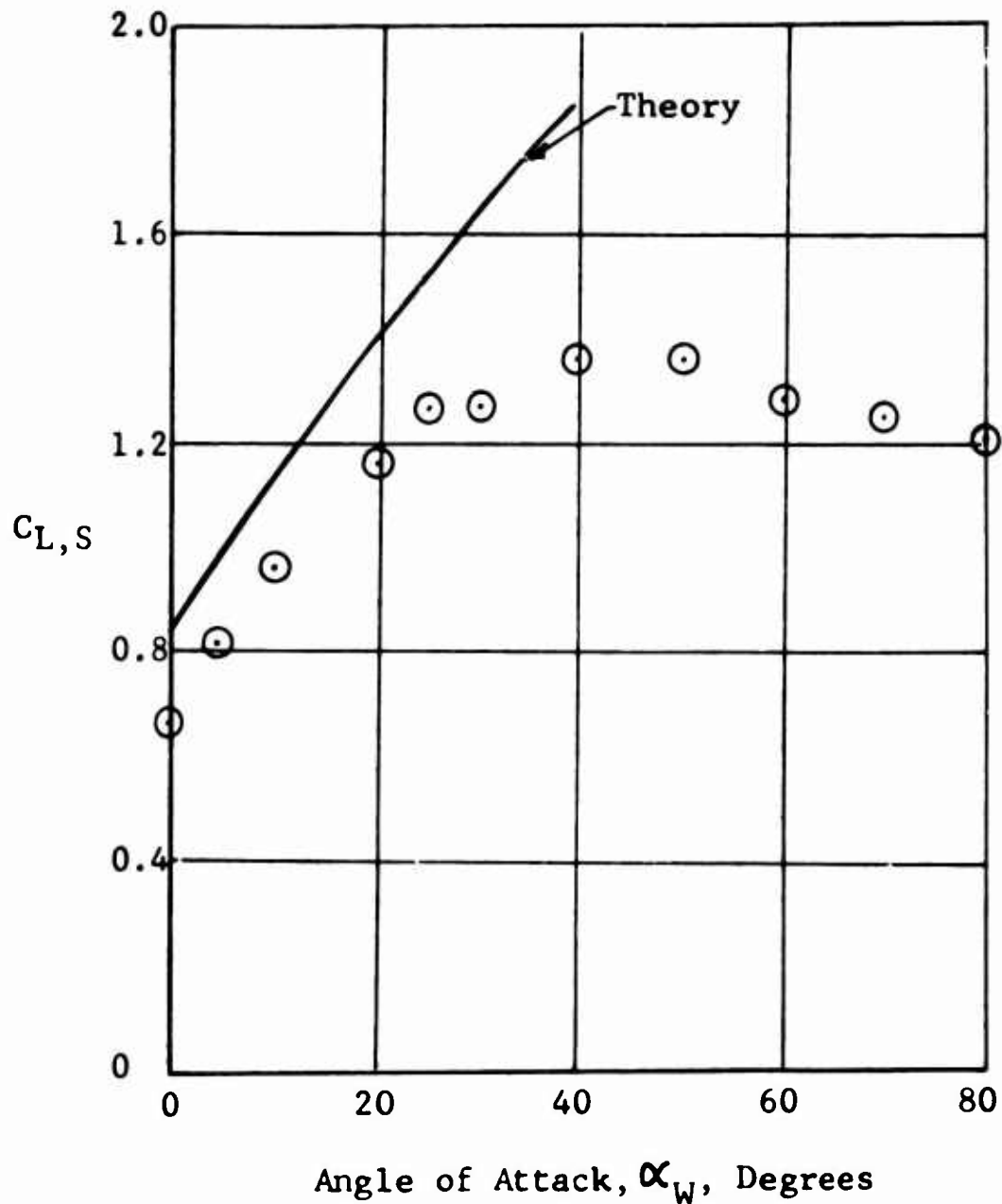


FIGURE 25: CORRELATION OF PREDICTED AND EXPERIMENTAL LIFT COEFFICIENTS, CONFIGURATION F,  $C_{T,S} = 0.91$  AND  $\delta_f = 50$  DEGREES

$$c/D = 0.76 \quad V_o = 24.6 \text{ ft/sec}$$

$$i_W = 0^\circ \quad \frac{V_o}{V_j} = 0.300$$

$$N = 4 \quad R_n = 0.8 \times 10^6$$

⊙ TEST DATA REFERENCE 16

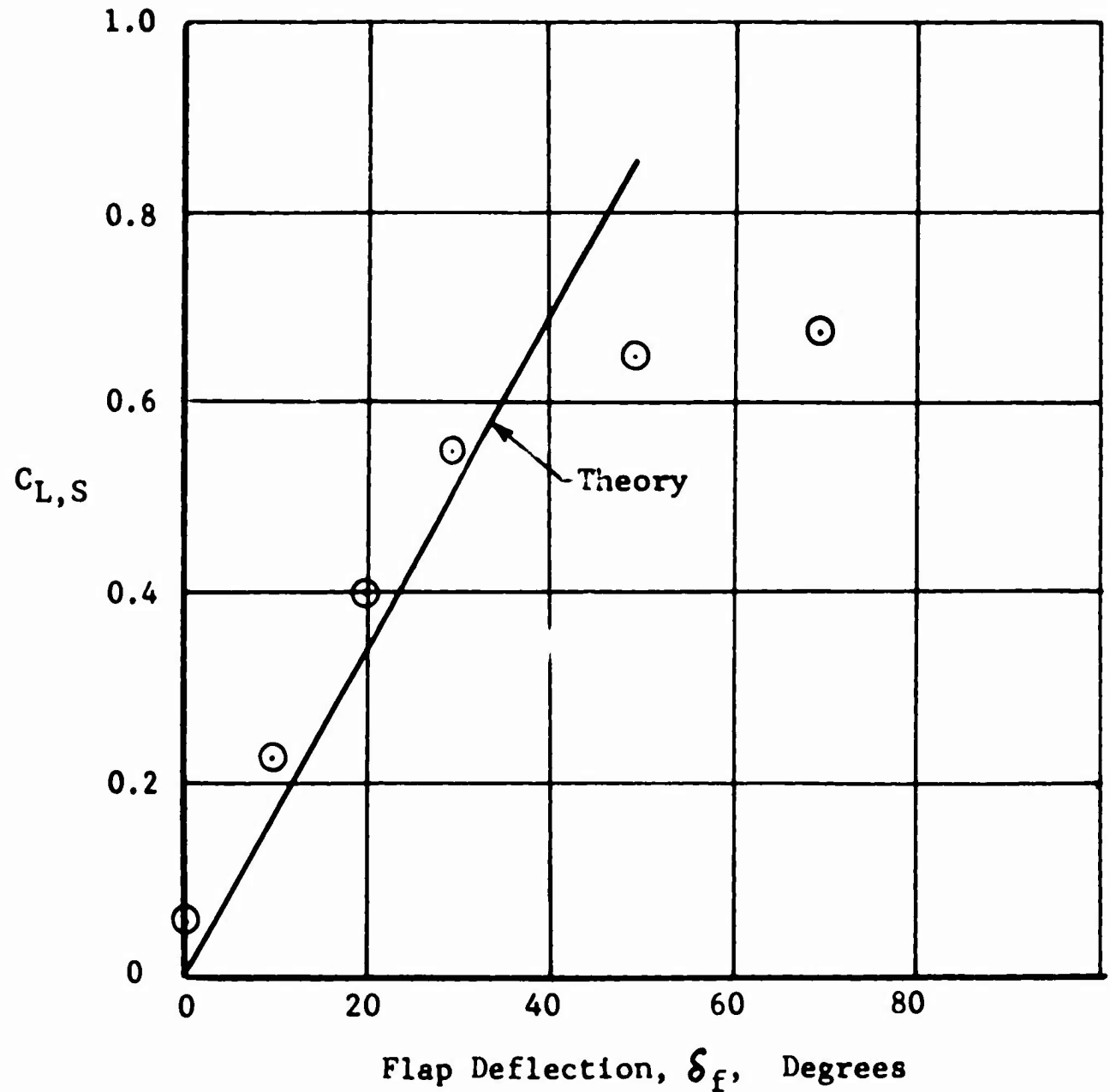


FIGURE 26: CORRELATION OF PREDICTED AND EXPERIMENTAL LIFT COEFFICIENTS AS A FUNCTION OF FLAP DEFLECTION CONFIGURATION F,  $C_{T,S} = 0.91$  AND  $\alpha_W = 0$  DEGREES

$$\begin{aligned}
 c/D &= 0.76 & V_o &= 24.6 \text{ ft/sec} \\
 i_w &= 0^\circ & \frac{V_o}{V_j} &= 0.300 \\
 N &= 4 & R_n &= 0.8 \times 10^6
 \end{aligned}$$

△ TEST DATA REFERENCE 16

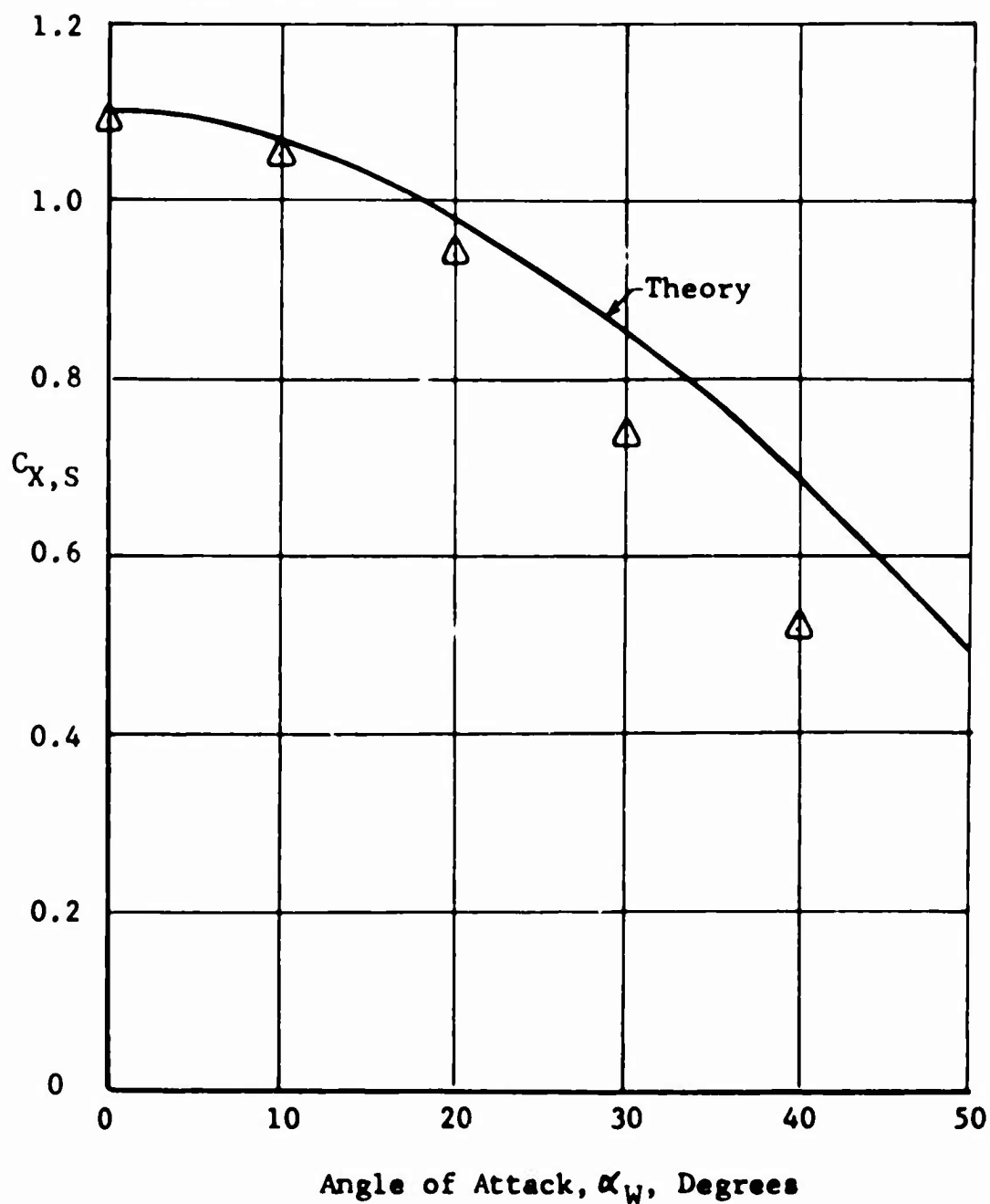


FIGURE 27: CORRELATION OF PREDICTED AND EXPERIMENTAL LONGITUDINAL FORCE COEFFICIENTS, CONFIGURATION F,  $C_{T,S} = 0.91$  AND  $\delta_f = 0$  DEGREES

$$c/D = 0.76 \quad V_o = 24.6 \text{ ft/sec}$$

$$i_w = 0 \quad \frac{V_o}{V_j} = 0.300$$

$$N = 4 \quad R_n = 0.8 \times 10^6$$

△ TEST DATA REFERENCE 16

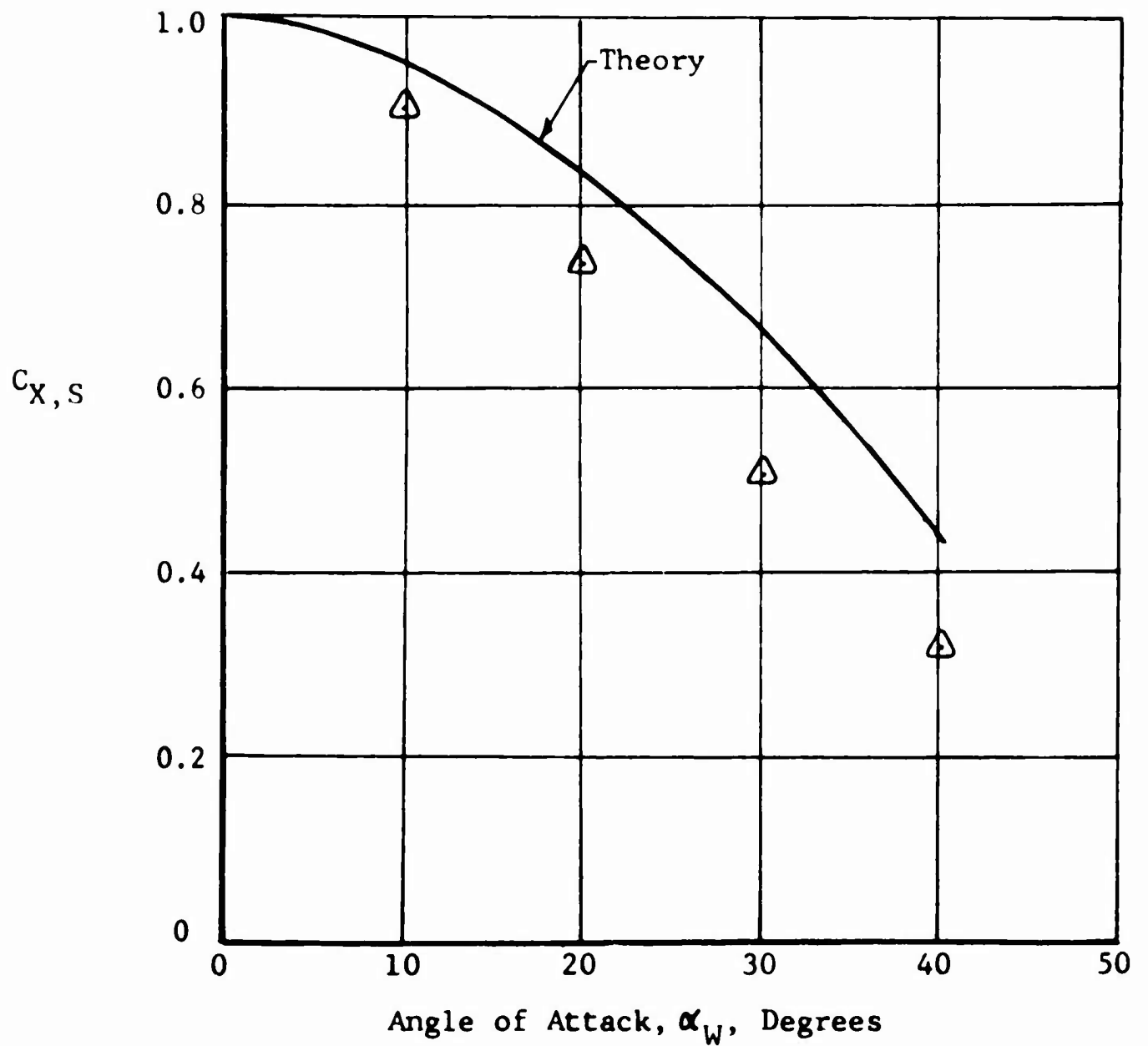


FIGURE 28: CORRELATION OF PREDICTED AND EXPERIMENTAL LONGITUDINAL FORCE COEFFICIENTS, CONFIGURATION F,  $C_{T,S} = 0.91$  AND  $\delta_f = 20$  DEGREES

$$c/D = 0.76 \quad V_o = 24.6 \text{ ft/sec}$$

$$i_W = 0^\circ \quad \frac{V_o}{V_j} = 0.300$$

$$N = 4 \quad R_n = 0.8 \times 10^6$$

$\triangle$  TEST DATA REFERENCE 16

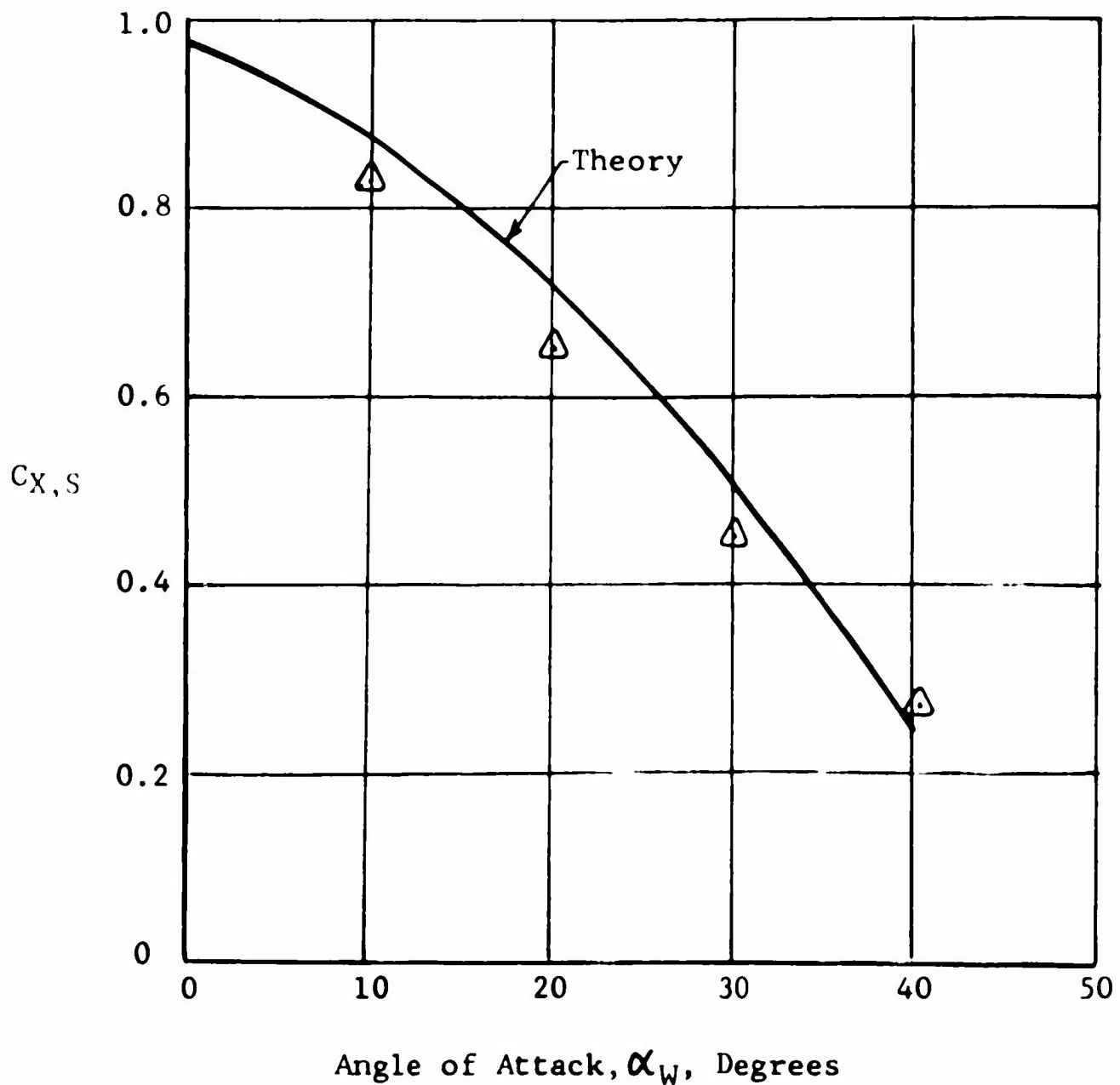


FIGURE 29: CORRELATION OF PREDICTED AND EXPERIMENTAL LONGITUDINAL FORCE COEFFICIENTS, CONFIGURATION F,  $C_{T,S} = 0.91$  AND  $\delta_f = 30$  DEGREES



$$c/D = 0.76 \quad V_o = 44.1 \text{ ft/sec}$$

$$i_w = 0^\circ \quad \frac{V_o}{V_j} = 0.538$$

$$N = 4 \quad R_n = 0.8 \times 10^6$$

△ TEST DATA REFERENCE 16

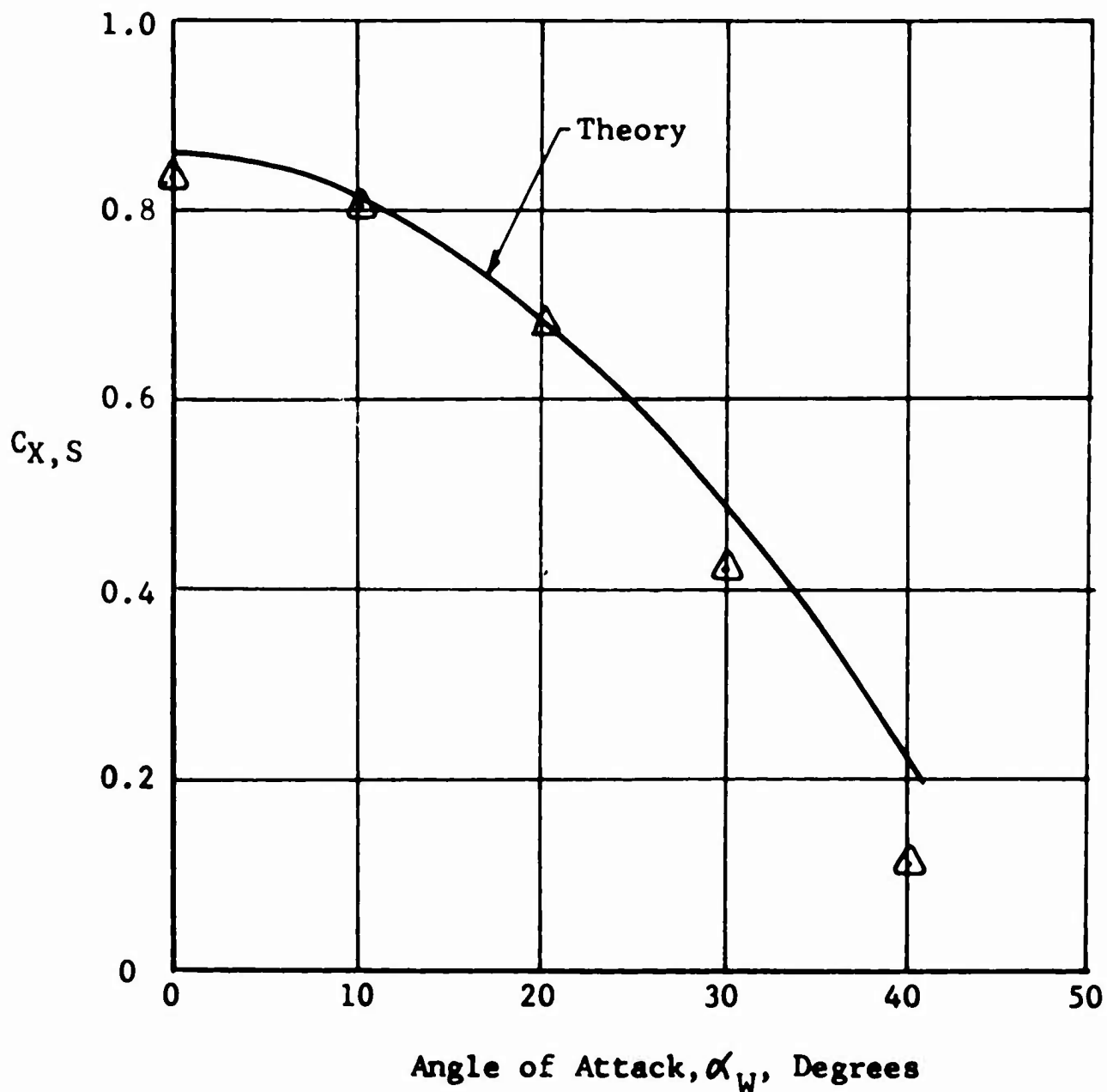


FIGURE 30: CORRELATION OF PREDICTED AND EXPERIMENTAL LONGITUDINAL FORCE COEFFICIENTS, CONFIGURATION F,  $C_{T,S} = 0.71$  AND  $\delta_f = 0$  DEGREES

$$c/D = 0.76 \quad V_o = 44.1 \text{ ft/sec}$$

$$i_w = 0^\circ \quad \frac{V_o}{V_j} = 0.538$$

$$N = 4 \quad R_n = 0.8 \times 10^6$$

△ TEST DATA REFERENCE 16

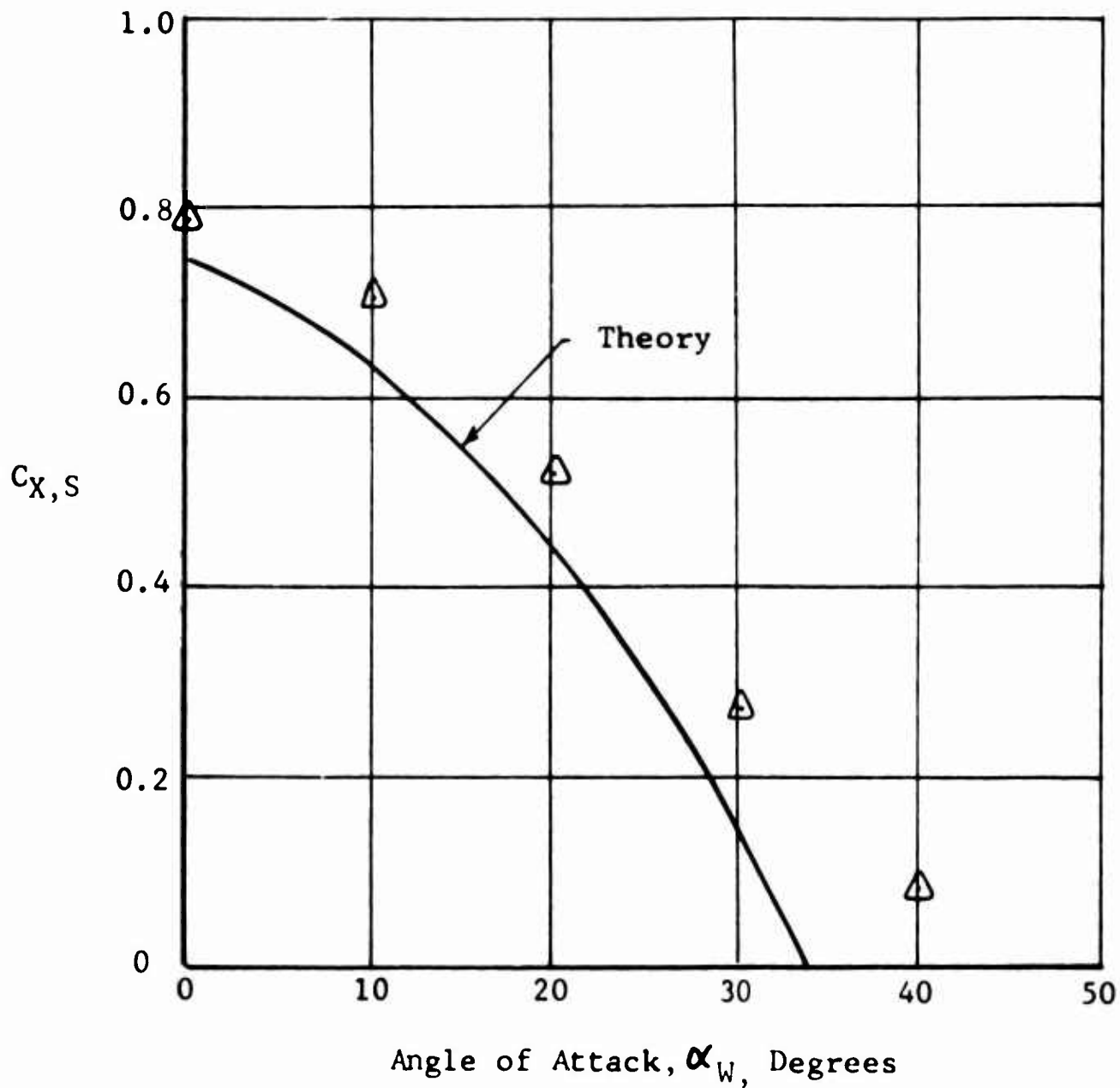


FIGURE 31: CORRELATION OF PREDICTED AND EXPERIMENTAL LONGITUDINAL FORCE COEFFICIENTS, CONFIGURATION F,  $C_{T,S} = 0.71$  AND  $\delta_f = 30$  DEGREES

the analysis as presented in Section III gives the best overall correlation with test data.

In summary, the correlation performed indicates that the accuracy of the analysis is not greatly affected by variations in  $\mu$ ,  $\alpha_w$ ,  $c/D$ ,  $\delta_f$ , wing planform, and propeller position; and that agreement is good up to the point of stall for all cases.

#### B. STALL CONSIDERATIONS

During the analysis of the model configurations previously discussed, it became evident that the degree of correlation between the calculated and measured values of  $C_{L,S}$  and  $C_{X,S}$  is affected by the stalling of the wing. Solving Equation (4.2) for the angle of stall,  $\alpha_{stall}$ ,

$$\alpha_{stall} = \frac{(C_{lmax})\pi c}{r_o (1 + \mu^2)} \quad (5.1)$$

Furthermore, from Equations (3.4) and (3.9),

$$\alpha_{stall} = i_w + \tan^{-1} \left[ \frac{V_o \sin \alpha_T}{\sqrt{(V_o \cos \alpha_T)^2 + \frac{T}{\frac{\rho}{2} \frac{\pi D^2}{4}}}} \right] - \alpha_{LO} + \delta_f \quad (5.2)$$

It is seen from Equation (5.1), that an increase of  $\mu$  (i.e., a decrease of  $C_{T,S}$ ) corresponds to a decrease of  $\alpha_{stall}$ . Furthermore, from Equation (5.2) for a given  $\alpha_{stall}$ , an increase of  $\alpha_w$  must be compensated for by a decrease of the flap deflection,  $\delta_f$ .

By use of Equation (5.1), the value of  $\alpha_{stall}$  for the configuration discussed in Figure 12 is 13.6 degrees and  $\alpha_w = 24$  degrees. Indeed, this value for  $\alpha_{stall}$  appears to be in agreement with the test data presented in Figure 12. Similarly, for the test conditions illustrated in Figure 11,  $\alpha_{stall} = 20$  degrees, and from Equation (5.2) there results that stall will not occur within the slipstream for any value of  $\alpha_w$ . Again, correlation between test data and calculated values of  $C_{L,S}$  support this conclusion. A further examination of the calculated values for  $C_{L,S}$  shows, however, that the limit of correlation between theory and test data is not always predicted by Equations (5.1) and (5.2).

Whereas these equations did not indicate any stall in the range of values of  $\alpha_w$ , shown in Figure 14 and Figures 17 through 25, the leveling off of the test data appears to indicate, however, the existence of wing stall.

A more detailed investigation of stall is warranted before an expression can be formulated for predicting the onset of stall for a wide range of parameters.

### C. CORRELATION OF CALCULATED STOL LANDING AND TAKE-OFF PERFORMANCE WITH FLIGHT TEST DATA

The analysis presented in the Appendix was used to calculate the take-off and landing performance of STOL aircraft. The results are as follows:

#### 1. Landing Distances Over a 50-Foot Obstacle

Landing distances for several STOL aircraft obtained from flight test data are shown in Figure 38. The data is seen to fall within the limits of the predicted routine landings and the maximum performance landings.

#### 2. Take-Off Distance

Propeller performance plays an important role in the determination of take-off distances as discussed in Reference 18. The accuracy of the calculations thus depends upon the accuracy of the propeller performance data. For the STOL aircraft shown in Figure 38, complete propeller performance data was not available; thus it was necessary to utilize other existing performance curves for similar propellers. Take-off distances were calculated for the Grumman Mohawk (a typical STOL aircraft) using propeller data from Reference 15.

A ground roll of 547 feet was obtained for the Mohawk using the procedure in the Appendix. The calculated data showed that the aircraft remained in transition above an altitude of 50 feet. The ground distance corresponding to the 50-foot altitude during transition was calculated accordingly, and found to be 220 feet. The total distance to clear a 50-foot obstacle is 547 feet plus 220 feet, or 767 feet. The flight test data indicated a corresponding distance of 880 feet.

### 3. Results

The calculated take-off and landing performance was found to be in good agreement with the available test data. As comprehensive aircraft and test data become available, further calculations should be performed to determine the degree of validity of the assumptions made. On the basis of the comparison with the limited test data, it appears that the landing and take-off performance of STOL aircraft can be predicted with reasonable accuracy using the methods presented herein.

#### D. RANGE OF CORRELATION FOR THEORY AND TEST DATA

The range of correlation between the theory presented herein and lift and longitudinal force data is as follows:

<u>PARAMETERS</u>	<u>RANGE OF APPLICABILITY</u>	<u>RANGE OF CORRELATION</u>
Number of Propellers	Any	2 and 4
Disc Loading (psf)	Any	0 to 8.0
Thrust Coefficient	Any	0 to 1.0
Jet Velocity to free-stream Velocity ratio " $\mu$ "	0 to 1.0	0 to 1.0
Propeller Axis Inclination Relative to Wing (deg.)	Not Established	0
Slipstream Overlap	0 to D/3	0 to D/3
Wing Aspect Ratio	>1	3.33 to 7.5
Wing Angles of Attack(deg.)	Below section stall in slipstream	-20°to stall
Flap Angles (deg.)	Below section stall in slipstream	0°to 35°
Flap Types	Not Established	Plain & Fowler
Wing Planform	Rectangular and moderate deviation therefrom	Taper ratio from 1.0 to 0.715

---

## VI. V/STOL AIRCRAFT STABILITY AND CONTROL

### A. INTRODUCTION

In this section a study is made of the effects of propeller slipstream on the stability and control characteristics of tilt-wing V/STOL aircraft. The feasibility of improving the slow speed and transition handling qualities by proper use of the slipstream is also investigated.

### B. SCOPE OF INVESTIGATION

#### 1. Discussion of V/STOL Stability Analysis

The stability and control characteristics of tilt-wing types of VTOL aircraft are discussed in References 21 and 22. Reference 21 treats the tilt-wing configuration employing semi-empirical expressions for the propeller slipstream contributions to the wing lift and drag. The investigation discussed herein utilizes the analysis of Reference 21, except for the slipstream contributions for which the analytical expressions developed in Section III are utilized.

#### 2. Assumptions of the Analysis

The major assumptions utilized in the development of the VTOL dynamic stability analysis are as follows:

- a. Small amplitude analysis is utilized, i.e., the equations of motion are linearized.
- b. The airframe is considered to be a rigid body.
- c. There is no coupling between the lateral and longitudinal modes of motion.
- d. The wing tilt angle is fixed during the analysis.

#### 3. Area of Present Investigation

The present investigation is concerned with the hovering flight condition, which, as shown in Reference 21, represents the most severe stability problems for the tilt-wing aircraft configuration.

## C. STABILITY ANALYSIS OF V/STOL AIRCRAFT AS AFFECTED BY THE PROPELLER SLIPSTREAM

The determination of the slipstream effects on the stability characteristics is accomplished by examining the effects of slipstream terms on the stability derivatives and the roots of the characteristic equation.

### 1. Equations of Motion

As given in Reference 21, the longitudinal equations of motion in coefficient form for the hovering case reduce to

$$\underline{C_{X_V}} V + C_{X_{\dot{V}}} \dot{V} + C_{X_{\theta}} \theta + \underline{C_{X_{\dot{\theta}}}} \dot{\theta} = 0 \quad (6.1)$$

$$\underline{C_{M_V}} V - C_{M_{\dot{\theta}}} \dot{\theta} + C_{M_{\ddot{\theta}}} \ddot{\theta} = 0 \quad (6.2)$$

The perturbation variables used are the free-stream velocity,  $V$ , and the aircraft pitch attitude,  $\theta$ . The derivatives involving slipstream terms are underlined. These derivatives are now further investigated.

### 2. Evaluation of Stability Derivatives Involving Slipstream Terms

#### a. Total Derivatives

The derivative relating to the change in longitudinal force with a change in forward velocity,  $C_{X_V}$ , is given as follows:

$$C_{X_V} = \frac{\partial C_{X,i}}{\partial V} + \frac{\partial C_{X,g}}{\partial V} + \frac{\partial C_{X,R}}{\partial V} + \frac{\partial C_{X,t}}{\partial V} + \frac{\partial C_{X,w}}{\partial V} + \frac{\partial C_{X,s}}{\partial V} + \frac{\partial C_X}{\partial C_T} \left| \frac{\partial C_T}{\partial V} \right|_{\alpha, V} \bigg|_{\alpha} \quad (6.3)$$

Neglecting small terms, this derivative can be simplified to be

$$C_{X_V} = \frac{\partial C_{X,S}}{\partial V} + \frac{\partial C_{X,R}}{\partial V} . \quad (6.4)$$

The change in pitching moment coefficient with a change in forward speed,  $C_{M_V}$ , is given by

$$\begin{aligned} C_{M_V} = & -X_a \frac{\partial C_{Z,S}}{\partial V} - Z_a \frac{\partial C_{X,S}}{\partial V} - Z_t \frac{\partial C_{X,t}}{\partial V} - X_a \frac{\partial C_{Z,W}}{\partial V} - \\ & Z_a \frac{\partial C_{X,W}}{\partial V} + \frac{\partial C_{M,CF}}{\partial V} + \frac{\partial C_{M,ac}}{\partial V} - X_R \frac{\partial C_{Z,R}}{\partial V} - \\ & Z_R \frac{\partial C_{X,R}}{\partial V} + \left. \frac{\partial C_M}{\partial C_T} \right|_{\alpha, V} \left. \frac{\partial C_T}{\partial V} \right|_{\alpha} . \end{aligned} \quad (6.5)$$

Considering the major contributors to this derivative in hovering, there results

$$C_{M_V} = -Z_a \frac{\partial C_{X,S}}{\partial V} - Z_R \frac{\partial C_{X,R}}{\partial V} . \quad (6.6)$$

The change in longitudinal force with a change in pitch rate is given as follows:

$$C_{X_{\dot{\theta}}} = \frac{\partial C_{X,t}}{\partial \dot{\theta}} + \frac{\partial C_{X,R}}{\partial \dot{\theta}} + \frac{\partial C_{X,S}}{\partial \dot{\theta}} . \quad (6.7)$$

The change in pitching moment with a change in pitch rate is given as

$$\begin{aligned} C_{M_{\dot{\theta}}} = & \frac{\partial C_{M,CF}}{\partial \dot{\theta}} + \frac{\partial C_{M,S}}{\partial \dot{\theta}} - X_R \frac{\partial C_{Z,R}}{\partial \dot{\theta}} - \\ & Z_R \frac{\partial C_{X,R}}{\partial \dot{\theta}} - X_t \frac{\partial C_{Z,t}}{\partial \dot{\theta}} . \end{aligned} \quad (6.8)$$

The slipstream terms affecting these stability derivatives are presented in the next section.



b. Slipstream Terms

The slipstream terms to be considered in the evaluation of the stability derivatives are  $\Delta C_{L,S}$ ,  $\Delta C_{D,S}$ ,  $\partial \Delta C_{L,S} / \partial V$  and  $\partial \Delta C_{D,S} / \partial V$ . The slipstream lift and longitudinal force coefficients are

$$\Delta C_{L,S} = 1.87 \alpha_s \frac{r_o}{c} (1 - \mu^2) + \frac{q}{q_s} a \alpha \quad (6.9)$$

and

$$C_{D,S} = C_{D0} + (\Delta C_{L,S})^2 \frac{N S}{\pi A R S_s} \quad (6.10)$$

Differentiating Equation (6.9) with respect to  $V$ ,

$$\begin{aligned} \frac{\partial \Delta C_{L,S}}{\partial V} = & K \frac{\partial \alpha_s}{\partial V} r_o (1 - \mu^2) + K \alpha_s \frac{\partial r_o}{\partial V} (1 - \mu^2) + \\ & K \alpha_s r_o (-2\mu \frac{\partial \mu}{\partial V}) + \frac{q}{q_s} a \frac{\partial \alpha}{\partial V} + \\ & \frac{a \alpha}{q_s} \rho V - \frac{a \alpha q}{q_s^2} \frac{\partial q_s}{\partial V} \end{aligned} \quad (6.11)$$

$$\text{where } K = \frac{1.87}{c} \quad (6.12)$$

The partial derivatives appearing in Equation (6.11) are as follows:

$$\frac{\partial \phi}{\partial V} = \frac{\partial \alpha_s}{\partial V} = \frac{\left( V \frac{\partial T}{\partial V} - 2T \right) \cdot \left( -\frac{1}{2} \cos^2 \phi \right)}{\left( \frac{\rho}{2} \right) \frac{\pi D^2}{4} \sin^2 \alpha_T \left[ V^2 \cot^2 \alpha_T + \frac{2T}{\sin^2 \alpha_T \rho \frac{\pi D^2}{4}} \right]^{3/2}} \quad (6.13)$$

$$\frac{\partial r_o}{\partial V} = - \frac{D^2}{32r_o} \frac{\left[ \frac{2T \frac{\partial T}{\partial V} V}{\rho \frac{\pi D^2}{4} \cos^2 \alpha_T} \right] - \left[ \frac{4T}{\rho \frac{\pi D^2}{4} \cos^2 \alpha_T} \right]}{\left[ V^2 + \frac{2T}{\rho \frac{\pi D^2}{4} \cos^2 \alpha_T} \right] \left[ V^2 + \frac{2T}{\rho \frac{\pi D^2}{4} \cos^2 \alpha_T} \right]^{\frac{1}{2}}} \quad (6.14)$$

and

$$\begin{aligned} \frac{\partial \mu}{\partial V} = & \frac{V^2 \sin 2(\alpha_T - \phi) \left( - \frac{\partial \phi}{\partial V} \right)}{\left[ V^2 + \frac{2T}{\rho \frac{\pi D^2}{4}} \right]} + \\ & \frac{\cos^2 (\alpha_T - \phi)}{\left[ V^2 + \frac{2T}{\rho \frac{\pi D^2}{4}} \right]^{3/2}} \cdot \left[ 2 \frac{\partial T}{\partial V} V \frac{1}{\rho \frac{\pi D^2}{4}} - \frac{4T}{\rho \frac{\pi D^2}{4}} \right]. \end{aligned} \quad (6.15)$$

For the hovering case, ( $V = 0$ ),

$$\left. \frac{\partial \phi}{\partial V} \right|_{V=0} = \frac{\sin \alpha_T}{\sqrt{\frac{2T}{\rho \frac{\pi D^2}{4}}}} \quad (6.16)$$

$$\left. \frac{\partial r_o}{\partial V} \right|_{V=0} = \frac{D}{4\sqrt{2}} \frac{\cos \alpha_T}{\sqrt{\frac{2T}{\rho \frac{\pi D^2}{4}}}} \quad (6.17)$$

$$\left. \frac{\partial \mu}{\partial V} \right|_{V=0} = \frac{-2 \cos^2 \alpha_T}{\sqrt{\frac{2T}{\rho \frac{\pi D^2}{4}}}}. \quad (6.18)$$

Differentiating, next, Equation (6.10) with respect to  $V$ , there results

$$\frac{\partial \Delta C_{D,S}}{\partial V} = \frac{2 \Delta C_{L,SS}}{\pi AR S_s} \cdot \frac{\partial \Delta C_{L,S}}{\partial V} \quad (6.19)$$

#### (1) Numerical Computation of Slipstream Terms

For the purpose of comparison and compatibility with the data of Reference 21, the slipstream terms were evaluated using the following data from that reference:

##### Performance Data

$V = 0$ ft./sec.	$\alpha_T = 87$ degrees
$C_{T,S} = 1.0$	$\Omega R = 702$ ft./sec.
$C_T = 0.0195$	$T = 1615$ lb.

##### Wing Characteristics

$S = 114.7$ ft. <sup>2</sup>	$i_W = 0$ degrees
$AR = 5.25$	$\alpha_{LO} = -4$ degrees
$c = 5.25$ ft.	$a = 3.05$ /rad.

##### Propeller Characteristics

$N = 2$
$D = 9.5$ ft.
$\frac{\pi D^2}{4} = 70.6$ ft. <sup>2</sup>

Using these values and the equations of Section III,

9)

$$U = \sqrt{\frac{2T}{\rho \frac{\pi D^2}{4}}} = 139 \text{ ft./sec.}$$

$$V_j = U = 139 \text{ ft./sec.}$$

$$q_s = \frac{1}{2} \rho V_j^2 = 22.9 \text{ lb./ft.}^2$$

$$\phi = \tan^{-1} \left( \frac{V \sin \alpha_T}{V \cos \alpha_T + U} \right) = 0$$

$$\alpha_s = i_W \cdot \phi - \alpha_{LO} = 4 \text{ degrees} = 0.07 \text{ radians}$$

$$r_o = \frac{D}{2} \sqrt{\frac{1}{2} \left( \frac{2V \cos \alpha_T + U}{V \cos \alpha_T + U} \right)} = 3.36 \text{ ft.}$$

$$\mu = \frac{V \cos (\alpha_T - \phi)}{V_j} = 0$$

$$\Delta C_{L,S} = 1.87 \alpha_s \frac{r_o}{c} (1 - \mu^2) = 0.0924$$

$$\Delta C_{D,S} = C_{DO} + (\Delta C_{L,S}^2) \frac{N S}{S_s \pi AR} = 0.0213$$

$$\frac{\partial \phi}{\partial V} = \frac{\sin \alpha_T}{\sqrt{\frac{2T}{\rho \frac{\pi D^2}{4}}}} = 0.00717$$

$$\frac{\partial r_0}{\partial V} = \frac{D}{4\sqrt{2}} \frac{\cos \alpha_T}{\sqrt{\rho \frac{\pi D^2}{4}}} = 0.00063$$

$$\frac{\partial \mu}{\partial V} = - \frac{2\cos^2 \alpha_T}{\sqrt{\rho \frac{\pi D^2}{4}}} = - 0.000039$$

$$K = \frac{1.87}{c} = 0.394 .$$

There follows that

$$\frac{\partial \Delta C_{L,S}}{\partial V} = 0.0095$$

$$\frac{\partial \Delta C_{D,S}}{\partial V} = 0.00027 .$$

## (2) Effect of Slipstream on Stability Derivatives

Using the derivations presented in Reference 21, the derivative  $C_{X_V}$  can be written as

$$C_{X_V} = - \left[ \frac{2}{V_j} \frac{\partial V_j}{\partial V} \Delta C_{L,S} + \frac{\partial \Delta C_{L,S}}{\partial V} + \Delta C_{D,S} \frac{\partial \alpha_s}{\partial V} \right] \sin(\alpha_T - \phi) +$$

$$\frac{\partial C_{X,R}}{\partial V} - \left[ \frac{2}{V_j} \frac{\partial V_j}{\partial V} \Delta C_{D,S} + \frac{\partial \Delta C_{D,S}}{\partial V} - \Delta C_{L,S} \frac{\partial \alpha_s}{\partial V} \right] \cos(\alpha_T - \phi) .$$

(6.20)

Neglecting small terms, this derivative can be written for the hovering flight condition as follows:

$$C_{X_V} = - \frac{\partial \Delta C_{L,S}}{\partial V} \sin (\alpha_T - \phi) + \frac{\partial C_{X,R}}{\partial V} \quad (6.21)$$

Similarly, from Equation (6.6), the pitching moment derivative with velocity can be written as

$$C_{M_V} = z_a \frac{\partial \Delta C_{L,S}}{\partial V} \sin (\alpha_T - \phi) - z_R \frac{\partial C_{X,R}}{\partial V} \quad (6.22)$$

The derivatives  $C_{X_{\dot{\theta}}}$  and  $C_{M_{\dot{\theta}}}$  are given as:

$$C_{X_{\dot{\theta}}} = \frac{\partial C_{X,t}}{\partial \dot{\theta}} + \frac{\partial C_{X,R}}{\partial \dot{\theta}} - z_R \frac{\partial C_{L,S}}{\partial V} \cos (\alpha - \alpha_T - \phi_p) \quad (6.23)$$

$$C_{M_{\dot{\theta}}} = \frac{\partial C_{M,CF}}{\partial \dot{\theta}} - x_t \frac{\partial C_{Z,t}}{\partial \dot{\theta}} - z_R \frac{\partial C_{X,R}}{\partial \dot{\theta}} - \frac{z_a^2}{c} \frac{\partial \Delta C_{L,S}}{\partial V} \quad (6.24)$$

It should be noted that the stability derivatives  $C_{X_V}$ ,  $C_{M_V}$ ,  $C_{X_{\dot{\theta}}}$ , and  $C_{M_{\dot{\theta}}}$  are affected by the slipstream derivative,  $\partial \Delta C_{L,S} / \partial V$ .

### 3. Effect of the Slipstream on the Hovering Stability Characteristics

The characteristic equation in hovering is as follows:

$$B \lambda^3 + C \lambda^2 + D \lambda + E = 0 \quad (6.25)$$

where, using the numerical values obtained above,

$$\begin{aligned} B &= C_{X_V} C_{M_{\ddot{\theta}}} \\ &= 0.0091 \end{aligned} \quad (6.26)$$

$$C = C_{X_V} C_{M\ddot{\theta}} + C_{X\dot{V}} C_{M\dot{\theta}} \quad (6.27)$$

$$= 0.212 \frac{\partial \Delta C_{L,S}}{\partial V} + 0.00407$$

$$D = C_{X_V} C_{M\dot{\theta}} - C_{M_V} C_{X\dot{\theta}} \quad (6.28)$$

$$= -1.615 \left( \frac{\partial \Delta C_{L,S}}{\partial V} \right)^2 + 0.0623 \left( \frac{\partial \Delta C_{L,S}}{\partial V} \right) + 0.00004$$

$$E = -C_{M_V} C_{X\theta} \quad (6.29)$$

$$2.17 \left( \frac{\partial \Delta C_{L,S}}{\partial V} \right) + 0.0059$$

The solution of the characteristic equation for the hovering flight condition yields the roots as shown in Figure 32. One root is aperiodic and convergent, while the other pair of roots represents an unstable oscillation.

As was previously shown, the slipstream term  $\partial \Delta C_{L,S} / \partial V$  affects the stability derivatives  $C_{X_V}$ ,  $C_{M_V}$ ,  $C_{X\dot{\theta}}$  and  $C_{M\dot{\theta}}$ . In order to determine the effect of the slipstream, the magnitude of  $\partial \Delta C_{L,S} / \partial V$  was varied between zero and 200 percent of its original value of 0.0095, and the resulting roots of the characteristic equation were calculated and are also shown in Figure 32. It can be seen from Figure 32 that a decrease of  $\partial \Delta C_{L,S} / \partial V$  increases the period of the unstable oscillation while at the same time reducing its instability.

$$\lambda = a + ib$$

$$B\lambda^3 + C\lambda^2 + D\lambda + E = 0$$

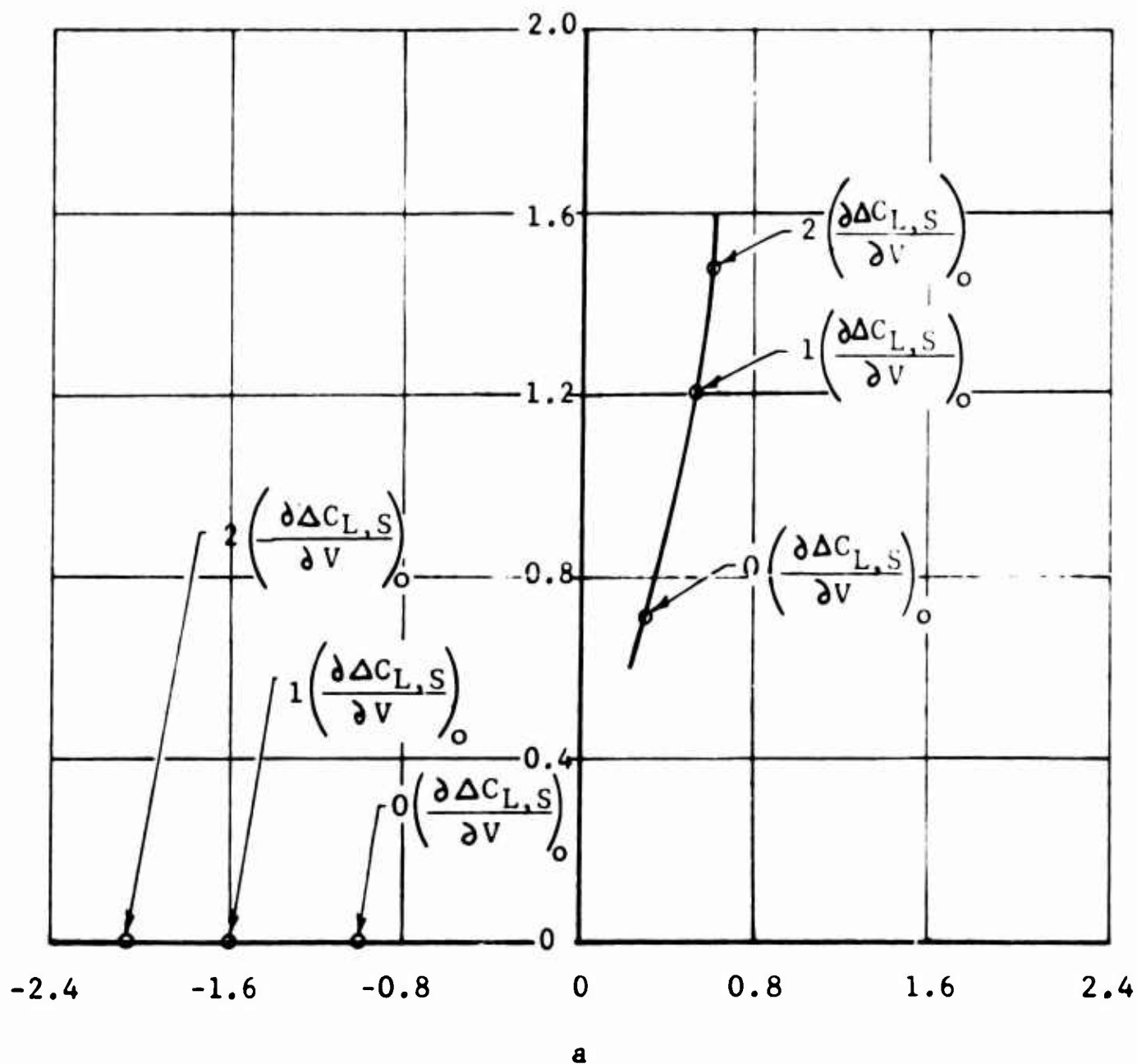


FIGURE 32: EFFECT OF SLIPSTREAM ON THE ROOTS OF THE CHARACTERISTIC EQUATION FOR HOVERING FLIGHT



D. STABILITY AUGMENTATION OF V/STOL AIRCRAFT UTILIZING THE SLIPSTREAM VELOCITY

The high disc loadings, compared to those of helicopters, of tilt-wing VTOL aircraft points toward the use of slipstream air flow for improving the stability characteristics of these aircraft. An investigation was performed, therefore, to gain an insight into the effectiveness of the slipstream air flow for this purpose. It was assumed that the stability augmentation is provided by means of a movable flap at the trailing edge of the wing immersed in the slipstream wake. This flap is deflected by changes in the aircraft attitude. The flap deflection angle,  $\delta_f$ , is then given by

$$\delta_f = k_\delta \theta . \quad (6.30)$$

Substituting Equation (6.30) into Equation (3.9) the effective angle of attack in the slipstream,  $\alpha_s$ , is written as

$$\alpha_s = i_w + \phi - \alpha_{LO} + k_\delta \theta . \quad (6.31)$$

In hovering, the slipstream lift derivative with respect to attitude becomes

$$\frac{\partial \Delta C_{L,S}}{\partial \theta} = K r_o \frac{\partial \alpha_s}{\partial \theta} \quad (6.32)$$

where

$$\frac{\partial \alpha_s}{\partial \theta} = k_\delta .$$

There follows that

$$\frac{\partial \Delta C_{L,S}}{\partial \theta} = K r_o k_\delta . \quad (6.33)$$

Also, the pitching moment derivative with respect to attitude is

$$\frac{\partial C_M}{\partial \theta} = \frac{Z_a}{c} \frac{\partial \Delta C_{L,S}}{\partial \theta} . \quad (6.34)$$

Substituting Equation (6.34) into Equation (6.33),

$$\frac{\partial C_M}{\partial \theta} = \frac{Z_a}{c} K r_o k_s . \quad (6.35)$$

Also,

$$\frac{\partial C_X}{\partial \theta} = \frac{\partial \Delta C_{L,S}}{\partial \theta} \left( -\sin (\alpha_T - \phi) \right) . \quad (6.36)$$

Evaluating Equations (6.35) and (6.36),

$$\frac{\partial C_M}{\partial \theta} = 0.401 k_s \quad (6.37)$$

and

$$\frac{\partial C_{X,S}}{\partial \theta} = -1.32 k_s . \quad (6.38)$$

The coefficients of the characteristic equation in hovering are thus changed by the addition of the derivative  $\partial C_M / \partial \theta$ , and also by a change in the derivative  $C_{X_\theta}$ , due to Equations (6.37) and (6.38). These coefficients are as follows:

$$\begin{aligned} B &= C_{X\dot{V}} C_{M\dot{\theta}} \\ &= 0.0091 \end{aligned}$$

$$\begin{aligned}
C &= C_{X_V} C_{M\ddot{\theta}} + C_{X\dot{V}} C_{M\dot{\theta}} \\
&= 0.00608 \\
D &= C_{X_V} C_{M\dot{\theta}} - C_{M_V} C_{X\dot{\theta}} + \underline{0.401k_\zeta} C_{X_V} \\
&= 0.000486 - 0.019k_\zeta \\
E &= - C_{M_V} (C_{X\ddot{\theta}} - \underline{1.32k_\zeta}) + \underline{0.401k_\zeta} C_{X_V} \\
&= 0.0266 + 0.0187k_\zeta \qquad (6.39)
\end{aligned}$$

The underlined terms represent the contributions due to flap deflection.

The roots of the characteristic equation were calculated for various values of  $k_\zeta$ , and the results are shown in Figure 33. It is seen from this figure that a decrease of  $k_\zeta$  results in an improvement of the oscillatory mode while at the same time decreasing the stability of the aperiodic mode. It is also shown that for the example configuration analyzed here, a value of  $k_\zeta = -1.0$  results in dynamic stability of both modes of motion. It is seen, therefore, that proper use of the propeller slipstream could improve the dynamic stability of a tilt-wing aircraft.

$$\lambda = a \pm ib$$

$$B\lambda^3 + C\lambda^2 + D\lambda + E = 0$$

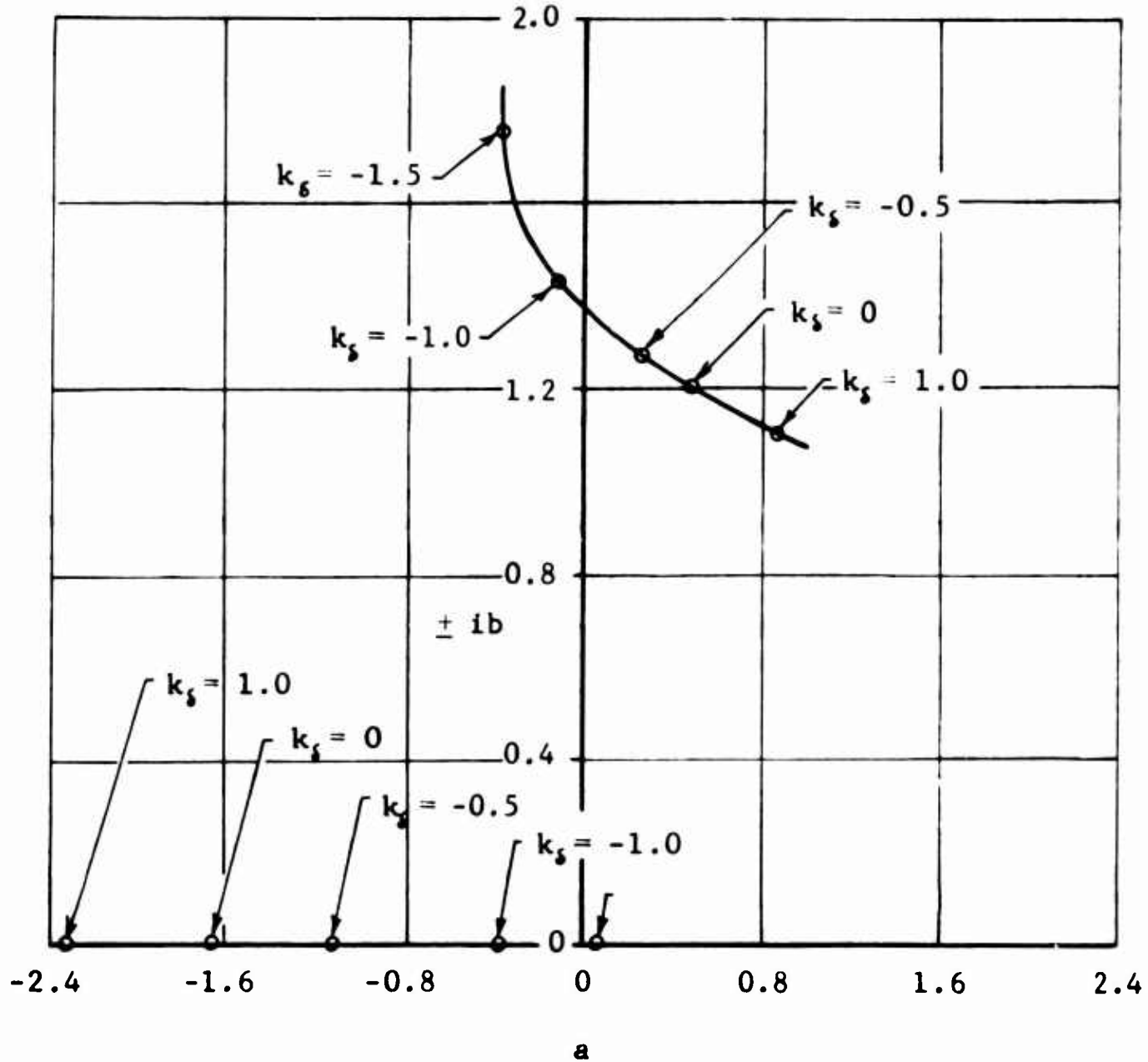


FIGURE 33: EFFECT OF TRAILING EDGE FLAP STABILIZER ON THE ROOTS OF THE CHARACTERISTIC EQUATION FOR HOVERING FLIGHT

## VII. CONCLUSIONS AND RECOMMENDATIONS

An analysis is presented of the lift and longitudinal force acting on various propeller-wing combinations. The analysis includes a theoretical treatment of the important effects of propeller slipstream-wing interaction. Correlation of the theory with test data of both two- and four-propeller-wing combinations shows good agreement. Application of the theory to predict the take-off and landing performance of typical STOL aircraft is also presented.

Preliminary stability and control analysis indicates that the slipstream can be utilized for improving the dynamic stability of a tilt-wing aircraft in hovering flight.

Based on the findings of this report it is suggested that this work be extended to include:

1. A more detailed investigation of the onset of stall in the slipstream.
2. The application of such a stall investigation to the determination of a propeller-wing combination which would be free from the adverse effects of wing stall throughout transition.
3. The extension of the stability and control analysis, giving detailed consideration to: propeller normal force and moments, tail moments, wing center of pressure location as effected by the slipstream, the deflection of flaps in the slipstream, and the effects of ground proximity.
4. The quantitative determination of slipstream effects on VTOL stability and control.

## VIII. BIBLIOGRAPHY

1. Koning, C., "Influence of the Propeller on Other Parts of the Airplane Structure," Aerodynamic Theory Edited by W. F. Durand, Volume IV, 1943
2. Rethorst, S., Royce, W., and Wu, T., Lift Characteristics of Wings Extending Through Propeller Slipstreams, Vehicle Research Corporation Report No. 1., 1958
3. Smelt, R. and Davis, H., Estimate of Increase on Lift Due to Slipstream, Air Ministry; Aeronautical Research Committee Reports and Memoranda, R. and M. 1788, 1937
4. Graham, E. W., Lagerstrom, P. A., Licher, R. M., and Beane, B. J., A Preliminary Theoretical Investigation of the Effects of Propeller Slipstream on Wing Lift, Douglas Report SM-14991, 1953
5. Squire, H. B., and Chester, W., Calculation of the Effect of Slipstream on Lift and Induced Drag, Ministry of Supply; Aeronautical Research Council Reports and Memoranda, R. and M. No. 2368, 1945
6. Franke, A. and Weinig, F., The Effect of the Slipstream on Airplane Wing, NACA TM 920, 1939
7. Jones, R. T., Properties of Low-Aspect-Ratio Pointed Wings at Speeds Below and Above the Speed of Sound, NACA Report No. 835, 1946
8. Dwight, Tables of Integrals and Other Mathematical Data, the MacMillan Co., 1947
9. Diederich, F. W., A Planform Parameter for Correlating Certain Aerodynamic Characteristics of Swept Wings, NACA TN 2335, 1951

10. Kuethe, A. M., and Schetzer, J. D., Foundations of Aerodynamics, John Wiley and Sons, 1950
11. Gessow, A., and Myers, G. C., Aerodynamics of the Helicopter, The MacMillan Co., 1952
12. Taylor, Robert T., Wind-Tunnel Investigation of Effect of Ratio of Wing-Chord to Propeller Diameter with Addition of Slats on the Aerodynamic Characteristics of Tilt-Wing VTOL Configurations in the Transition Speed Range, NASA TN D-17, September 1959
13. Hoerner, S. F., Fluid-Dynamic Drag, 1958
14. Kuhn, R. E., Take-Off and Landing Distances and Power Requirements of Propeller Driven STOL Airplanes, IAS Preprint No. 690, 1957
15. Hemke, P. E., Elementary Applied Aerodynamics, Prentice Hall, New York, 1946
16. Kuhn, R. E., and Draper, J. W., An Investigation of a Wing Propeller Configuration Employing Large Chord Plain Flaps and Large-Diameter Propellers for Low-Speed Flight and Vertical Take-Off, NACA TN 3307, December 1954
17. Kuhn, R. E., Hayes, W. C., Jr., Wind-Tunnel Investigation of Longitudinal Aerodynamic Characteristics of Three-Propeller Driven VTOL Configurations in the Transition Speed Range Including Effects of Ground Proximity, NASA TN D-55, February 1960
18. Neal, B., The Effect of Thrust Variation with Forward Speed on the STOL Performance of an Overloaded Tilt-Wing VTOL Aircraft, National Research Council of Canada, Report No. LR-373A, July 1963

19. Williamson, G. G., Dynamic Stability Analysis of a VTOL Vectored Slipstream Vehicle During Transition, Princeton University Report No. 535, April 1961 (AD 260 719)
20. Paiewonsky, B. H., The Dynamic Stability Characteristics of a VTOL Type Aircraft in Hovering and Transition Flight, Princeton University Report No. 345, May 1956
21. Hargraves, C. R., An Analytical Study of the Longitudinal Dynamics of a Tilt-Wing VTOL, Princeton University Report No. 561, June 1961
22. Cromwell, C. H., and Payne, H. E., A Stability Analysis of Tilt-Wing Aircraft, Princeton University Report No. 477, May 1960
23. Perkins and Hage, Airplane Performance, Stability and Control, John Wiley, 1949
24. LeSueur, M., Ground Effect on the Take-Off and Landing of Airplanes, NACA TM 771, July 1935
25. Pegg, R. J., Summary of Flight-Test Results of the VZ-2 Tilt-Wing Aircraft, NASA TN D-989, February 1962
26. Johnson, G. W., Factors Affecting the Field Length of STOL Aircraft, AGARD Report 81, August 1956
27. Kuhn, R. E., and Grunwald, K. J., Lateral Stability and Control Characteristics of a Four-Propeller Deflected-Slipstream VTOL Model Including the Effects of Ground Proximity, NASA TN D-444, January 1962
28. Grunwald, K. J., Aerodynamic Characteristics of a Four-Propeller Tilt-Wing VTOL Model with Twin Vertical Tails, Including Effects of Ground Proximity, NASA TN D-901, June 1961



29. Kuhn, R. E., and Grunwald, K. J., Longitudinal Aerodynamic Characteristics of a Four-Propeller Deflected-Slipstream VTOL Model Including the Effects of Ground Proximity, NASA TN-248, November 1960
30. Kuhn, R. E., Investigation of the Effects of Ground Proximity and Propeller Position on the Effectiveness of a Wing with Large-Chord Slotted Flaps in Redirecting Propeller Slipstreams for Vertical Take-Off, NACA TN 3629, March 1956
31. Fink, M. P., and Lastinger, J. L., Aerodynamic Characteristics of Low-Aspect-Ratio Wings in Close Proximity to the Ground, NASA TN 926, July 1961
32. Recant, J. G., Wind-Tunnel Investigation of Ground Effects on Wings with Flaps, NACA TN 705, May 1939
33. Reid, E. G., Applied Wing Theory, McGraw-Hill Book Company, Inc., New York, 1932
34. Heyson, H. H., Jet-Boundary Correction for Lifting Rotors Centered in Rectangular Wind Tunnels, NASA TR R-71, 1960
35. Heyson, H. H. Linearized Theory of Wind Tunnel Jet-Boundary Corrections and Ground Effect for VTOL-STOL Aircraft, NASA TR R-124, 1962
36. Neal, B. and Lyster, H. N. C., Estimation of Minimum Field Requirements of Two Overloaded, Propeller-Driven Tilt-Wing VTOL Aircraft, National Research Council of Canada Aeronautical Report LR-373, January 1963
37. Neal, B., The Static and Forward Speed Testing of a Flapped Wing with Boundary Layer Control for use in Deflecting Propeller Slipstreams Downward for Vertical Take-Off Part II: at Incidence and Ground Proximity Effects, National Research Council of Canada Aeronautical Report LR-383, July 1963.

38. Anon., YAO-1 Demonstration Progress and Data Report, Contract NOas 57-841c, Grumman Aircraft Engineering Corporation, Report FP-134-2 & 5-001, May 30, 1959
39. Wetmore, W. C., "Foreign Interest Revived in Breguet 941," Aviation Week, Volume 79 Number 3, July 15, 1963, pp. 73-80
40. Craig, A. J., Evaluation of the Performance Stability and Control of the Helio Courier Airplane, The University of Wichita, Kansas, Report No. 264, February 1957
41. Goland, L., and Miller, N., Effects of Propeller Slipstream on V/STOL Aircraft Performance and Stability Phase II Report, Dynasciences Corporation, Report No. DCR-130, November 1963

## APPENDIX

### STOL TAKE-OFF AND LANDING PERFORMANCE ANALYSIS

This performance analysis consists of developing methods to predict STOL take-off and landing distances and velocities. The landing analysis will be discussed first.

#### A. LANDING ANALYSIS

As indicated in Reference 14, the landing maneuver analysis is assumed to be made up of three stages: the approach, transition, and the ground run as shown in Figure 34.

##### 1. Approach Distance

The approach distance from a 50-foot obstacle is given by

$$l_a = \frac{50}{\tan \theta_p} \quad (A1)$$

Thus, the approach distance is determined by the approach angle,  $\theta_p$ . The approach angle is given in terms of the approach velocity,  $V$ , and the rate of descent,  $V_v$ , as follows:

$$\sin \theta_p = \frac{V_v}{60V} \quad (\text{for } V_v \text{ in ft./min.}) \quad (A2)$$

Rates of descent of 500 to 700 feet/minute would appear reasonable based on flight experience with helicopters and V/STOL aircraft. Using the small angle assumption that  $\sin \theta_p = \tan \theta_p$  (although this assumption is not valid at very low speeds, the discrepancy will be shown to be small), the approach distance can be written as

$$l_a = 3000 \frac{V}{V_v} \quad \left( \begin{array}{l} \text{for } V \text{ in ft./sec.} \\ \text{and } V_v \text{ in ft./min.} \end{array} \right) \quad (A3)$$

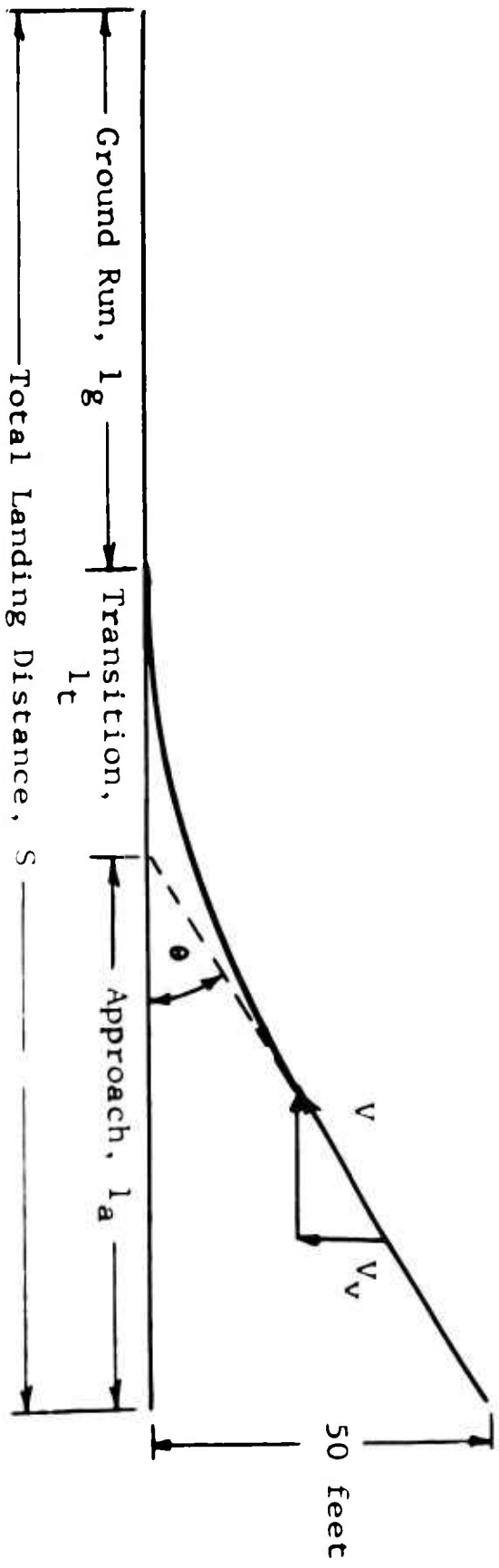


FIGURE 34: PROFILE OF LANDING PATH

or

$$l_a = 5070 \frac{V_k}{V_v} \quad \left( \begin{array}{l} \text{for } V_k \text{ in knots} \\ \text{and } V_v \text{ in ft./min.} \end{array} \right) \quad (A4)$$

This relation from Reference 14 is shown as a function of the approach speed for several rates of descent in Figure 35. The small-angle discrepancy is small as shown by the dashed line on Figure 35.

## 2. Transition Distance

The transition distance, obtained by assuming that the flight path occurs along a circular arc, is given by

$$l_t = \frac{v^2 \tan\left(\frac{\theta_p}{2}\right)}{g \Delta n} \quad (A5)$$

Using the small-angle assumption together with Equation (A2), the transition distance can be written as

$$l_t = \frac{V V_v}{120 g \Delta n} \quad (V_v \text{ in ft./min.}) \quad (A6)$$

If a rate of descent of 500 feet/minute is assumed for routine landings, then Equation (A6) can be written as

$$l_t = \frac{4.16 V}{g \Delta n} \quad (\text{for } V \text{ in ft./sec}) \quad (A7)$$

or

$$l_t = \frac{7 V_k}{g \Delta n} \quad (V_k \text{ in knots}) . \quad (A8)$$

The transition distances are plotted in Figure 36 for typical values of normal acceleration. The effect of the small-angle assumption is seen to be very small.

$$l_a = \frac{5070 V_K}{V_V}$$

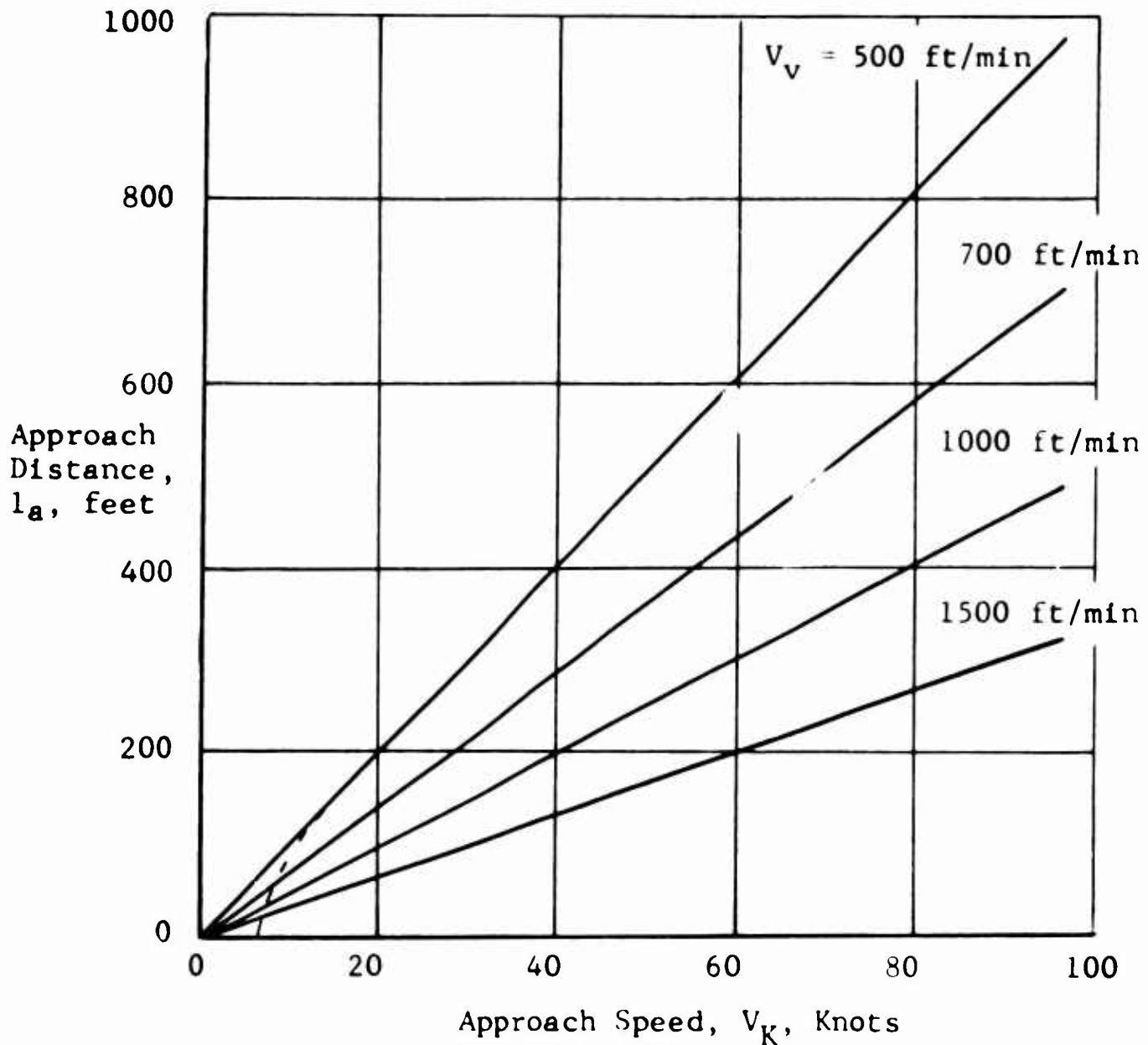


FIGURE 35: LANDING APPROACH DISTANCE FROM REFERENCE 14

$$l_t = \frac{7 V_K}{g \Delta n}$$

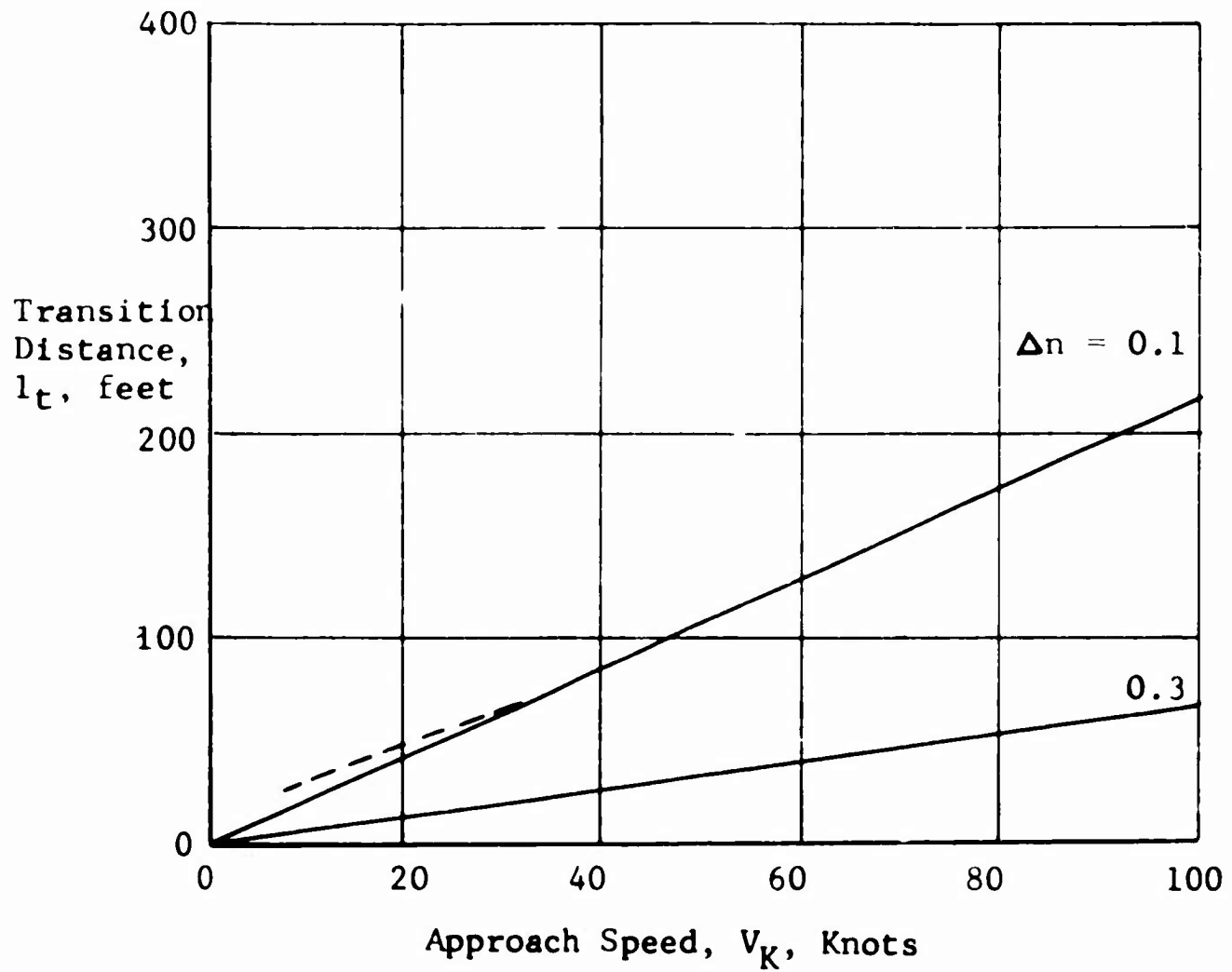


FIGURE 36: LANDING TRANSITION DISTANCE

### 3. Ground Run

The forces acting on the aircraft during the landing run are given by

$$D + C_F (W - L) = \frac{W}{g} a_c$$

$D$  = drag force (A9)

$C_F(W - L)$  = braking force

At touchdown, the braking force available for deceleration can be increased by a decrease of lift. This condition can be achieved through piloting technique. The drag force can be considered small compared to the braking force. The landing distance is then given for a constant deceleration in terms of the coefficient of friction as

$$l_g = \frac{v^2}{2 C_F g} \quad (A10)$$

or

$$l_g = \frac{2.86 V_k^2}{2 C_F g} \quad (\text{for } V_k \text{ in knots}) \quad (A11)$$

Decelerations from 0.8g to 1.0g (represented by  $C_F$  0.8 and 1.0) are possible during landing on dry concrete; these are, however, beyond the range of routine operations. The braking force (and the deceleration) could be increased by increasing the normal force on the wheels. This could be accomplished possibly by producing negative lift through the use of flaps deflected upward. Thus, this should be considered as a means to reduce landing distances for future STOL aircraft; however, at present, a deceleration of 0.3g represents a realistic value for normal landings.

The ground run for various friction coefficients is shown in Figure 37.



$$l_g = \frac{2.86 V_K^2}{2 C_F g}$$

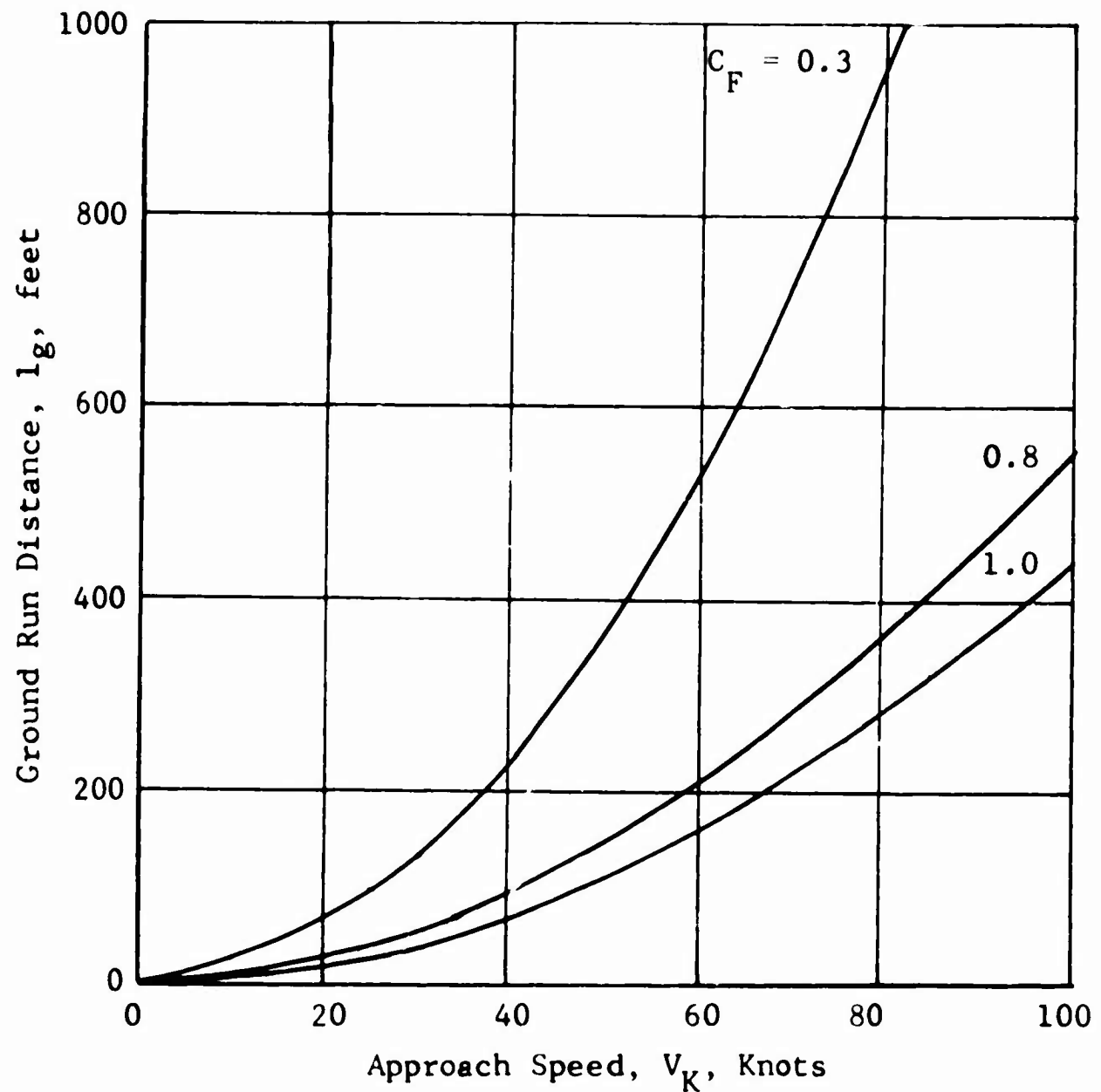


FIGURE 37: LANDING GROUND RUN DISTANCE FROM  
REFERENCE 14

#### 4. Total Landing Distance

The total landing distance is obtained from the summation of the approach, the transition, and the ground run. This distance can be obtained for a range of aircraft operations from routine landings to maximum performance landings using the following assumptions:

a. for routine landings

$$\begin{aligned}V_V &= 500 \text{ ft./min.} \\ \Delta n &= 0.1g \text{ (during transition)} \\ C_F &= 0.3 \text{ (landing deceleration } 0.3g)\end{aligned}$$

b. for maximum performance landings

$$\begin{aligned}V_V &= 1000 \text{ ft./min.} \\ V_{\text{transition}} & \\ C_F &= 0.8 \text{ (landing deceleration } 0.8g)\end{aligned}$$

The total landing distances corresponding to these values are shown in Figure 38.

In order to determine the total landing distance, it is necessary to know the approach speed of the aircraft. Standard practice has been to relate this approach speed to the aircraft stall speed as follows:

$$V = V_{\text{approach}} = KV_{\text{stall}} \quad \text{where } K > 1.0 \quad (\text{A12})$$

The approach speed is assumed to be 10 percent greater than the stall speed to allow a margin of safety for control during landing. Equation (A12) can thus be written as follows:

$$V_{\text{approach}} = 1.1 \sqrt{\frac{2 \left( \frac{W}{S} \right)}{\rho C_{L_{\text{max}}}}} \quad (\text{A13})$$

The maximum lift coefficient can be determined through standard methods such as those given in Reference 15.

- ◇ Grumman Mohawk, Reference 38
- Breguet 941, Reference 39
- △ DeHavilland DHC-2 Beaver, Reference 26
- Helio Courier, Reference 40

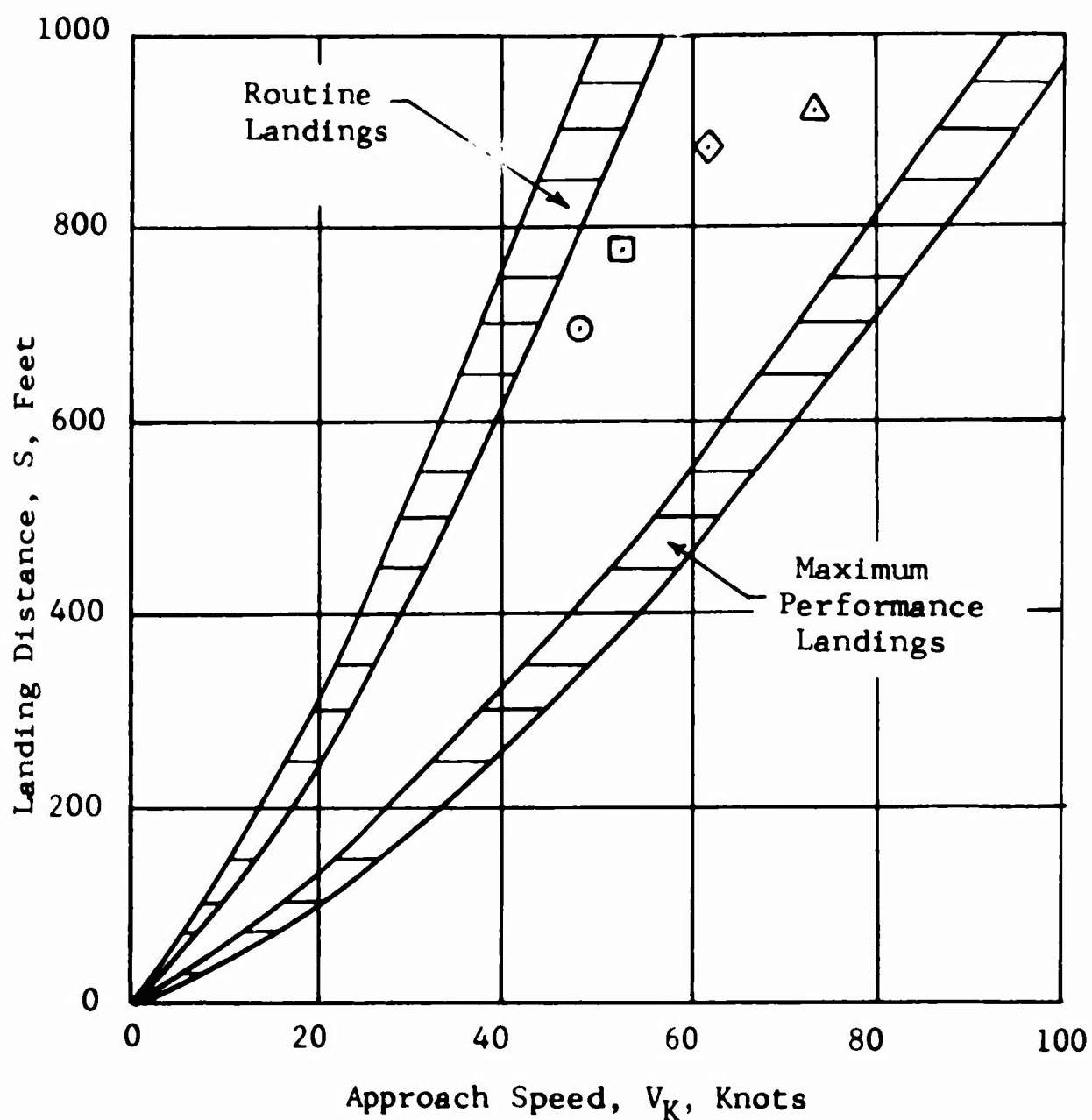


FIGURE 38: TOTAL LANDING DISTANCE OVER A 50-FOOT OBSTACLE

## B. TAKE-OFF ANALYSIS

The take-off maneuver can be considered to be made up of the ground run, the transition, and the climb.

### 1. Ground Run

The ground run of an aircraft consists of the take-off distance from start to the point at which the wheels leave the ground. The take-off distance is given by

$$S_{TO} = \int_{V=0}^{V=V_{TO}} \frac{VdV}{a_1} \quad (A14)$$

The acceleration  $a_1$  is obtained by a solution of the equations of the forces acting on the aircraft (parallel and perpendicular to the ground) to obtain

$$a_1 = \frac{g}{W} \left[ F_x - \mu_L(W - L) \right]. \quad (A15)$$

With this expression, Equation (A14) can be integrated numerically:

$$S_{TO} = \sum_{V=0}^{V=V_{TO}} \frac{W}{g} \left[ \frac{V}{F_x - \mu_L(W-L)} \right] \Delta V. \quad (A16)$$

The calculation of take-off distance from equation (A16) is performed as follows:

- a. The minimum flying speed,  $V_{min}$ , is calculated from

$$V_{\min} = \sqrt{\frac{2}{\rho} \frac{W}{C_{L\max} S}} \quad (A17)$$

The determination of the lift coefficient  $C_{L\max}$  is presented in Section IV.

b. Increments of velocity,  $\Delta V$ , are selected starting from  $V = 0$  to  $V_{T0} = 1.2 V_{\min}$ .

c. At each station  $V + n \Delta V$  ( $n =$  positive integer 0, 1, 2), the longitudinal force,  $F_x$ , is calculated from Equation (3.25), and the lift is obtained by multiplying the total lift coefficient,  $C_{L,S}$ , from Equation (3.17) by  $q_s S$ .

d. The value of the expression given in Equation (A16) is calculated at each station selected in c. above.

e. The value of step d. above is numerically integrated from  $V = 0$  to  $V = V_{T0}$  to obtain the take-off distance.

## 2. Transition

The transition distance, which accounts for the distance required from take-off to achieve a steady-state climb, is assumed to occur along a circular arc, similar to that of the landing transition distance. Thus,

$$l_{TT} = \frac{V^2}{g \Delta n} \tan \left( \frac{\theta_c}{2} \right) \quad (A18)$$

where  $\Delta n =$  increment of normal acceleration, g's, and  $\theta_c$  is the climb angle given by

$$\theta_c = \sin^{-1} \left( \frac{V_c}{V} \right) \quad (A19)$$

where  $V_c$  = rate of climb .

It is necessary to obtain the climb angle in order to calculate the transition distance. This angle is obtained as discussed in the next section. The normal acceleration during transition is dependent upon the lift coefficient at take-off as well as the take-off velocity. If the take-off velocity is assumed to be 20 percent greater than the stall speed and the lift coefficient is  $0.9 C_{Lmax}$ , then the maximum normal acceleration is  $0.23g$ . The transition maneuver and the climb are assumed to be performed at the take-off velocity.

### 3. Climb

For the case of climbing flight with V/STOL aircraft, the climb angles involved could be large compared to conventional aircraft climb angles. Therefore, this fact must be taken into account in the analysis of the climb maneuver. The forces parallel and perpendicular to the flight path of an aircraft in steady climbing flight are

$$T - D - W \sin \theta_c = 0 \quad (A20)$$

and

$$L - W \cos \theta_c = 0 \quad (A21)$$

The climb angle,  $\theta_c$ , is given as

$$\theta_c = \sin^{-1} \left( \frac{V_c}{V} \right) \quad (A22)$$

where  $V_c$  is the rate of climb.

Substituting (A22) into (A20),

$$TV - (DV + W V_c) = 0 \quad (A23)$$

The first term represents power available and the second term is the horsepower required. Solving for  $V_c$  from Equation (A23),

$$V_c = \frac{TV - DV}{W} \quad (A24)$$

The total drag can be written as

$$D = D_o + D_i, \quad (A25)$$

or in coefficient form,

$$D = (C_{Do} + C_{Di}) q S \quad (A26)$$

where  $C_{Do}$  is the equivalent profile drag coefficient of the entire aircraft, and  $C_{Di}$  is the induced drag coefficient of the wing. For the case where the lift contribution and induced drag of the wing outside of the slipstream are negligible, the induced drag coefficient can be expressed as

$$C_{Di} = \frac{C_L^2}{\pi A R e}$$

Equation (A26) becomes

$$D = C_{Do} q S + \frac{C_L^2 q S}{\pi A R e} \quad (A27)$$

The lift coefficient  $C_L$  pertains to climbing flight, and must be compatible with Equation (A21),

$$C_L = \frac{L}{q S} = \frac{W \cos \theta_c}{q S} \quad (A28)$$

Substituting Equation (A28) into (A27), there results

$$D = C_{Do} q S + \frac{W^2 \cos^2 \theta_c}{\pi A R e q S} \quad (A29)$$

Substituting Equation (A29) into (A24) and solving for  $V_c/V$  while noting that

$$\cos \theta_c = \frac{\sqrt{V^2 - V_c^2}}{V} = \sqrt{1 - \left(\frac{V_c}{V}\right)^2}$$

$$\frac{V_c}{V} = \sin \theta_c = \frac{A}{2} \pm \sqrt{\left(\frac{A}{2}\right)^2 - B} \quad (A30)$$

where  $A = \frac{\pi AR e q S}{W}$ , and

$$B = \frac{A}{W} \left[ \frac{TV}{V} - C_{DO} q S \right] - 1$$

The rate of climb and climb angle can be determined from Equation (A30) for the given flight velocity,  $V$ , and the aircraft characteristics ( $C_{DO}$  and power available can be obtained from standard methods as given in References 15 and 23.) The distance required to climb to a 50-foot altitude can be obtained as

$$l_c = \frac{V}{V_c} (50-h) \cos \theta_c = \frac{(50-h)}{\tan \theta_c} = \frac{50 - \frac{2V^2}{g \Delta n} \sin^2 \frac{\theta_c}{2}}{\tan \theta_c} \quad (A31)$$

The total distance over a 50-foot obstacle can be obtained by summing the distances for ground run, transition, and climb, with the exception of the case of some STOL aircraft which could reach a 50-foot altitude during transition. In this case, the total distance over a 50-foot obstacle consists of a ground run (obtained previously) and a transition which is now determined as follows:

The vertical height achieved during transition is

$$h = \frac{2V^2}{\Delta n g} \sin^2 \left( \frac{\theta_c}{2} \right) \quad (A32)$$



If this height is greater than 50 feet, then the following is to be used:

For a height of 50 feet, the corresponding angle  $\theta_c$ , from Equation (A31), is

$$\theta = 2 \sin^{-1} \left( \frac{50 \Delta ng}{2v^2} \right)^{\frac{1}{2}} = 2 \sin^{-1} \frac{5}{v} \sqrt{\Delta ng} \quad (A33)$$

The transition distance would be given by,

$$l_{T50} = 50 \sqrt{\frac{v^2}{2S (\Delta ng)} - 1} \quad (A34)$$

The total distance over a 50-foot obstacle is

$$S_T = l_g + l_{T50} \quad (A35)$$

### C. GROUND EFFECT

Test data (References 24 through 32) on the performance of conventional wings and V/STOL propeller wing combinations in ground proximity indicates that a marked change in aerodynamic characteristics occurs in ground effect. The primary effects are a reduction in wing induced drag and large variations in pitching moment accompanied by secondary changes in lift coefficient.

As a result of ground effect on aircraft characteristics, "out of ground effect" analysis is at times inadequate for the accurate estimation of V/STOL take-off and landing performance. Hence, a V/STOL analysis considering ground effect is desirable. As part of this program, it was undertaken to adapt existing ground effect analyses (examples of which are presented in References 34 through 38) to the V/STOL performance analysis of this report. The first approach was based upon a ground effect analysis for propeller slipstreams developed by Heyson (References 35 and 36), and modified to account for a wing with a flap immersed in the slipstream by Neal (Reference 33). This analysis uses out-of-ground-effect slipstream characteristics to estimate interference velocities at the propeller disc caused by the presence of a ground plane in the propeller wake. It is shown in Reference 38, that this method gives good lift, drag, and downwash angle correlation in ground effect. This type of analysis, however, requires the use of digital computer facilities. Also, in its present form the analysis can be applied only to the case where the entire wing is immersed in the slipstream.

Another approach to ground effect analysis is developed by Reid in Reference 34 for conventional monoplanes or multiplanes. This is a relatively straightforward method which is suited to the case where part of the wing is out of the slipstream. An investigation was conducted during Phase II of this program (Reference 41) to adapt this method to the propeller slipstream analysis presented herein. It was found, however, that this method did not give consistently accurate estimates of ground effect.

In view of the complexity of the first method described and the inadequacy of the second method, additional effort is required to develop an analysis suited to preliminary performance calculations.

## DISTRIBUTION

U. S. Army Materiel Command	2
U. S. Army Mobility Command	2
U. S. Army Aviation Materiel Command	5
Chief of R&D, D/A	1
U. S. Army Transportation Research Command	75
U. S. Army Research and Development Group (Europe)	1
U. S. Army Natick Laboratories	1
U. S. Army Engineer Research and Development Laboratories	3
U. S. Army Signal Research and Development Laboratory Liaison Office , USACDC	1
Army Research Office-Durham	1
U. S. Army Combat Developments Command Experimentation Center	1
U. S. Army Aviation School	1
U. S. Army Transportation Center and Fort Eustis	1
U. S. Army Aviation Maintenance Center	1
U. S. Army Aviation Test Board	1
U. S. Army Aviation Test Activity, Edwards AFB	2
Air Force Systems Command, Wright-Patterson AFB	4
Air University Library, Maxwell AFB	1
Chief of Naval Operations	1
Bureau of Ships	1
Bureau of Naval Weapons	4
U. S. Naval Postgraduate School	1
Naval Air Test Center	1
U. S. Naval Ordnance Test Station	1
David Taylor Model Basin	2
Ames Research Center, NASA	2
NASA-LRC, Langley Station	2
Lewis Research Center, NASA	2
NASA Representative, Scientific and Technical Information Facility	2
Research Analysis Corporation	2
National Aviation Facilities Experimental Center	1
Defense Documentation Center	10
U. S. Government Printing Office	1

**BLANK PAGE**

**BLANK PAGE**

Dynasciences Corporation, Fort  
Washington, Pa., EFFECT OF  
PROPELLER SLIPSTREAM ON V/STOL  
AIRCRAFT PERFORMANCE AND STA-  
BILITY, L.Goland, et al., TRECOM  
Technical Report 64-47, August  
1964 105 pp. (Contract DA 44-177-  
AMC-48(T)) USATRECOM TASK  
ID121401A14203

UNCLASSIFIED REPORT

This report presents the results  
of an investigation of propeller  
slipstream effects on V/STOL

Dynasciences Corporation, Fort 1.  
Washington, Pa., EFFECT OF  
PROPELLER SLIPSTREAM ON V/STOL  
AIRCRAFT PERFORMANCE AND STA-  
BILITY, L.Goland, et al., TRECOM 2.  
Technical Report 64-47, August  
1964 105 pp. (Contract DA 44-177-  
AMC-48(T)) USATRECOM TASK  
ID121401A14203

UNCLASSIFIED REPORT

This report presents the results  
of an investigation of propeller  
slipstream effects on V/STOL

1. PROPELLER  
SLIPSTREAM  
EFFECTS  
2. Contract No.  
DA 44-177-  
AMC-48(T)

Dynasciences Corporation, Fort  
Washington, Pa., EFFECT OF  
PROPELLER SLIPSTREAM ON V/STOL  
AIRCRAFT PERFORMANCE AND STA-  
BILITY, L.Goland, et al., TRECOM  
Technical Report 64-47, August  
1964 105 pp. (Contract DA 44-177-  
AMC-48(T)) USATRECOM TASK  
ID121401A14203

UNCLASSIFIED REPORT

This report presents the results  
of an investigation of propeller  
slipstream effects on V/STOL

Dynasciences Corporation, Fort 1.  
Washington, Pa., EFFECT OF  
PROPELLER SLIPSTREAM ON V/STOL  
AIRCRAFT PERFORMANCE AND STA-  
BILITY, L.Goland, et al., TRECOM 2.  
Technical Report 64-47, August  
1964 105 pp. (Contract DA 44-177-  
AMC-48(T)) USATRECOM TASK  
ID121401A14203

UNCLASSIFIED REPORT

This report presents the results  
of an investigation of propeller  
slipstream effects on V/STOL

1. PROPELLER  
SLIPSTREAM  
EFFECTS  
2. Contract No.  
DA 44-177-  
AMC-48(T)

1. PROPELLER  
SLIPSTREAM  
EFFECTS  
2. Contract No.  
DA 44-177-  
AMC-48(T)

aircraft performance and stability. An analysis is presented of the lift and longitudinal force acting on various V/STOL propeller wing combinations. Correlation of the theory with test data shows good agreement. A STOL take-off and landing analysis and a preliminary VTOL stability analysis are also presented.

aircraft performance and stability. An analysis is presented of the lift and longitudinal force acting on various V/STOL propeller wing combinations. Correlation of the theory with test data shows good agreement. A STOL take-off and landing analysis and a preliminary VTOL stability analysis are also presented.

aircraft performance and stability. An analysis is presented of the lift and longitudinal force acting on various V/STOL propeller wing combinations. Correlation of the theory with test data shows good agreement. A STOL take-off and landing analysis and a preliminary VTOL stability analysis are also presented.

aircraft performance and stability. An analysis is presented of the lift and longitudinal force acting on various V/STOL propeller wing combinations. Correlation of the theory with test data shows good agreement. A STOL take-off and landing analysis and a preliminary VTOL stability analysis are also presented.